Faculdade de Engenharia da Universidade do Porto

Artificial blood to assess bacterial infections in central venous catheters

António Costa Gomes de Sá Cachada

Mestrado em Engenharia Biomédica

Supervisor: Prof. Dr. João Mário Miranda (PhD)

October, 2024

Fundação para a Ciência e a Tecnologia

REPÚBLICA PORTUGUESA | CIÊNCIA, TECNOLOGIA E ENSINO SUPERIOR

© António Cachada, 2024

Resumo

As infeções pela utilização de cateteres venosos centrais são um problema de saúde significativo. De facto, este e outros tipos de cateteres são utilizados por 75% dos pacientes em unidades de cuidados intensivos. Estes dispositivos têm várias aplicações, tais como a administração de medicamentos ou a recolha de sangue. O longo contacto dos cateteres venosos centrais com a corrente sanguínea faz com que o paciente tenha maior propensão para infeções. Estas infeções podem ter consequências graves e, em último caso, provocar a morte do paciente.

O sangue tem um papel fundamental no normal funcionamento do corpo. De facto, o sangue tem como principais funções o fornecimento de oxigénio e nutrientes às células e a remoção do dióxido de carbono produzido nos processos metabólicos. Para isso, este fluído apresenta uma composição específica, onde se destaca a elevada presença de glóbulos vermelhos. Para além disso, a presença significativa de glóbulos vermelhos faz com que o comportamento reológico do sangue seja altamente marcado por estas células sanguínea, pelo que, este fluído é caracterizado como um fluido não newtoniano.

Este trabalho está inserido no âmbito do projeto "Multiblood" (2022.08598.PTDC). O principal objetivo é o desenvolvimento de um fluído análogo ao sangue com a capacidade de transportar oxigénio. Para isso, é necessário produzir um fluído particulado, onde as partículas apresentem propriedades semelhantes aos glóbulos vermelhos (dimensão, entre outros), bem como a capacidade de transportar oxigénio. Na literatura, existem duas grandes correntes de fluídos nesta temática: os análogos do sangue (propriedades mecânicas semelhantes) e os substitutos do sangue (função específica semelhante, como o transporte de oxigénio). Os substitutos do sangue são divididos em dois grandes grupos: os baseados em hemoglobina e os baseados em perfluorocarbonos. No âmbito deste trabalho, foram estudados os fluídos particulados baseados em perfluorocarbonos, em particular a perfluorodecalina.

No sentido de estudar um fluído análogo ao sangue que concilie as propriedades mecânicas semelhantes ao sangue e a capacidade de transportar oxigénio, neste trabalho, foram desenvolvidas algumas ferramentas. Foram estudadas soluções para a produção de um fluído particulado baseado em perfluorodecalina utilizando o método de emulsificação por membrana, tendo sido obtida uma versão final utilizada para os testes posteriores. Para além disso, foram desenvolvidos dois micro-reómetros utilizando microcanais fabricados pela técnica de "soft

lithography". Por fim, foi desenvolvido e testado um sensor de oxigénio, utilizando uma solução de PtOEP encapsulada em PDMS.

Um fluído particulado baseado em perfluorodecalina (10%) foi produzido com sucesso, tendo sido utilizado para testes posteriores. O fluído apresenta partículas com dimensões de 10 μm ou inferiores e os fenómenos de coalescência foram reduzidos com a adição de PVA (3%). No desenvolvimento do micro-reómetro, foi possível fazer estimativas de valores de viscosidade para fluídos particulados, mas são recomendados testes adicionais para otimizar o método e tirar conclusões mais claras. Por fim, foi desenvolvido um sensor de oxigénio que deteta a variação de oxigénio. Este sensor foi testado com um scavenger (Na_2SO_3), tendo sido possível medir a variação da fluorescência ao longo do tempo. Foram executados testes com microrganismos, mas os resultados foram pouco conclusivos, devido a problemas associados à resolução espacial do sensor.

Palavras chave: Microfluídica, sangue artificial, fluído análogo ao sangue, Glóbulos vermelhos, sensor de oxigénio, Micro-reómetro, fluído particulado, perfluorodecalina.

Abstract

Infections related to use of central venous catheters are a significant problem. In fact, this and other types of catheters are used in 75% of patients in intensive care units. These devices have various applications, such as administering medications or collecting blood. The prolonged contact of central venous catheters with the bloodstream increases the patient's susceptibility to infections. These infections can have severe consequences and, in extreme cases, lead to the patient's death.

Blood plays a key role in the normal operation of the body. Blood's primary functions are to supply oxygen and nutrients to cells and remove the carbon dioxide produced in metabolic processes. To do this, this fluid has a specific composition, with a high presence of red blood cells (45%). Additionally, the high concentration of red blood cells significantly influences its mechanical behavior, characterizing blood as a non-Newtonian fluid.

This work is part of the "Multiblood" project (2022.08598.PTDC). The primary objective is the development a blood-analog fluid capable of transporting oxygen. To achieve this, it is necessary to produce a particulate fluid where the particles have mechanical properties similar to red blood cells (such as size) and the ability to transport oxygen. In the literature, there are two main categories of fluids in this field: blood analogs (with similar mechanical properties) and blood substitutes (with a similar specific function, such as oxygen transport). Blood substitutes are divided into two main groups: hemoglobin-based and perfluorocarbon-based. This work focused on studying particulate fluids based on perfluorocarbons, particularly perfluorodecalin.

In this work, to study a blood analogue fluid that combines similar mechanical properties to blood and the ability to transport oxygen, several tools were developed. Solutions for producing a particulate fluid based on perfluorodecalin were explored using the membrane emulsification method, resulting in a final version used for subsequent tests. Additionally, two micro-rheometers were developed using microchannels fabricated by the soft lithography technique. Finally, an oxygen sensor was developed and tested using a PtOEP solution encapsulated in PDMS.

PFD (10%) particulate fluid with Tween 80 and PVA (3%) presents particles of PFD with the majority of them showing dimensions of 10 μm or smaller. Also, coalescence phenomena was prevented by the use of PVA. In developing the micro-rheometer, it was possible to estimate viscosity values for particulate fluids, but additional tests are recommended to optimize the

method and draw clearer conclusions. Finally, an oxygen sensor was developed that detects oxygen variation. This sensor was tested with a scavenger (Na_2SO_3) and it was possible to measure the variation in fluorescence over the time. Tests with microorganisms were conducted, but the results were inconclusive due to issues related to the sensor's spatial resolution.

Keywords: Microfluidics, artificial blood, blood analogue fluid, red blood cells, oxygen sensor, Micro-rheometer, particulate fluid, perfluorodecalin.

Acknowledgment

First of all, I would like to thank to my supervisor, Prof. Dr. João Mário Miranda, for the help, the availability and the attention in this journey. All the hard work that he shown through the follow-up process of the investigation were vital to the final result of this investigation.

To Transport Phenomena Research Center (CEFT) and their researchers, Ana Cerdeira, Ana Moreira, João Carneiro, Violina Barbosa and others, thank you for the contributes for my investigation, for welcoming me in the laboratory and for helping me when I needed.

To Faculdade de Engenharia da Universidade do Porto (FEUP), I would like the opportunity of growing in the last 2 years, in the conclusion of a 5-year journey, that started at my 18 years in Escola Superior de Biotecnologia da Univerdade Católica Portuguesa. The constant challenges make me a better person and prepared me to the future. To my teachers, thank you for creating the better environment for developing my personal, academical and professional skills.

To my parents, family and friends, a big thank you for helping and the supporting me among this journey. Without you all, achieving this goal wouldn't be possible.

Finally, this work was financially supported by national funds through the FCT/MCTES (PIDDAC), under the project 2022.08598.PTDC. I would like to thank FCT/MCTES (PIDDAC) for the research scholarship under this project.

“Deus quer, o homem sonha, a obra nasce.”

Fernando Pessoa

Contents

Introduction 1

1.1. Current Situation 1

1.2. Objectives and Expected results 2

1.3. Dissertation Structure 2

Context and State of Art review 4

2.1. Blood and oxygen transport 4

2.1.1. Circulatory System 4

2.1.2. Blood composition and oxygen transport 6

2.2. Blood alternative fluids 8

2.2.1. Rheology 8

2.2.2. Rheological analogue fluids 10

2.2.3. Blood substitutes 11

2.3. Microfluidics and Emulsions 14

2.4. Vortex pre-emulsification and membrane emulsification 19

2.5. Oxygen measuring and control 20

2.5.1. Oxygen measuring 20

2.5.2. Oxygen control 22

2.6. Biofilms formation 24

Methods **26**

3.1. Particulate fluid production 26

3.2. Microfabrication 27

3.3. Oxygen Plasma Treatment 30

3.4. Particle and droplet characterization 30

3.5. Interfacial tension 33

3.6. Micro-Rheometer 35

3.6.1. Flow-focusing device 35

3.6.2. T-junction device 37

3.7. Oxygen optical tests 38

3.7.1. Development of the oxygen sensor device setup 38

3.7.2. Oxygen sensor implementation 40

3.7.3. Oxygen sensor tests 41

3.8. Test with microorganisms 43

Results and discussion **45**

4.1. Microchannels production 45

4.2. Particulate fluids 47

4.3. Micro-Rheometers 48

4.3.1. Flow-focusing device 48

4.3.2. Preliminary results from T-junction device 54

4.4. Oxygen sensor 55

4.5. Test with microorganisms 58

Conclusions **62**

5.1. Conclusions 62

5.2. Future works 63

References **66**

List of Figures

Figure 1: Circulatory system. 5

Figure 2: Heart anatomy, adapted from [10]. 5

Figure 3: Examples of different levels of oxygen A - Levels of oxygen in different tissues; B - Glossary to describe exposure different levels of oxygen. [23]. 7

Figure 4: Shear stress versus rate of shearing strain graphic [38]. 9

Figure 5: Schematic of an experimental setup to measuring PFL and DI [14]. 9

Figure 6: Schematic of an example to the steady-state and oscillatory shear rheology test [39]. 10

Figure 7: Oxygen solubility in PFCs and water [45]. 12

Figure 8: HBOCs solutions [17]. 12

Figure 9: $O2$ content (in mL/dL) variation according to the variation of the P$O2$ (mmHg) [48]. 13

Figure 10: Some of the most common types of designs: a) T-junction design; b) Flow-focusing design; c) Co-flow design; d) Droplet formation using capillaries [54]. 15

Figure 11: Schematic of the formation of droplets in multiphase fluids. 16

Figure 12: Example of a $O_1/W/O_2$ double emulsification process [67]. 16

Figure 13: Formation of perfluorocarbon-alginate microparticles schematic, adapted from [70]. 17

Figure 14: Schematic of the double emulsion process. 18

Figure 15: Schematic of double emulsion solutions. A – Double emulsion process in two channels. B - Double emulsion process in one channel. 19

Figure 16: Alginate droplets formed by premix emulsification membrane method, with 3 passages by the filter [13]. 20

Figure 17: Schematic of an oxygen sensor setup using PtOEP [24, 81]. 21

Figure 18: PtOEP sensor characterization from [80]. 22

Figure 19: Examples of experimental setups to oxygen level control [23]. 23

Figure 20: Biofilm formation [96]. 24

Figure 21: Schematic from the biofilm formation under flow [94]. 24

Figure 22: PFD particulate fluid method of production. A – Preparation of water solution with Tween 80 (1%) and PVA (3%) and the addition of PFD (10%). B – Membrane Emulsification process, executed 3 times, using a filter of 10 μm and a plastic syringe. 27

Figure 23: New T-junction channel drawing process (Inskape). 28

Figure 24: Paper molds production. 29

Figure 25: Plasma asher treatment example. 30

Figure 26: Experimental setup of visualization of the formation of droplets, using a microscope, a syringe pump and a High Speed Camera. A – Schematic version. B – Real experimental setup. 31

Figure 27: Image import process. 32

Figure 28: Example of the measuring procedure in Image J - 2.5x microscope objective. 33

Figure 29: Force tensiometer Sigma 701. 34

Figure 30: Schematic of the micro-rheometer trials - flow-focusing microchannels. 36

Figure 31: Schematic of the T-junction channel with 2 different flows (h as the thickness of the fluids). 37

Figure 32: Schematic of the implementation of a fluorescence oxygen sensor. 38

Figure 33: Spin-coater new program ("Cavidade" program). A – Step 1 (Acceleration); B – Step 2 (Rotation); C – Step 3 (Slowdown). 38

Figure 34: Glass slide with a rectangular piece of paper. 39

Figure 35: Implementation of the initial fluorescence substance without drying the substance. 39

Figure 36: Glass slides after 5 minutes drying in the oven (80º C). 40

Figure 37: Fluorescence sensor implementing the drying procedure. A – Microchannel device with fluorescence droplet dried. B – Microchannel device where the dried conditions were not enough to ensure that the fluorescence substance maintains in the first layer of PDMS 20:1. ...40

Figure 38: Oxygen sensor test experimental scheme. 42

Figure 39: Selected areas of oxygen sensor to the measures or intensity of fluorescence (Image J). A – Agglomerate zone. B – Normal zone. 42

Figure 40: Microorganism test setup. 43

Figure 41: Microchannel molds (T-junction and Flow-focusing). 45

Figure 42: Example of microchannels procuded by soft litography (Flow-focusing design). ...46

Figure 43: T-junction microchannel with imperfections. 46

Figure 44: Particulate fluids images (20x objective). A – PFD (10%) particulate fluid without PEG; B – PFD (10%) particulate fluid with PEG (1%). C – PFD (10%) particulate fluid with PVA (3%). Scale bar: 100 μm. 47

Figure 45: Example of the measuring of the width of the microchannel in Image J - 2.5x Microscope Objective. 48

Figure 46: Length of the droplet's variation through the variation of oil flow to a flow of water (of 25 µL /min. 49

Figure 47: Droplet formation. A – Water + Glycerol (40%) flow: 10 µLmin; B – Water + Glycerol flow: 15 µLmin; C – Water + Glycerol flow: 20 µLmin; D – Water + Glycerol flow: 25 µLmin. Variable flow of oil (continuous phase) for a fixed value of dispersed phase. 2.5x microscope objective used. 50

Figure 48: Speed of the droplet's variation through the variation of oil flow to a flow of water + glycerol (40%) of 20 µL /min. 51

Figure 49: Ca x *L/W* graphic – Micro-rheometer. 52

Figure 50: Ratio Micro-rheometer with the standard curves and estimations for alginate particulate fluid [13] and PFD (10%) particulate fluid. Ratio 3 standard curve is represented by blue dashed line and Ratio 5 standard curve is represented by gray dashed line. 53

Figure 51: T-junction micro-rheometer trial example. $Qoil = QPF = 10\ \mu L$/min. 54

Figure 52: Oxygen sensor implementation - glass slide with PtOEP encapsulated. 55

Figure 53: Images of the sensor fluorescence variation with the decrease of the oxygen level. 56

Figure 54: Fluorescence variation according to the time of the trial. Blue dots – Agglomerate zone (Figure 39 A); Orange dots – Normal zone (Figure 39 B). 57

Figure 55: Oxygen sensor detection of fluorescence in a limit zone. A – Fluorescence light on; B – Image without fluorescence. 58

Figure 56: Recorded images from the microorganism's trials. A - *Saccharomyces cerevisiae* suspension; B – Scavenger ($Na2SO3$ + water); C – Water; D – Diluted scavenger (5:1); E – Diluted Scavenger (10:1); F – PFD particulate fluid + diluted scavenger (5:1). 59

List of Tables

Table 1: Blood composition and characteristics, adapted from [8].....6

Table 2: Water and some PFCs oxygen solubility [45]. 11

Table 3: Composition from particulate fluids produced by membrane emulsification filter. 3 passages in a 10 μm filter applied in all the fluids.....27

Table 4: High Speed Camera calibration values. 32

Table 5: Interfacial tension values. 34

Table 6: Glycerol properties at 293K. 36

Table 7: Fixed values of dispersed phase flow used in the trials. 49

Table 8: PFD (10%) particulate fluid results. 53

Table 9: T-junction micro-rheometer results with PFD (10%) particulate fluid and oil. $Q1/Q2 = 1$.....54

Table 10: Mean Gray Value from Figure 57 images 59

Abbreviations, Acronyms and Symbols

A – Interfacial area

Ca – Capillarity number

CEFT – Transport Phenomena Research Center

CFL – Cell-Free Layer

$C_{28}H_{31}CIN_2O_3$ – Rhodamine B

COC – Cyclic olefin copolymer

CO_2 – Carbon Dioxide

CVC – Central venous catheter

DI – Deformability index

h – thickness

Hb – Hemoglobin

HBOC – Hemoglobin-based oxygen carriers

I – Fluorescence intensity in the presence of oxygen

I_0 – Fluorescence intensity in the absence of oxygen

K_{sv} – Stern-Volmer constant

L/W – Normalized droplet length

Na_2SO_3 – Sodium Sulfite

O_1/W/O_2 – oil-in-water-in-oil

O_2 – Oxygen

PC – Polycarbonate

PO_2 – Oxygen partial pressure

PDMS – Polydimethylsiloxane

PFC – Perfluorocarbon

PFD – Perfluorodecalin

PFL – Particle-free layer

PFOC – Perfluorocarbon-based oxygen carriers

PEG – Poly(ethylene glycol)

PMMA – Polymethylmethacrylate

PS – Polystyrene

PtOEP – Platinium (II) octaethylporphyrin

PVA – Polyvinyl alcohol

Q_c – Continuous phase flow

Q_d – Dispersed phase flow

RBC – Red Blood Cell

T – Temperature

$v_{droplet}$ – speed of the droplet

v_{fluid} – speed of the fluid

WBCs – White Blood Cells

W1/O/W2 – water-in-oil-in-water

μ – Viscosity

γ – Interfacial tension

ΔG – Cost of energy (Gibbs-enthalpy)

ΔS – Gain of disorder (entropy)

Chapter 1

Introduction

1.1. Current Situation

Central venous catheters (CVCs) and other types of catheters are used in 75% of the patients in a critical state in the intensive healthcare units [1]. CVCs can be used in a large set of applications, such as drugs or vasopressors administration, frequent blood sampling or parenteral nutrition [2]. The use of this device is important to improve the management of intensive health care patients, but complications associated with this process can emerge [2]. It is also relevant to consider that the number of infections resulting from the use of CVCs is increasing [3].

The use of CVCs is often associated to patients who need a long-term solution to access the central venous system and this situation causes a long time of contact between the device and the bloodstream, which can origin infections [4]. This situation can result in the administration of intravenous antibiotics or the early removal of the CVC [4]. Also, the patient can suffer severe sepsis [4], which ultimately can cause the patient's death.

Bacterial infections in intravenous devices, such as CVCs, are consequence of the formation of biofilms in this type of devices [5]. The formation of biofilms is the result of the adhesion of the bacterias and the following growth and proliferation, which is improved by the components of the human blood [5]. There are many approaches to prevent CVC infections, but the use of more rigid procedures in hygiene control and the development of new designs and materials to prevent cell adhesion and growing of bacterial biofilms are the most relevant ones [6]. These new designs and materials are subject to a long procedure of tests to evaluate their effectiveness, starting with *in vitro* tests. In this work, it is analysed if a blood analogue fluid with the capacity to transport oxygen can be useful to substitute blood in this type of testing and the path to achieve that fluid.

1.2. Objectives and Expected results

The main goal of this master's dissertation, that was inserted in "Multiblood" project (2022.08598.PTDC), was to assess the capacity of a particulate fluid as a blood substitute in the development of medical devices, such as CVCs, especially in the study of new solutions for the design of the device and for coatings (use of anti-fouling surfaces), to decrease the number of infections due to the use of medical devices. Considering this, one of the most important topics of this investigation is to understand how a blood analogue fluid, with particles that replicate the function of RBCs, affects the oxygenation of biofilms that are formed on the surface of a catheter.

Transport Phenomena Research Center (CEFT) usually works with fluids that have rheological properties similar to the original fluid. In a blood analogue fluid, the mechanical properties should be similar to blood and they can be used in trials that don't depend on the functionality of the fluid. However, in tests with microorganisms, the function of oxygen transport is required. Considering the need to add the capacity of transporting oxygen to study the biofilms growing on a surface, one of the targets was to study particulate fluids with the capacity to transport oxygen. This is particularly relevant because this type of test needs to have real conditions, so it is necessary to replicate the values of concentration of oxygen that are observed in the tissues and cells. Considering that the measuring and control of the levels of oxygen are key to the development of a blood substitute, one of the other main goals was to study and develop a fluorescence oxygen sensor with capacity of detection variations of the levels of oxygen and to fluoresce in low levels of oxygen. Other objective was to create new alternatives to measure the viscosity of particulate fluids, due to the small amount of analogue fluid that is available for tests. of the small samples available could not be enough to test in conventional methods.

This master dissertation work was expected to: i) develop a particulate fluid, with the help of microfluidics methodologies, such as membrane emulsification or droplet microfluidics; ii) to use microfabrication techniques to develop an oxygen sensor device that is capable of presenting fluorescence in the absence of oxygen and iii) to study and develop successfully an alternative methodology to determine the viscosity of a fluid.

1.3. Dissertation Structure

This dissertation includes 5 chapters and the references. The first chapter is the Introduction (the one where this section is included) and describes the current situation that validates the importance of this study, the objectives of this investigation and the timeline that was followed to achieve the goals that were proposed. In the second chapter, the most recent developments in the field and the characterization of key concepts were made. After characterizing the State of the Art, the methodologies related to the study are described in Chapter 3. In addition, Chapter 4 presents the results obtained in the investigation and the reflection that was made. Chapter 5 summarizes the conclusions and future works.

Chapter 2

Context and State of Art review

2.1. Blood and oxygen transport

Blood is vital to the function of the cells and organs [7]. The constitution of blood is particularly important to explain the functionality of the human body. Blood has a key role in the exchanges of gases (oxygen and carbon dioxide) and nutrients, but also as impact in the immunological and temperature regulation and coagulation, among other functions [8]. Considering this, the circulatory system is one of the most important ones in the normal function of the human body.

2.1.1. Circulatory System

Circulatory system is the responsible for the blood circulation, allowing the fluid to reach all body parts. Considering this, the circulatory system is a key part in the normal functionality of the organism, enabling that blood circulates correctly in the body. According to this, circulatory system (Figure 1) is a complex bionetwork of blood vessels (arteries, veins and capillaries) that transport blood through the body [9]. Heart (Figure 2) is the pump that makes blood circulate through the organism. In fact, heart is a muscular organ located in the left side of the chest (anatomic view), above the diaphragm [10, 11]. This organ is divided in four parts (Figure 2), two atria (right and left) and two ventricles (right and left), and the wall is constituted by three parts: epicardium, myocardium and endocardium [10, 12].

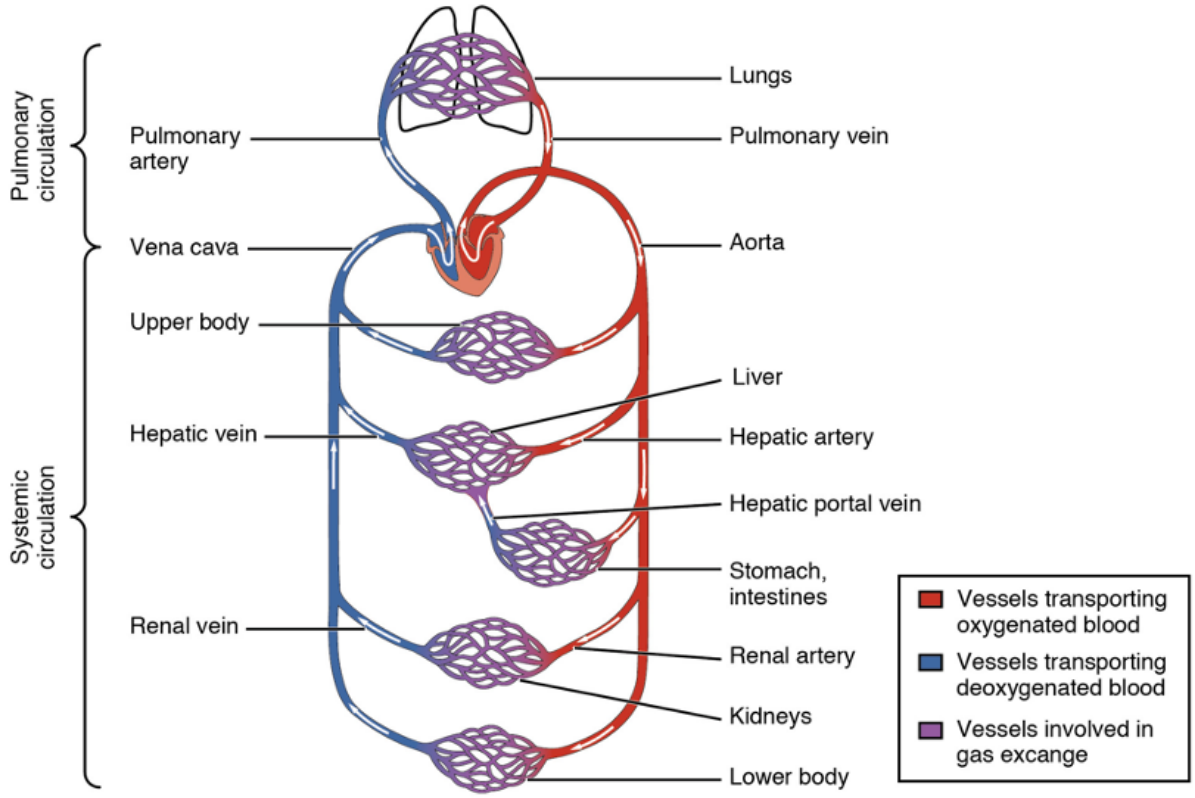


Figure 1: Circulatory system.

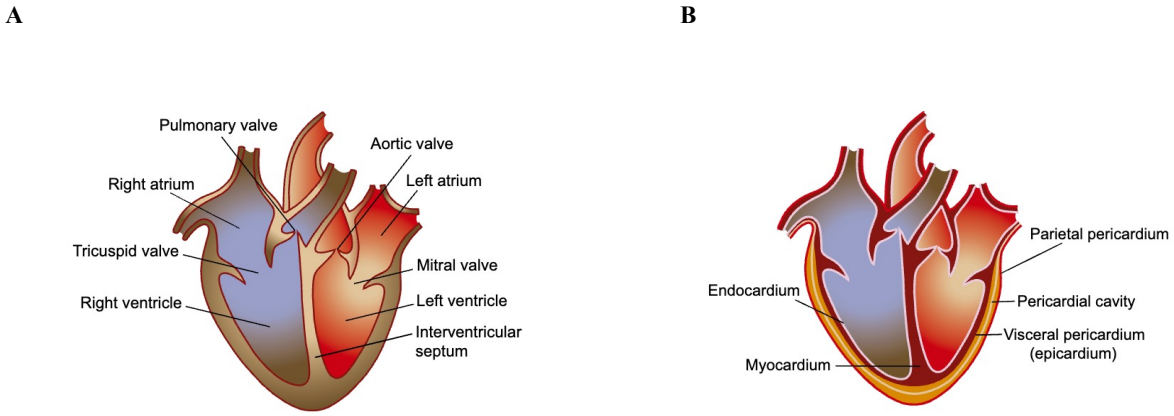


Figure 2: Heart anatomy, adapted from [10].

As presented in Figure 1, the circulation of the blood can be divided in two types: Systemic and Pulmonary. In Systemic circulation, the blood is transported from the heart through aorta and the following arteries until reaching the capillary level, where the exchanges are executed. Through the following path from the vessels, from arteries to capillaries, the dimensions of the vessels decrease to promote the exchanges of oxygen and carbon dioxide at the capillary level.

The dimensions of the capillaries (diameter bellow the 300 μm) are responsible for a phenomenon called Cell-Free Layer (CFL) [13, 14]. After the exchanges, blood returns to the heart through veins, finishing the systemic circulation. The Pulmonary circulation is the one responsible for the oxygenation of blood, the release of CO_2 from the system and the supplying of blood with O_2.

2.1.2. Blood composition and oxygen transport

Blood is complex biofluid constituted by red blood cells (RBCs), white cells and platelets suspended in plasma [8, 13, 14] (Table 1). Blood is a particulate fluid with a critical importance in the correct function of the organism. Considering the values of composition of blood, RBCs represent around 45% of the volume of blood [15] and are the most plentiful type of cells in the bloodstream [16]. In fact, the rheological behaviour of blood is ultimately affected by RBC cells [14].

Table 1: Blood composition and characteristics [8].

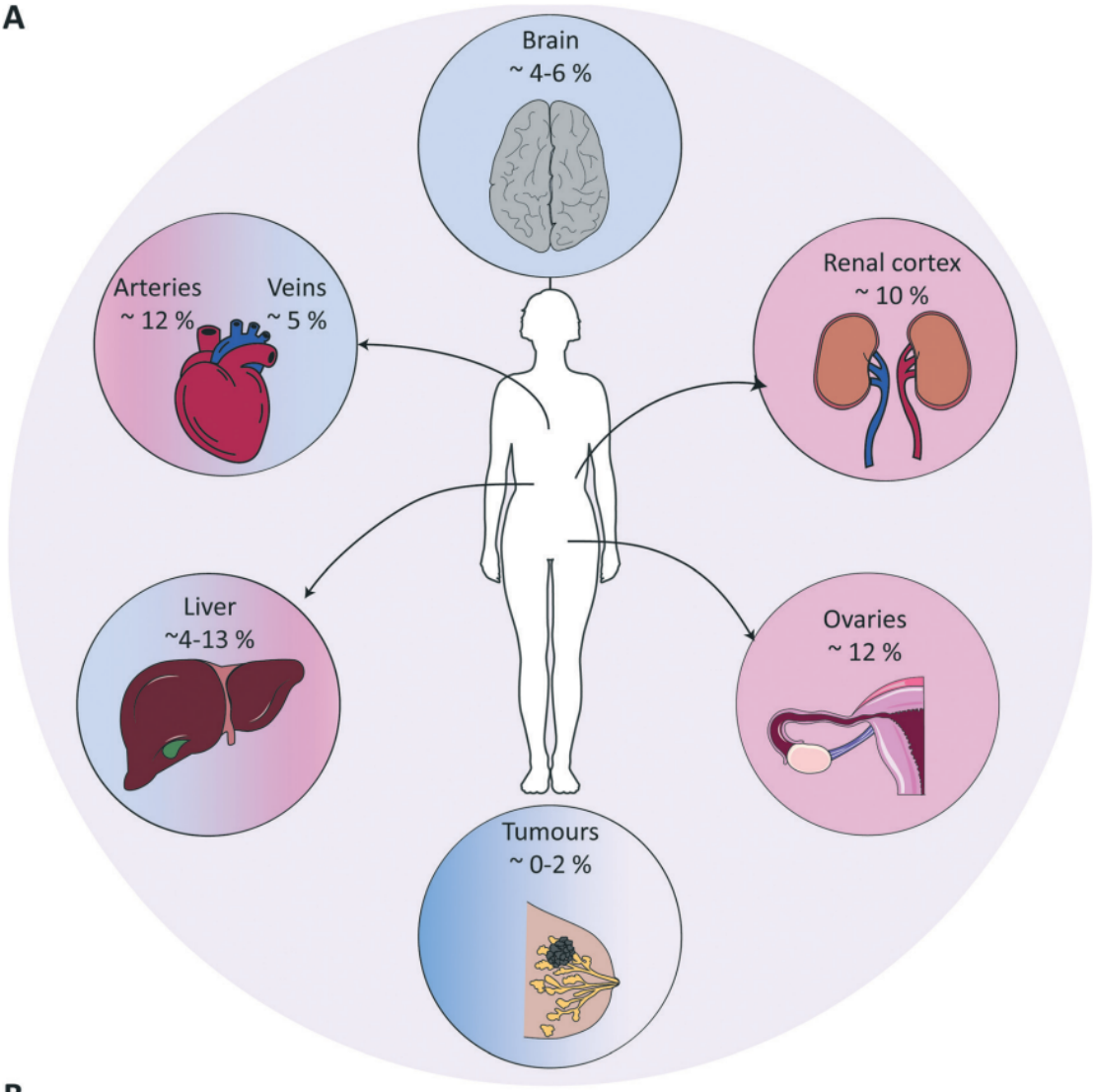
	Whole blood (%)	Diameter (μm)	Shape	Density (Kg m^{-3})	Viscosity (mPa.s)
RBCs	~ 45 %	~ 8	Biconcave disk	~ 1100	6 - 7
WBCs	~ 1 %	6 - 20	Spherical	~ 1090	-
Platelets	~ 1 %	~ 2	Oval discoid	~ 1060	-
Plasma	~ 55 %	-	Liquid	~ 1050	1.10 - 1.35 (37 °C)
Whole blood	-	-	Liquid	~ 1055	4 – 5 (37 °C)

According to Table 1, RBCs present a diameter of approximately 8 μm and a high viscosity value (6-7 mPa.s) [8]. RBCs are cells with a biconcave discoidal shape and present Hemoglobin in their constitution [15]. These cells are one of the components of blood that makes it such an important biofluid, as explored previously. In fact, RBCs are responsible for key exchanges in the body, like the supply of oxygen and the removal of carbon dioxide [16]. The main function of this type of cell is to carry oxygen from the lungs, where the concentration is high to the tissues and cells where the concentration is low [17].

RBCs present a tendency to deform and cell deformability is a significant factor that affects the viscosity of a biofluid like blood at a microscale [8, 18]. The aggregation, disaggregation and deformation of RBCs explain the non-Newtonian shear-thinning behaviour of blood [14]. In other words, when RBCs are exposed to low shear rates they aggregate and adopt a coin structure and in opposite conditions, this process is reversed [14]. Considering this, the non-Newtonian behavior of blood is ultimately a consequence of the high presence of RBCs in is constitution [8, 19]. Also, the properties of RBCs are responsible for viscoelastic characteristics of blood [20-22].

The transport of oxygen is, as presented before, critical for the viability of the tissues and cells. However, the levels of oxygen are not the same in the different tissues (Figure 3).

A



B

Anoxia	Exposure to extremely low levels of oxygen (< 0.02%), which often leads to necrosis
Hypoxia	Exposure to low levels of oxygen that activate adaptive responses of the cells or tissues. Depending on the tissue, this usually occurs below 3-5% oxygen
Physioxia	Exposure to normal levels of oxygen as happens inside the body, ranging from ~4-12% depending on the tissue
Normoxia	Exposure to atmospheric levels of oxygen (~20%). This is often hyperoxic for tissues in *in vitro* conditions
Hyperoxia	Exposure of cells and tissues to oxygen levels that are supraphysiological

Figure 3: Examples of different levels of oxygen A - Levels of oxygen in different tissues; B - Glossary to describe exposure different levels of oxygen. [23].

Considering the data from Figure 3, the percentage of oxygen in the troposphere (20.9%) decreases until approximately 12% in arterial blood and the value is even lower in venous blood,

as a consequence of the body consumption [23], and in cells, where oxygen is used to cellular respiration [24]. Also, it is possible to categorize the levels of oxygen in different tissues, using the categories presented in Figure 3B. For instance, hypoxia environments are commonly used to study the behavior of cells and it is relevant to consider that cancer cells proliferate in low oxygen conditions [23, 25-27].

2.2. Blood alternative fluids

As previously explored, blood is a key component for the correct function of the body, in particular, because of the transport of oxygen capacity. According to data from WHO from 2018, is estimated that 118 million donations were made worldwide (171 countries) [28]. However, blood transfusions are common procedures in the hospital environment and the availability of blood is insufficient [29, 30]. Also, in critical medical situations, blood transfusions have to be ensured to maintain the life of the patient, but the needs overpasses the offer [31]. Considering this, blood losses or treatments from diseases that affect directly blood, like diabetes or anaemia, need the availability of blood to transfusions or blood supplements [13]. Laboratory tests can represent an important loss of blood samples, ethical and economical challenges emerge and a storage is demanding [13, 15, 32, 33].

Blood transfusions are the only possibility to obtain blood, but complications are related to this procedure, like immunological and non-immunological side effects [31]. Also, some patients refuse blood transfusions due to religious beliefs [31, 34]. Considering this, blood alternative fluids are an important solution due to face challenges in the present and in the future. The most common currents of blood alternative fluids are the rheological analogue fluids and blood substitutes.

2.2.1. Rheology

Rheology is the area that studies characteristics like deformation and flow in matter, particularly, in fluids [35, 36]. Rheology has the objective of characterize the behavior of a fluid in a particular small set of flows [8]. Also, in rheological terms, fluids can be characterized in the dependence of time (time independent and time-dependent) and blood is time independent, both for *in vitro* and *in vivo* scenarios [8, 37, 38].

The rheological behavior of fluids can be categorized and Newtonian fluids and non-Newtonian fluids are the major groups. Newtonian fluids are the ones that present a linear relation between the shear rate and the rate of shearing strain [38]. Non-Newtonian fluids are the ones where this correlation doesn’t exit and can be classified by several ways, like it is presented in Figure 4. Considering that, blood is characterized as a Shear-Thinning fluid, ultimately because of the elevate presence of RBCs.

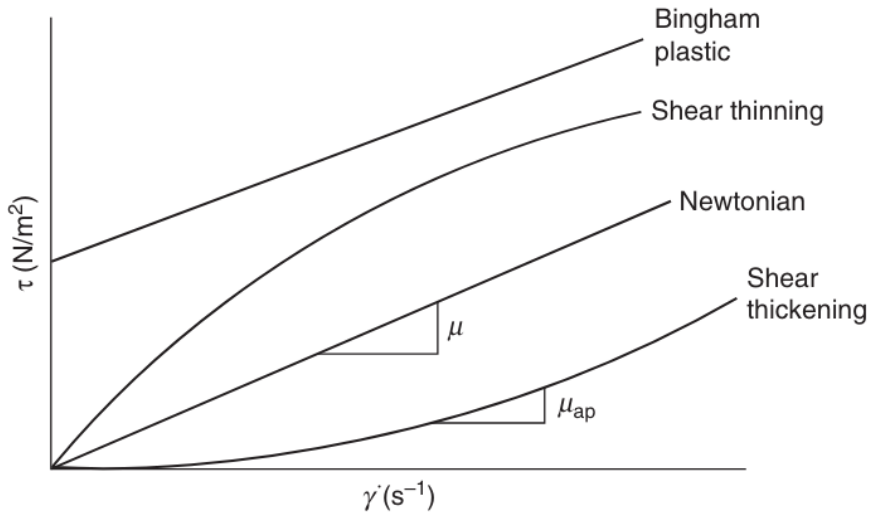


Figure 4: Shear stress versus rate of shearing strain graphic [38].

Particle-free layer (PFL) and deformability index (DI) are relevant parameters to characterize the particles. According to Carneiro, Lima [14], the measurement of this parameters can be performed using an experimental setup similar to the one represented in Figure 5. PFL and DI are performed by capturing the images using the High Speed Camera and the software "Image J" is used to do the analysis. To calculate PFL, the command "Z project function" is used in "Image J" [14]. DI is calculated by the equation (1) [14]:

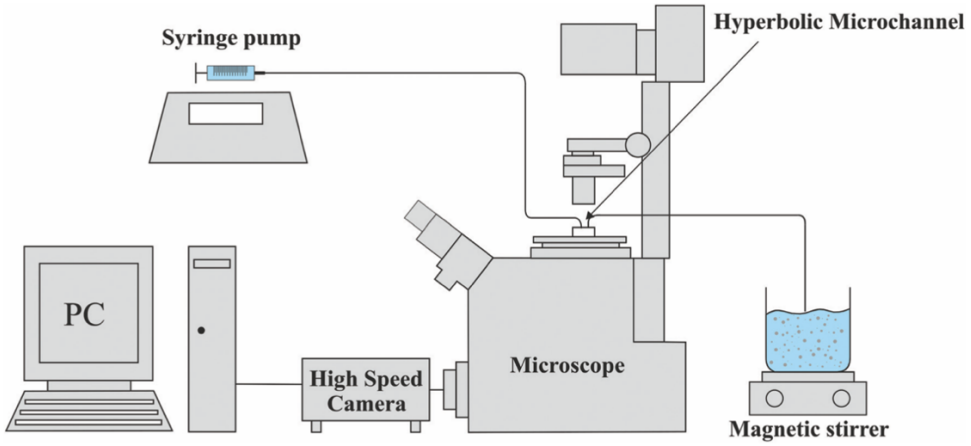
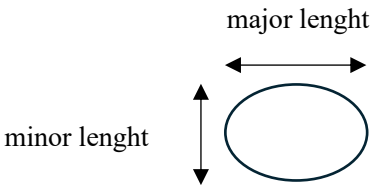


Figure 5: Schematic of an experimental setup to measuring PFL and DI [14].

$$DI = \frac{(major\ lenght - minor\ lenght)}{(major\ lenght + minor\ lenght)} \quad (1)$$



To characterize the steady-state and oscillatory shear rheology of a blood analogue fluid Sousa, Carneiro [39] protocol can be used [14, 40]. The protocol was developed to the study of all blood [39]. A rotational rheometer (Physica MCR301, Anton Paar) and a peltier temperature control system are used [14, 39, 40]. Figure 6 presents the schematic used in the original protocol.

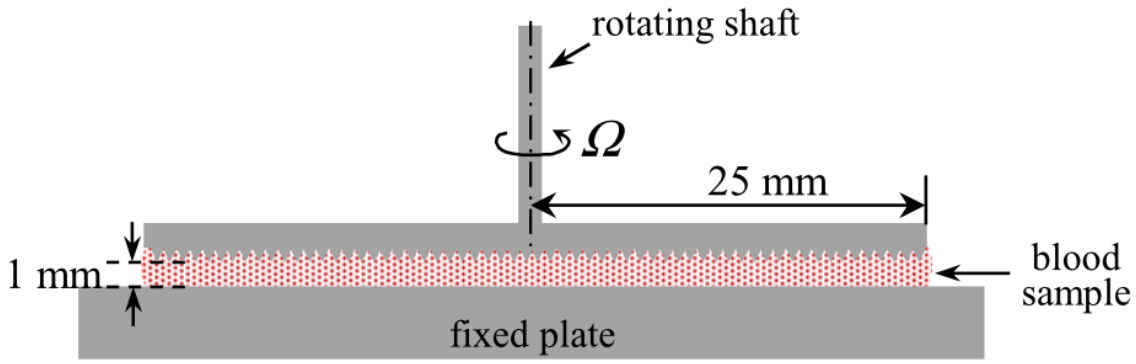


Figure 6: Schematic of an example to the steady-state and oscillatory shear rheology test [39].

2.2.2. Rheological analogue fluids

Blood flow has been studied using numerical simulations and *in vivo* tests, but *in vitro* solutions are a relevant one [7]. To perform *in vitro* tests, the analogue fluid that is used must present similar properties to real blood [7]. In the case of *in vitro* tests, the use of human blood is associated with several operational problems like coagulation, the storage of the sample or the cleaning of the microdevice [15]. Besides that, as explored previously, ethical and economic issues are some of the challenges associated with the use of blood in this type of study [15].

Rheological blood analogue fluids are fluids that present mechanical properties similar to blood mechanical properties. The complexity of a biofluid such as blood, which contains microparticles like RBCs, nutrients and compounds, is an important factor in the task of creating an analogue fluid [7]. Newtonian fluids (water/glycerol and water/dimethyl sulfoxide) and non-Newtonian fluids (water and/or glycerol with additives like xanthan gum, sodium iodide and urea) were explored as blood analogue fluids [15]. On one hand, Newtonian blood analogue fluids are the most simple ones and were used in a large set of applications in microfluidics [15]. On the other hand, non-Newtonian blood analogue fluids present a more realistic performance in the task of replicating real blood [41]. Although, these analogue homogenous fluids cannot mimic blood microstructure, the rheological behavior is similar at the macroscale, but at the microscale, the fluids were not capable of simulating blood [14, 42]. The low price, the easiness in preparation and cleaning and the similarity in the viscosity when compared to blood justify the use of these analogue fluids in experimental fluid dynamics studies [42].

In recent years, multiphase fluids have emerged as a solution to overcome the challenge of replicating blood microstructure. Multiphase fluids are composed by at least two immiscible phases, where it is present a continuous phase and a dispersed phase [14, 15]. Multiphase blood analogue fluids must present particles in a similar volume to RBCs in blood (around 45%) and

the particles must present likeness to RBCs in key characteristics, such as size, mechanical properties and shape [15]. To mimic blood in intravascular device tests, blood analogue fluid must present similar characteristics to the original fluid. Considering this, a blood analogue fluid should match blood in properties like shear rheology, viscoelasticity and particles characteristics (similar dimensions and properties to RBCs).

2.2.3. Blood substitutes

The name blood substitute suggests that this type of fluid is capable of substituting blood in a full way [43]. However, blood substitutes are usually fluids that can replicate one characteristic of the original fluid, such as the capacity to transport oxygen [43]. Considering this, blood substitutes are different from blood analogue fluids, that usually are not capable of transporting oxygen. Rheological properties are not enough to ensure that artificial blood has the same behavior as real blood at a microscale [15] and this explains the search for a fluid with the capacity to replicate blood functions like oxygen transport.

Blood substitutes based on the function of mimicking the supply of oxygen are divided into perfluorocarbon-based blood substitutes and hemoglobin-based blood substitutes [43, 44]. Considering this, Perfluorocarbons (PFCs) and Hemoglobin (Hb), which is present in the natural red blood cells, are important RBC substitutes, which present similar functional properties like the capacity to carry oxygen [17]. RBC substitutes present relevant advantages when compared to RBCs like the possibility of being sterilized (pasteurization and ultrafiltration can be used to reduce the biological risk of infection) and the fact of not presenting blood group antigens, which could be a relevant characteristic for the use of blood substitute in emergencies [17]. However, commonly blood substitutes don't present the same rheological properties as real blood. So, it is a critical challenge to have a functional and effective substitute to be used in a large set of applications.

PFCs are synthetic hydrocarbons that present fluorine atoms in substitution of hydrogen atoms [43, 45]. The presence of fluorine atoms in PFCs is important to the chemical properties of this type of particle, especially to the solubility of oxygen, which in PFCs is much higher than in water (Figure 7 and Table 2), fluid that is present in human blood plasma [45].

Table 2: Water and some PFCs oxygen solubility [45].

	Water	Perfluorodecalin (PFD)	Perfluorooctylbromide (PFOB)	Dodecafluoropentane (DDFP)
Formula	H_2O	$C_{10}F_{18}$	C_8BrF_{17}	C_5F_{12}
Molar mass	18 g/mol	462 g/mol	499 g/mol	288 g/mol
Density	0.997 g/cm^3	1.946 g/cm^3	1.89 g/cm^3	1.63 g/cm^3 (liquid, 25 °C), 0.012 g/cm^3 (gas, 37 °C)
Molar density	55.4 mol/L	4.2 mol/L	3.8 mol/L	0.04166 mol/L (gas, 37 °C)
Oxygen solubility (25 °C)	6.3 mL_{O2}/L_{H2O}	403 mL_{O2}/L_{PFD}	527 mL_{O2}/L_{PFOB}	29,421 mL_{O2}/L_{DDFP} (gas, 37 °C)
Molar oxygen solubility	0.11 mL_{O2}/mol_{H2O}	95.68 mL_{O2}/mol_{PFD}	139.14 mL_{O2}/mol_{PFOB}	7.06*10^5 mL/mol_{DDFP} (gas, 37 °C)
Molar ratio (oxygen/solute)	0.005 mol_{O2}/mol_{H2O}	4.27 mol_{O2}/mol_{PFD}	6.21 mol_{O2}/mol_{PFOB}	31.52 mol_{O2}/mol_{DDFP} (gas, 37 °C)

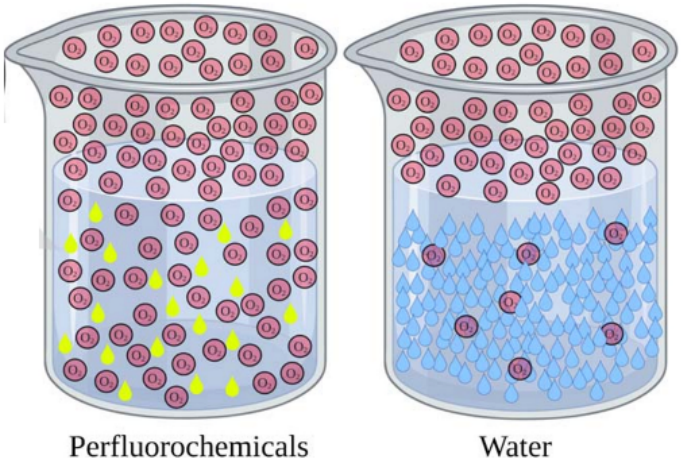


Figure 7: Oxygen solubility in PFCs and water [45].

The beginning of the study of PFCs as O_2 carriers goes back to 1966, when a famous experience was made [45, 46]. In fact, the experience of Leland C. Clark and Frank Gollan consisted in diving a mouse in a PFC, Fuorobutyltetrahydrofuran (FX-80). This trial was a huge breakthrough, as described by Jägers, Wrobeln [45], considering that in two different setups, the mice was capable of surviving for hours, situation that is impossible in a aqueous medium. Historically, PFCs are commonly used in several areas like the industrial and the medical ones [31, 47].

Hemoglobin-based blood substitutes use Hb, which is present in RBCs as an oxygen carrier, replicating its natural function. Hb is a protein with a globular structure, with two α and two β polypeptide subunits and each one of them contains a heme group, which is a porphyrin ring with Fe^{2+} in the centre [17, 43]. Each heme group can link to an oxygen molecule, so one Hb can carry four oxygen molecules [17]. However, Hb cannot be used in a blood substitute in its natural form, because of the limited time that is viable in circulation, which is approximately 6 hours, and for the toxins that are released in the dissociation of the structure of this protein [17].

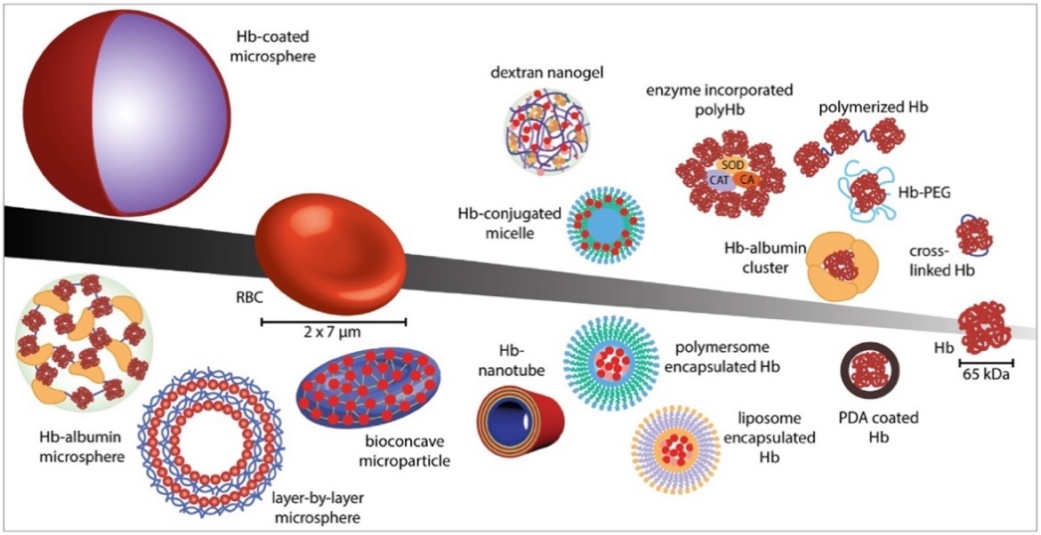


Figure 8: HBOCs solutions [17].

HBOCs can be divided into 3 different generations (Figure 8). The first and the second generation of hemoglobin-based oxygen carriers were focused on the chemical changes of Hb [17, 43]. However, the approach of the third generation of HBOCs consists in the encapsulation of Hb on a synthetic membrane [17].

Hb encapsulation appears because in blood substitutes this protein doesn't have the natural protection that the RBC membrane confers to them in real blood [17]. Encapsulation has several advantages like preventing the early removal from the system or the reduction of the viscosity, which is high, protecting the tissues and blood components [17].

As explored, the solubility of O_2 in PFCs is higher than in water. Also, this solubility can be compared to the blood and other fluids. Figure 9 presents the total content of oxygen in Blood (Hb = 140 g/L), in HBOC (70 g/L), in Perflubron (90%) and in Fluosol (20%).

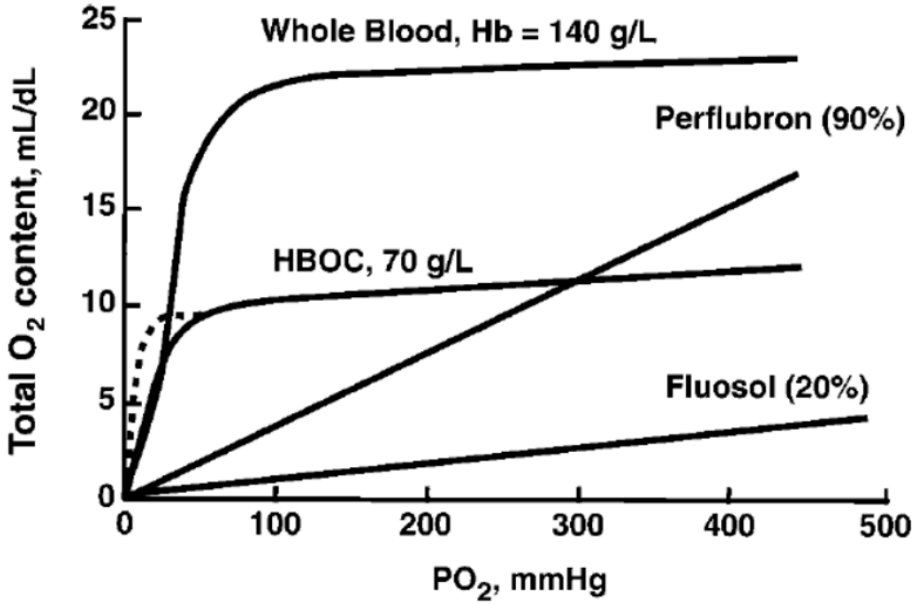


Figure 9: O_2 content (in mL/dL) variation according to the variation of the PO_2 (mmHg) [48].

Considering that HBOC uses similar oxygen transporter from the real Blood, the behavior of the curve is approximately the same, but the HBOC is not capable of reach the values of total O_2 (saturation around 10 mL/dL and the saturation of blood is higher than 20 mL/dL, less than half of the capacity of transporting of O_2). In this case, PFCs present a disadvantage that is the most significant one. In fact, as presented in Figure 9, PFOC are capable of reaching high values of total content of oxygen (higher than 15 mL/dL for the case of Perflubron), but present a linear behavior, so it is necessary a higher PO_2 value to reach the maximum capacity of storing oxygen [45, 48].

There were some attempts of replicate a fluid with the capacity of substitute blood. For instance, a blood substitute was tested in a robotic interrogator, with the target of testing if the fluid was capable maintaining the function of vascularized organs [13, 49]. The ideal blood substitute was not achieved and is challenging to meet all requirements to reach that goal. The

ideal blood substitute fluid needs to conciliate the function primary paper of the blood, but also the rheology properties of the fluid (approximation to the blood analogue fluids) [13]. Considering this, the ideal fluid would present the capacity of transporting O_2, similar rheological properties when compared to blood (shear-thinning behavior), a large number of particles with similar properties of RBCs (shape, size and other characteristics), matching the high percentage of RBCs in real blood and a similar behavior in microcirculation (capillarity level of circulation). [13, 15, 33, 50, 51]. Although, it is important to consider that even an "ideal fluid" would face challenges like the lack of capacity to transport CO_2, to interact with organs and the lack of immunological properties (conferred by WBCs).

2.3. Microfluidics and Emulsions

The study of fluids that are analogue to blood, in other words, that mimic the behaviour of the original fluid, is growing. According to Lima, Vega [7], in the 20 years that precede their study, several attempts were made to develop solutions to have a blood analogue fluid with the capacity to mimic multiphase effects that are observed in real blood. To achieve this goal, microfluidic techniques are an important solution.

Microfluidics offers the possibility of working with devices that use smaller volumes of reagent, present shorter reaction times and precision in the control of physical and chemical properties, due to the large surface area and the capacity of transferring high mass that these type of devices offer [52, 53]. Also, this type of technique allows the execution of experiments that are not possible or viable at a macroscale [52]. Currently, microfluidic techniques have a large set of applications in the biomedical field. Cell encapsulation, drug delivery or diagnosis are some of the areas where microparticles can be used [54]. Considering this, microfluidics can be used as an organ-on-chip systems [55].

Droplet microfluidics is a technique for the production of microparticles and is a key solution in the microbiology field [56]. In fact, this technique is capable of performing the production at a microscale [57, 58] and even at a nanoscale [58]. To be able to form droplets using this technique, it is necessary to have a microchannel. This technique can produce uniform droplets with a very small size range, in the scale of micrometres and nanometres [58]. Microfluidics approaches provide a great capacity of control over the dimension of particles that are formed [59]. This type of technique is increasingly related to the microbiology area. In fact, the study of microbiology using droplet microfluidics opens new possibilities, such as the testing of antibiotic susceptibility or the detection and identification of pathogens [56, 60]. Microfluidics has a significant number of advantages in the study of microbiology when compared to the traditional methods (for instance, the use of Petri dishes or the use of macroscale bioreactors), like the use of a very small amount of volume or the possibility of work with a large set of droplets [56].

The definition of the design and the type of mold to use, such as the method of production is critical. After that, microfabrication technique is applied to have microchannels. Considering this, the design (Figure 10) and fabrication of molds that are used are important to microfluidics approaches. As explored by Moreira, Carneiro [54], characteristics like the design of the channels and the materials that are used will affect the production rate, the size and shape of the droplets that are formed.

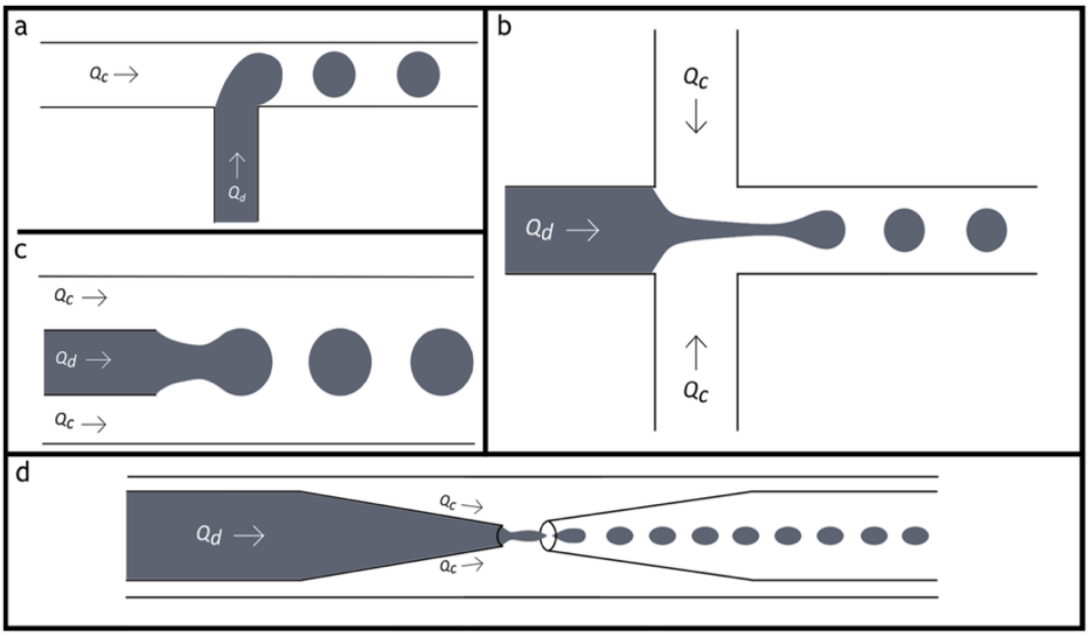


Figure 10: Some of the most common types of designs: a) T-junction design; b) Flow-focusing design; c) Co-flow design; d) Droplet formation using capillaries [54].

The emergence of multiphase fluids as a solution in the production of rheological analogue fluids (section 2.2.2) and the use of encapsulation as a solution to PFCs and Hb as a RBCS (section 2.2.3) were important breakthroughs in the biomedical field search for solutions to mimic blood. Considering this, it is necessary to have particles or encapsulated particles with properties similar to RBCs properties [15, 17]. For these, emulsification in microfluidic devices is critical.

Emulsification (Figure 11) is the process of dispersion of one fluid into another, when two or more immiscible fluids are mixed or get in touch [45, 61]. This process is largely used in several fields and is a relevant process in microscale experiments [61]. According to Tadros, Izquierdo [62], emulsification needs water, oil, surfactants and energy, because the emulsion formation is a non-spontaneous process. Also, is it considered by the authors that the emulsion of large droplets are easier and less demanding than the formation of small droplets (nanoscale), that need more energy or/and surfactants [62]. The formation of the droplets due to emulsification processes is a thermodynamic process described by an alternative version of the Gibbs-Helmholtz-Equation [45, 63]:

$$\Delta G = (\gamma A) - (\Delta S \times T) \quad (2)$$

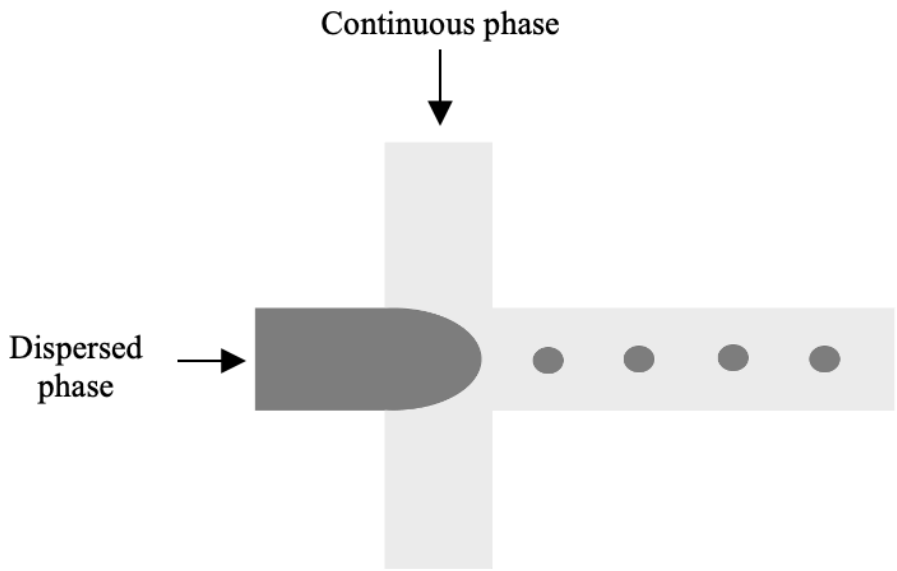


Figure 11: Schematic of the formation of droplets in multiphase fluids.

The use of emulsification in microfluidics and the need to have encapsulated particles led the study of this phenomenon to a relevant point. Double emulsification appeared in several works as an important and largely used solution [64]. Some of the most recent microfluidics research works are focused on double emulsion techniques, in particular to have the capacity to encapsulate particles that need to be protected to function, like Hb as a (3rd generation) HBOCs. Furthermore, emulsification offers other advantages, such as low energy cost or easy application [65].

The development of emulsification techniques leads to the growing of double emulsion approaches, that can be categorized in two different types: water-in-oil-in-water ($W_1/O/W_2$) emulsions and oil-in-water-in-oil ($O_1/W/O_2$) emulsions [65, 66]. An $O_1/W/O_2$ double emulsification process (Figure 12) was explored in the encapsulation of β-carotene in calcium alginate hydrogels [67].

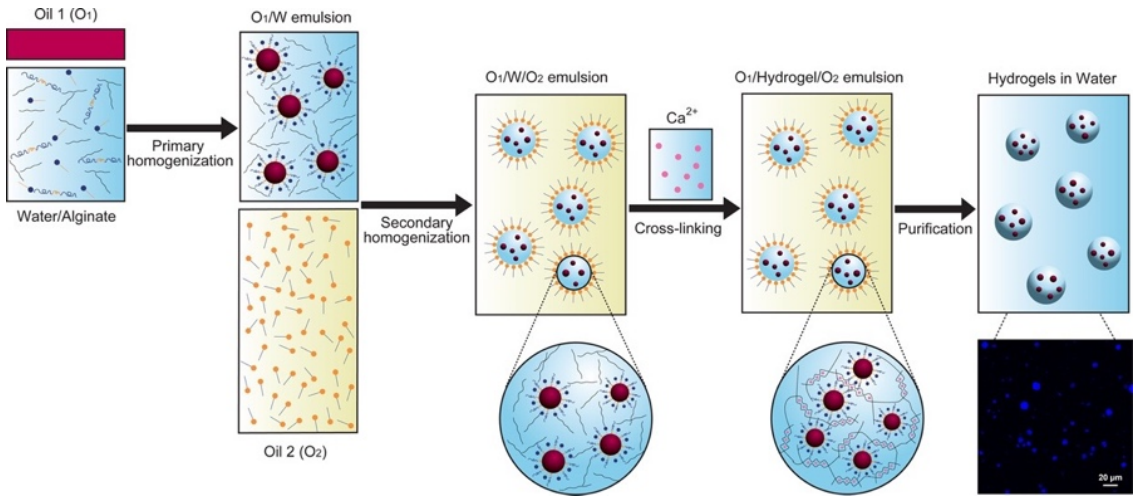


Figure 12: Example of a $O_1/W/O_2$ double emulsification process [67].

Double emulsion to encapsulate perfluorodecalin (PFD) is, at this step, a particular important solution to the breakthrough in the study of blood alternative fluids, and alginate, due to the properties that present, can be used. PFCs are extremely hydrophobic, so the use of emulsifiers like lipids, fluorinated compounds or proteins is required, to overtake the immiscibility in aqueous phases [45]. Alginate is a biopolymer that is largely produced by sea algae (like brown algae) and has several applications, like the ones in the biomedical field [68-70]. Also, alginate solutions present Non-Newtonian properties and are considered complex fluids, with high viscosity [70]. Properties such as biocompatibility are relevant to explain the use of alginate in biomedical applications [70]. Also, alginate rheological properties makes alginate microparticles a good candidate to incorporate a blood analogue fluid [13]. Figure 13 presents an experimental set-up for a double emulsion process of PFC in a polymer solution in air [70].

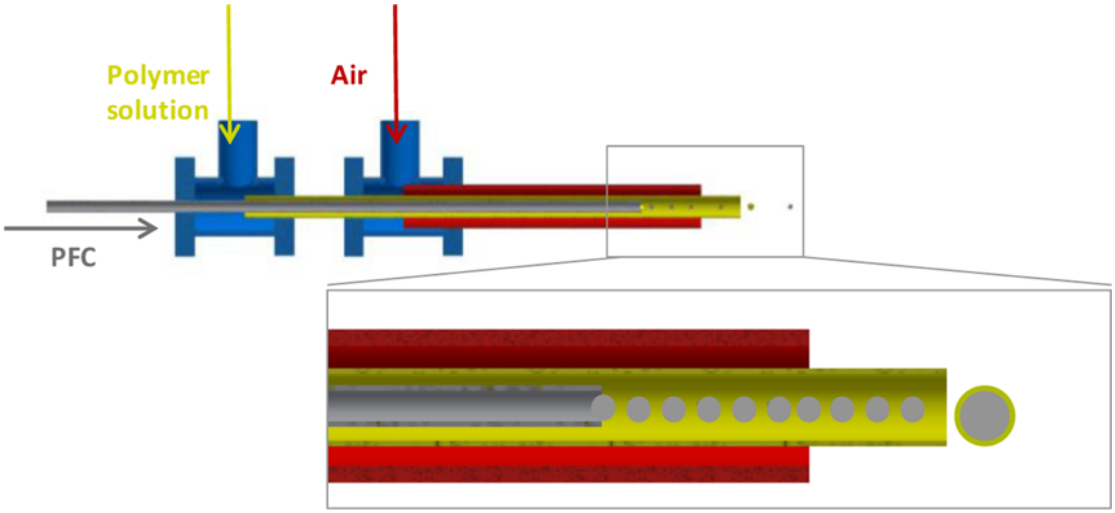


Figure 13: Formation of perfluorocarbon-alginate microparticles schematic, adapted from [70].

Considering the solutions explored, double emulsion of PFD can be performed using microfluidics approaches. In fact, the use of microchannels could be a solution to overcame significant problems associated to methodologies like membrane emulsification, such as the high waste of material to produce a small number of particles and the difficulties associated to controlling the dimensions of the particles, due to coalescence. For obtain the expected blood analogue fluid using the droplet microfluidics technique (double emulsion), it is necessary to perform a first emulsion of PFD in alginate that is followed by a second one of the particles of PFD in alginate in oil (Figure 14).

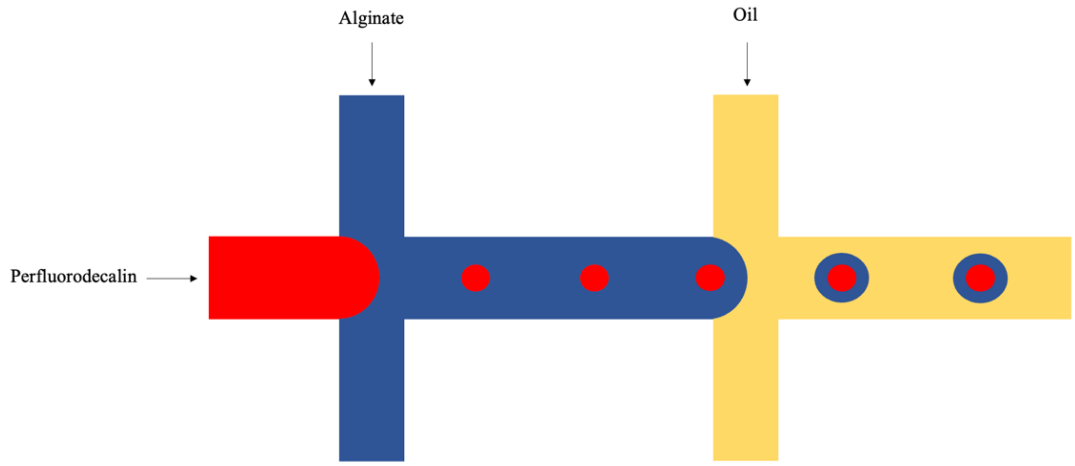
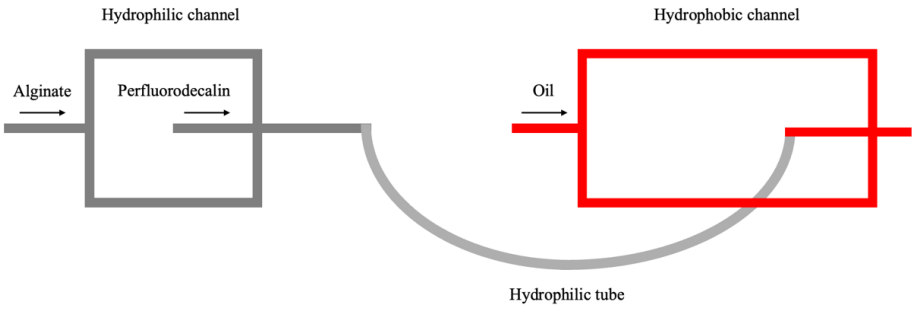


Figure 14: Schematic of the double emulsion process.

However, the process previously presented has problems related to the characteristics of the channels. In fact, for the first process of emulsification, it is necessary to have a hydrophilic channel and for the second one the channel must be hydrophobic (PDMS can be used). This problem comes up because in the first emulsification (perfluorodecalin in alginate) alginate is an aqueous solution and to function correctly as a continuous phase the fluid must present affinity to the wall of the channel, being hydrophilic. On the other hand, the continuous phase of the second emulsification (droplet of perfluorodecalin in alginate in oil) is oil, so it is required a hydrophobic wall.

Two different solutions could be applied. The first one is the use of two channels (Figure 15 A) one hydrophilic, where the first emulsion is performed, and one hydrophobic, connected to a hydrophilic tubing, to accomplish the second emulsification. Although, this process has several difficulties like the coalescence of the droplets in the tubing, that can result in a lack of control of the size of the microparticles. Another solution is the use of a single channel (Figure 15 B), with two different regions, one hydrophilic and another hydrophobic. The solution of a single channel is theoretically the best one to overcome the difficulties related to the coalescence of the particles, but the development of the device is difficult.

A



B

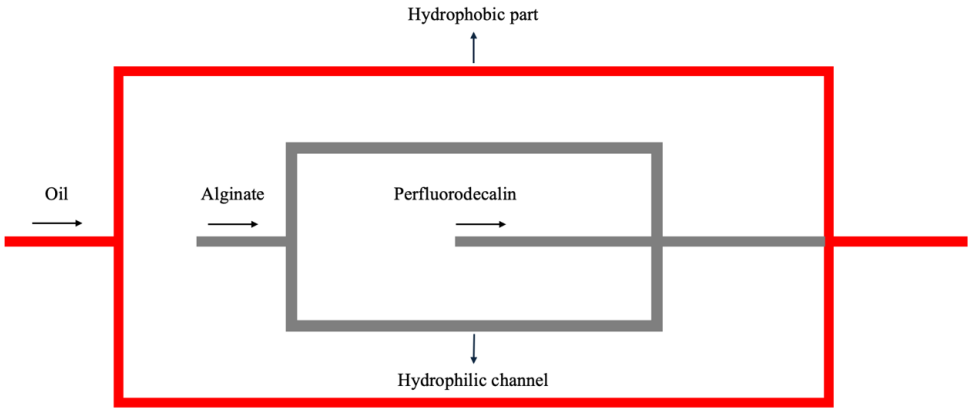


Figure 15: Schematic of double emulsion solutions. A – Double emulsion process in two channels. B - Double emulsion process in one channel.

It is possible to transform temporally a hydrophobic channel into a hydrophilic channel. For instance, CEFT has two different protocols for oxygen plasma treatments, one for PDMS-PDMS bonding and the other for PDMS-glass bonding, where the plasma asher is used to make PDMS temporarily hydrophilic. PDMS-glass oxygen plasma treatment is a solution channel sealing, which generates strong bonding connections between the surfaces [71, 72]. Also, oxygen plasma treatment presents the capacity of changing temporarily the surface of the channels, making them hydrophilic.

Surfactants are set of chemical surface-active substances that have important functions in several applications, due to their specific properties [73-75]. In fact, surfactants present a particular molecular structure, with hydrophilic heads, that are formed by polar groups, and hydrophobic tails (hydrocarbon chains) [73, 74]. Because of these characteristics, surfactants are amphiphilic compounds [76]. Considering this, surfactants can be used to lower interfacial tension between the fluids and to prevent phenomena like the droplet's coalescence [54, 75, 77].

2.4. Vortex pre-emulsification and membrane emulsification

Vortex emulsification followed by membrane emulsification (Figure 16) can be used in the production of particles. In this approach, a suspension of two immiscible fluids is prepared, with a continuous phase and a dispersed phase [14]. The suspension is agitated using a vortex. After this step, a membrane emulsification is performed. Membrane emulsification is the process where the droplets are formed by the use of two immiscible fluids by the use of a membrane [78]. In this process, particles can be subjected to filtration to guarantee that the diameter of the particles is uniform and is similar to the one presented by RBCs as described by [14]. The filtration process is executed to try to guarantee that particles are from the size pretended, but it could be necessary to repeat the process of filtrations to obtain the size desired to the particles and it is also a process with a large amount of loss of reagents [13]. In the case of alginate particles, that can be used to make particles that mimic properties from RBCs, 3 times filtration and a curing process are required [13].

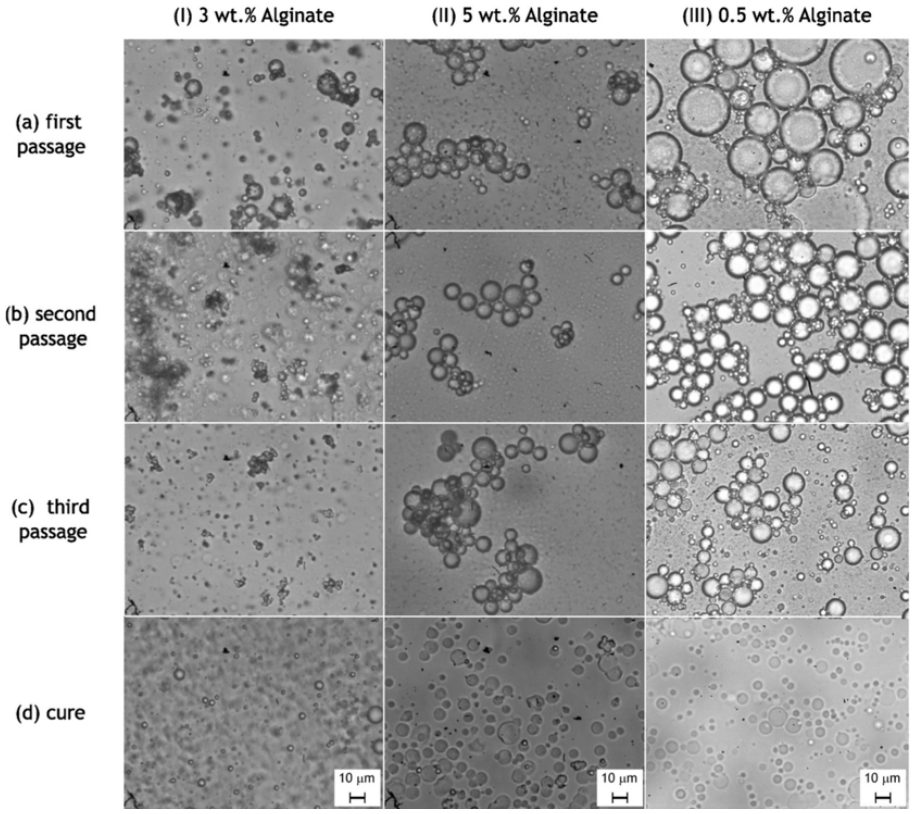


Figure 16: Alginate droplets formed by premix emulsification membrane method, with 3 passages by the filter [13].

2.5. Oxygen measuring and control

Oxygen quantification is vital to perform microbiological tests like the growth of biofilms or cell adhesion [24] and also to evaluate precisely the metabolism and viability of cells [79]. As previously presented, tissues present different levels of oxygen (Figure 3), between them and when compared with other levels of organization in the human body [23].

2.5.1. Oxygen measuring

In microfluidics, oxygen sensors can be integrated with the goal of experimentally characterize the experiment taking place in the device and there are two major approaches to the measuring of oxygen: electromechanical detection and optical detection [23, 24].

Electrochemical detection is a method of oxygen detection that uses incorporated electrodes [23]. The electrochemical sensors present several advantages, such as high sensitivity, short response time, easy implementation inside chips, capacity to make a correlation between oxygen concentration and other parameters, such as metabolic ones and other advantages [23, 24]. However, electromechanical detection techniques are expensive (chip integration), require specialized equipment and operators, the electrodes can generate a toxic environment, among other challenges [23, 24].

Optical detection is an important solution in on chip-systems and luminescence sensors are the most common solution that is applied [24]. This type of approach presents several advantages, that are important to overpass difficulties associated to the electrotechnical detection, such as, the easiness of implementation on a microscale [23, 24]. The lower price is also an important factor when both approaches are compared [24]. Optical detection, in particular fluorescence microscopy, is often used to live cell imaging [23]. According to [24], metal–ligand complexes, like Platinium (II) octaethylporphyrin (PtOEP), are largely used as oxygen sensors. In the case of PtOEP, the fluorescence will increase with the decreasing of levels of oxygen [24, 80, 81] (Figure 17 and 18).

Montagne, Komori [80] developed a sensor that presents the PtOEP scattered in a Polystyrene (PS) layer. The sensor was prepared using a solution of PS dissolved in toluene and PtOEP, that was prepared and scattered in a glass slide, using a spin-coater at 1000 rpm for a period of time of 30s [80]. According to the authors, PS was selected as the membrane polymer considering that is weakly auto-fluorescent and presents a good permeability to oxygen [80]. This type of sensor is particularly used in biological tests with a large set of advantages such as the continuous measurement in the period of the trial, the non-invasive character and the possibility of using different flow rates [24, 80, 81]. Figure 17 presents a schematic of an oxygen sensor using the setup described.

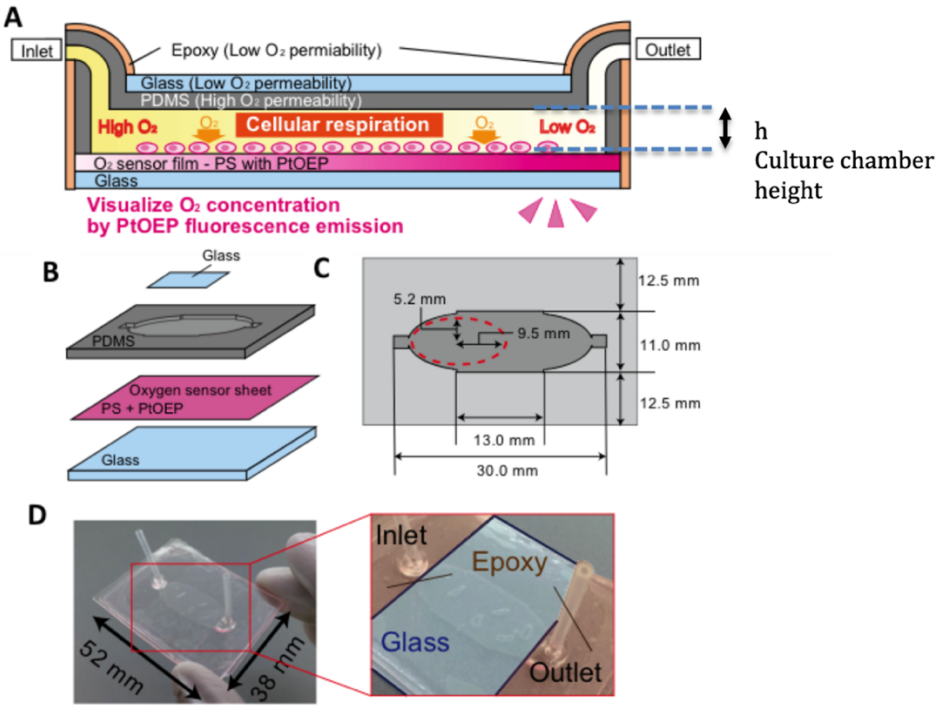


Figure 17: Schematic of an oxygen sensor setup using PtOEP [24, 81].

PtOEP presents two strong absorption bands at a wavelength of 383 and 536 nm (Figure 18) [80]. To a light source in the green scale (510-560 nm), PtOEP, in the absence of O_2 or in an environment of low % of O_2, emits a light in the red spectrum (expected emission at a wavelength of around 650 nm) [80]. As explored previously, the fluorescence of PtOEP is described by the Stern-Volmer equation, assuming a model where oxygen-sensitive dye is dispersed homogenously through the polymer and the oxygen is accessible:

$$\frac{I_0}{I} = 1 + K_{sv}[O_2] \quad (3)$$

As explored, the intensity of the fluorescence of PtOEP decreases with the increase of the levels of O_2. In Figure 18, it is possible to analyse the values of fluorescence according to the Stern-Volmer equation for the sensor presented by Montagne, Komori [80].

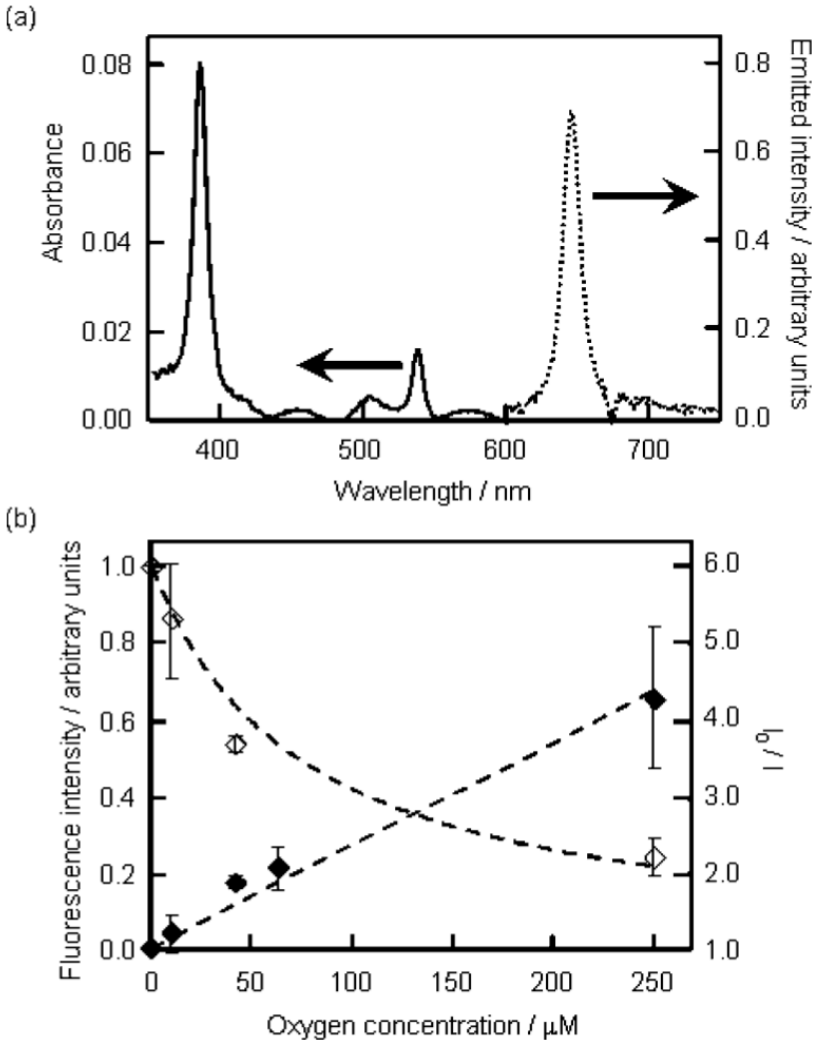


Figure 18: PtOEP sensor characterization from [80].

2.5.2. Oxygen control

The control of oxygen is also a factor that has to be taken in account, considering that the needs of oxygen (in %) are different to different organs, tissues or even cells (Figure 3). For instance, considering that PDMS is permeable to oxygen ($4.1 \times 10^{-5}\ cm^2\ s^{-1}$), without control of oxygen, the gas will enter in the channels through that material [23, 82]. To avoid the entrance of oxygen in the system, PDMS chip can be imperialize by using PMMA or PC substrate (Figure 19 A) [23, 25, 83-85]. Also, other materials (glass, SU-8 or COC) can be used instead of PDMS (Figure 19 B) [23, 86-89].

Scavengers can be used in oxygen control. In fact, scavengers are chemical substances that interact with oxygen, such as Sodium Sulfite (Na_2SO_3), removing it from the solution (Figure 19 C) [23]. Nitrogen (the use of gas canisters can difficult the experimental setup) can also work as a scavenger [23]. In cases where it is necessary more oxygen, oxygen generators can be used [23]. Considering these approaches, it is also possible to have a solution that mix and impermeable chip or an impermeable material and a scavenger, depending on the needs of oxygen in the environment of testing.

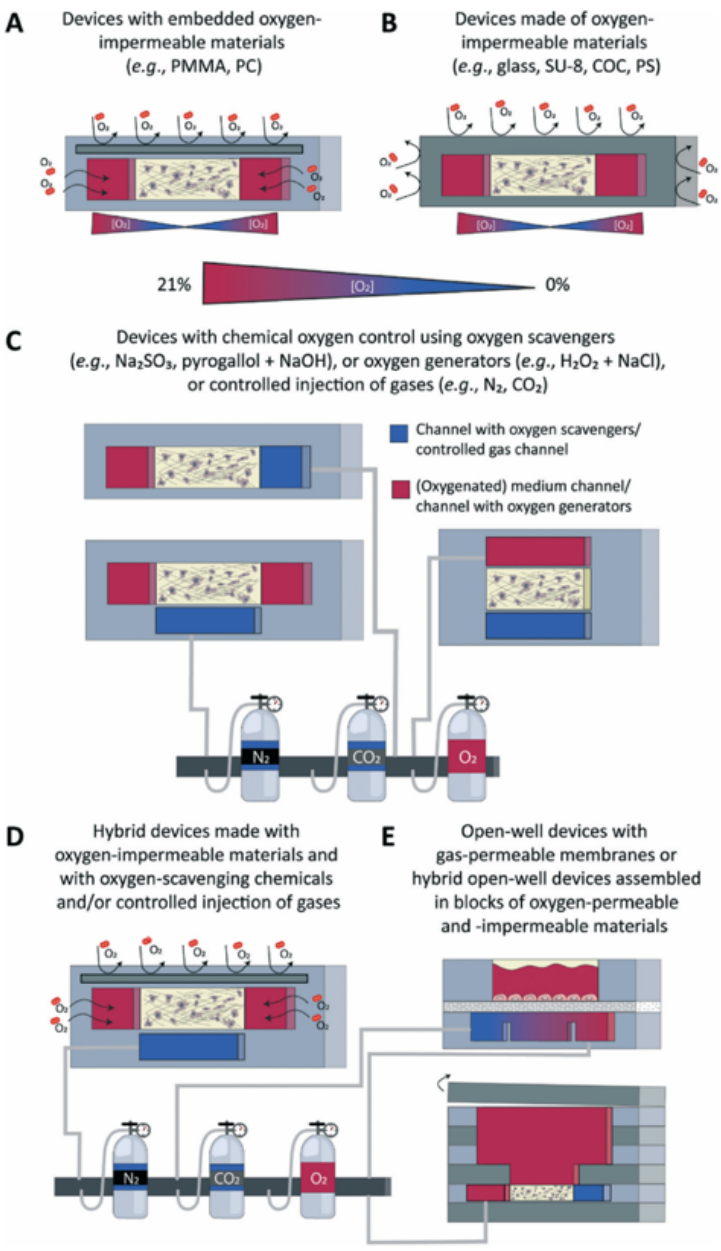


Figure 19: Examples of experimental setups to oxygen level control [23].

The use of scavengers is considered a chemical approach and presents some advantages when compared to engineering solutions (use of impermeable materials) like the possibility of having more flexibility in the changes of the oxygen levels, for instance, it is possible to create intermittent or chronic hypoxia [23, 90-92].

2.6. Biofilms formation

Biofilms are a community of microorganisms (for instance bacterias) that attach to a certain surface and grow, producing large amounts of microorganism that are, at a certain point, released [93-96]. Biofilms are originated by the attachment of microorganisms to a surface, reversible at a first stage and irreversible in a second one, followed by the growing of a colony (maturation) and consequent liberation of new microorganisms that are spread in the organism or stream where is placed [93, 94]. Biofilms formations (Figure 20) is described by presenting 5 stages: reversible attachment, irreversible attachment, maturation I, maturation II and dispersion [96].

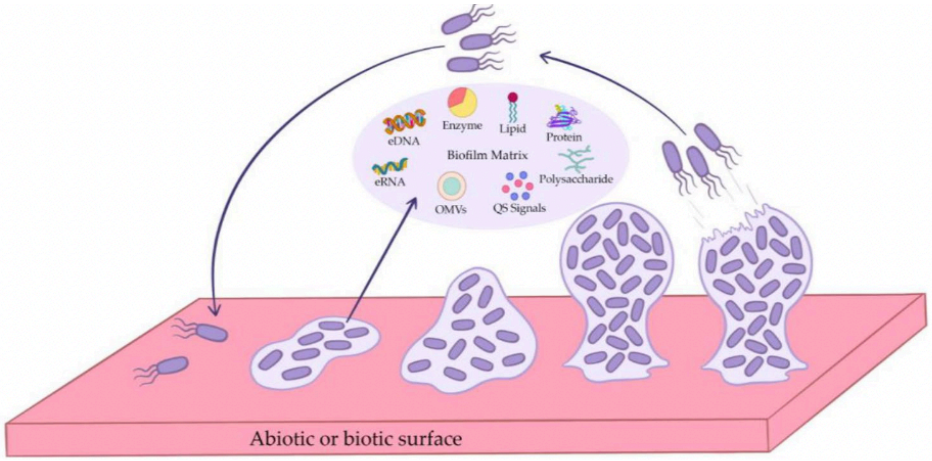


Figure 20: Biofilm formation [96].

Microfluidics and the study of biofilms are ultimately related. In the recent years, the use of microfluidics helped the development of the study of biofilms, due to the need of studying the behavior of biofilms in conditions where flow is a parameter in confrontation to the scenario where biofilms are formed in statical cultures [94]. In fact, flow is a factor in several bacterial environments [94]. Bacterial motility and adhesion, the genetic behavior of biofilms and the bacterial communications are some of the biofilms parameters that are affected by the flow [94]. Figure 21 presents a schematic of the formation of biofilms under flow.

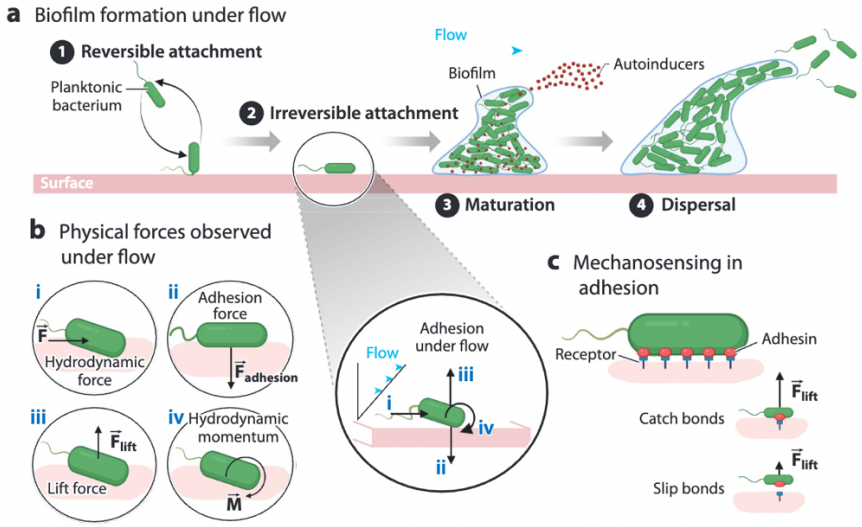


Figure 21: Schematic from the biofilm formation under flow [94].

Chapter 3

Methods

3.1. Particulate fluid production

Particulate fluids containing PFD were produced from multiphase mixtures by membrane emulsification.

Fluids: Perfluorodecalin 95% (P9900-25G) was used as dispersed phase and water was used as continuous phase. Tween® 80 (P1754–500 ML) was used as surfactant in all the fluids prepared. The surfactant was used make easier the separation between the microparticles formed and the continuous phase. Also, Poly(ethylene glycol) (94646-250G-F) and Polyvinyl alcohol (RM 6170) were used as stabilizers, to avoid the aggregation of the particles that are formed.

Syringe filters: 10 μm syringe filters (Versapor® Acrodisc® Syringe Filter, PALL) were used produce the microparticles of PFD.

Membrane emulsification (section 2.4): Membrane emulsification method was used to produce PFD particulate fluids. For that, distilled water, Tween 80 and Poly(ethylene glycol) (PEG) or Polyvinyl alcohol (PVA) were weighed, using an analytical balance ($\pm$ 0.0001g). The measurements were executed using mass values due to the high viscosity of Tween 80, that forbid the correct measurement when micropipettes were used. With the water solution and a PFD, the emulsification membrane technique was applied using a 10 μm syringe filter. PFD and water solution are measured using the balance and placed in a plastic syringe, with the syringe filter. The two immiscible phases are passed the filter three times, considering that after that number of passages was expected that the particles size didn't change significantly [13]. After that, PFD emulsion is obtained. Table 3 presents the composition from the particulate fluids produced and Figure 22 presents the schematic of the membrane emulsification approach used to form one of the PFD (10%) particulate fluids, using PFD, Water, Tween 80 (surfactant) and PVA (stabilizer), with a syringe filter of 10 μm.

Table 3: Composition from particulate fluids produced by membrane emulsification filter. 3 passages in a 10 μm filter applied in all the fluids.

Fluids	Composition
PFD (10%) particulate fluid with Tween 80	PFD (10%) Water (90%) - Tween 80 (1%)
PFD (10%) particulate fluid with Tween 80 and PEG	PFD (10%) Water (90%) - Tween 80 (1%) and PEG (1%)
PFD (10%) particulate fluid with Tween 80 and PVA	PFD (10%) Water (90%) - Tween 80 (1%) and PVA (3%)

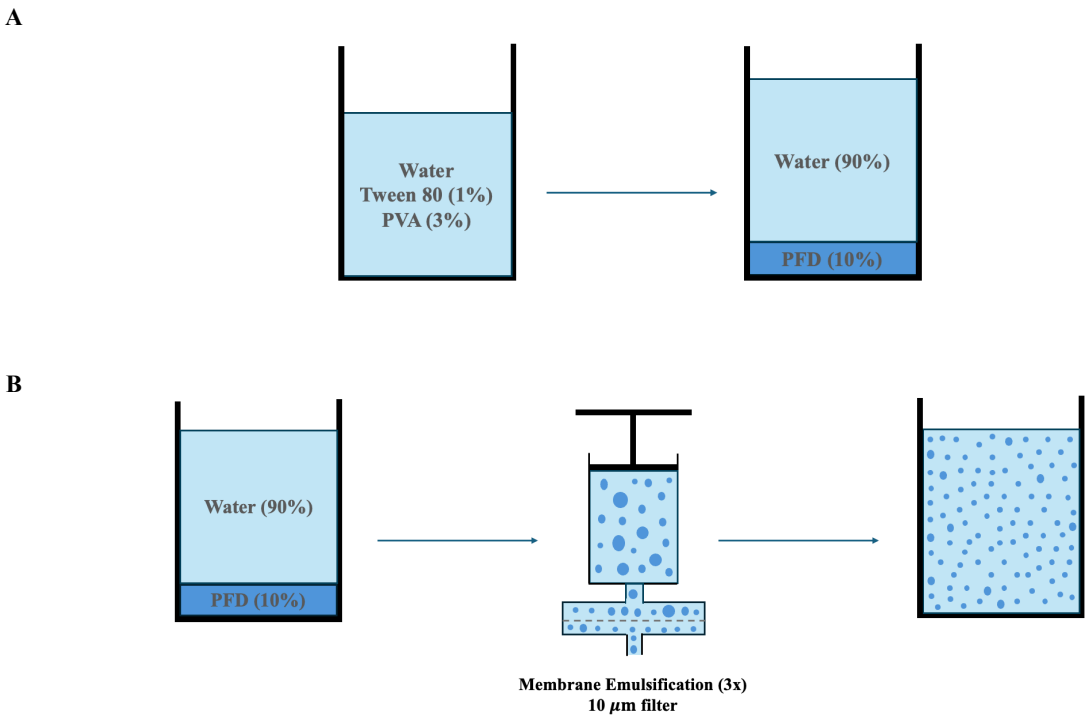


Figure 22: PFD particulate fluid method of production. A – Preparation of water solution with Tween 80 (1%) and PVA (3%) and the addition of PFD (10%). B – Membrane Emulsification process, executed 3 times, using a filter of 10 μm and a plastic syringe.

3.2. Microfabrication

In microfabrication, SU-8 molds and paper molds can be used. These molds are produced by different techniques. Photolithography is used to produce SU-8 molds. SU-8 is a photoresist material, that presents characteristics like thickness and good mechanical properties [97]. This material is a great option in microelectromechanical systems (MEMS) and SU-8 molds can be fabricated using Photolithography [97]. SU-8 molds are very useful because they can be used several times. However, the process of fabrication is demanding, expensive and has to be done by specialized companies [58]. Also, SU-8 molds need a previous preparation where the mold is placed in the fume hood and a few drops of trichlorosilane are added (it is important to be careful at this step and to wear latex gloves, as described in the protocol). The SU-8 molds are placed in

a Petri dish and left there for 30 minutes. This step is used to prevent the PDMS from getting stuck in the mold.

Xurography is another technique that can be used to fabricate microchannels, but this is used to produce paper molds. Xurography consists in a rapid prototype technique that uses a cutting plotter to create a specific micro-structure (thickness range of 25 and 1000 µm) [98]. Paper molds produced by the xurography method are a more viable solution in logistical and economical terms (they can be produced in the CEFT laboratory, using a cutting machine), but they usually can't be used more than one time.

Xurography was used to obtain paper molds to the production of microchannels, mainly with Flow-focusing design, to tests which involve the production of droplets. However, T-junction design was drawn as an alternative for the micro-rheometer studies. The new T-junction design was drawn using Inkscape software (Figure 23).

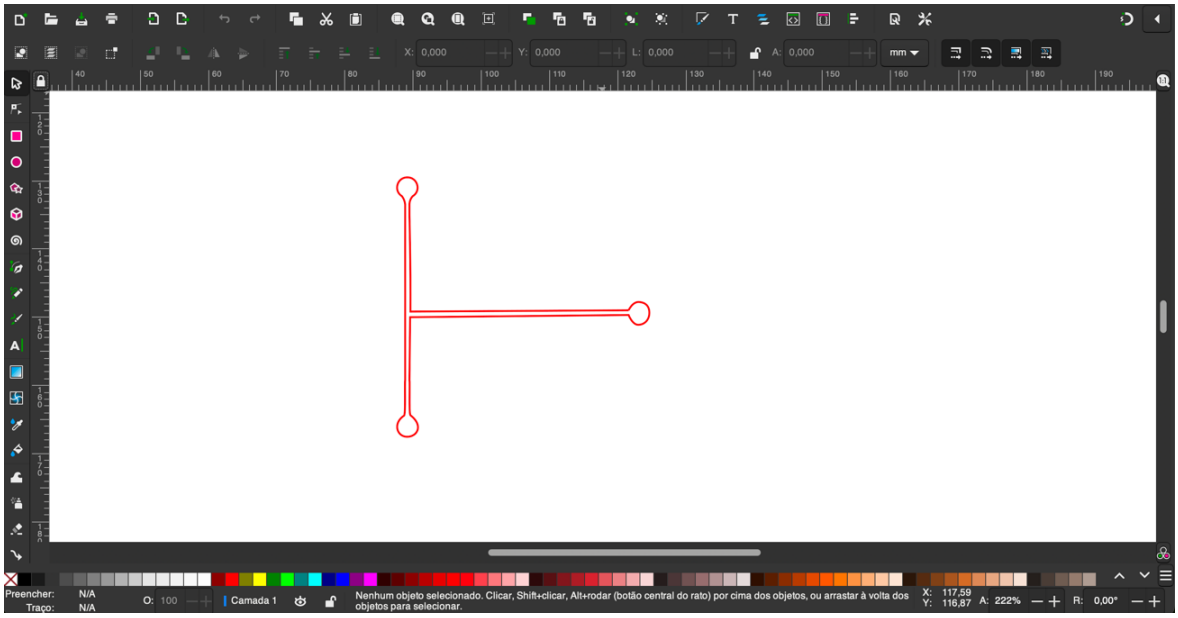


Figure 23: New T-junction channel drawing process (Inskape).

After making the drawing, the design was export to a software named Great Cut, that is a software used to command the cutting machine used. The import procedure was executed according to the following steps:

1. Export the design as a .ps file (Inkscape).
2. Import .ps file to a software called Corel Draw.
3. Copy the file to Great Cut software.

With the design in Great Cut, the printer was connected and a paper with an adhesive paper was placed in the cutting machine. After that, the design and the option cut were selected (with the correct parameters selected). Executing this procedure, the cutter makes the cutting and, after that, the adhesive paper is removed from the paper and is placed in a Petri dish (Figure 24). The

adhesive paper was removed from the normal paper using a tweezer and the adhesive paper with the design of the channels was placed in a petri dish. Alternatively, a transport paper can be used to try to decrease the imperfection resulting from the manual placement of the adhesive paper in petri dish.

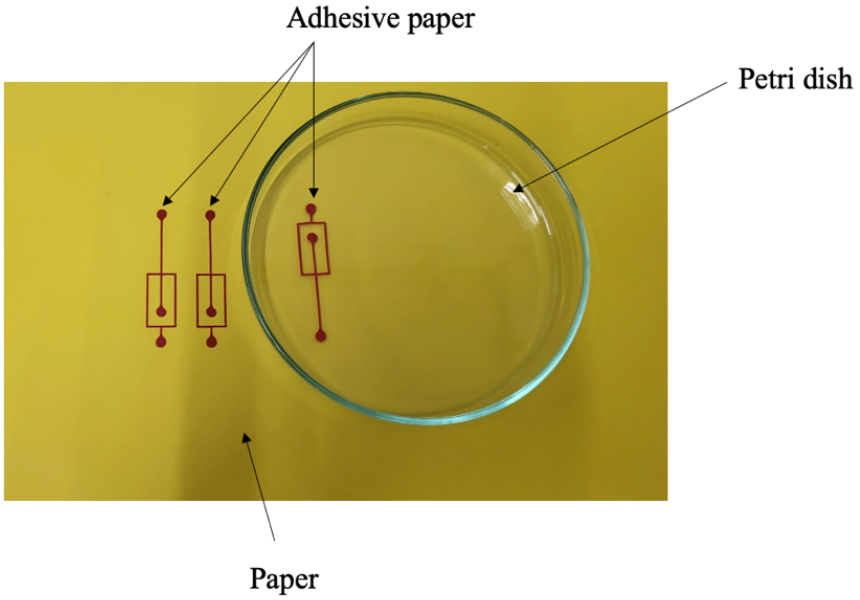


Figure 24: Paper molds production.

Several approaches can be applied in microfabrication. In fact, micromachining, soft lithography, in situ construction and micromolding are some of the options than can be used in microfluidics [52]. In CEFT, the microfabrication process follows a specific protocol, with soft lithography [52, 58, 99] as method. Soft lithography is a non-photolithography approach that uses replica molding to produce micro or nanostructures [99]. Soft lithography is an effective and low-cost solution to the manufacture of microstructures [99]. In soft lithography, polydimethylsiloxane (PDMS) and a curing agent (Sylgard 184, Dow Corning) were used in two different proportions (5:1 and 20:1). These two components are agitated for 10 minutes and the bubbles are removed, using a desiccator connected to a vacuum pump.

On one hand, the 5:1 mixture is used to fill the molds and after this is it necessary to remove the bubbles again. On the other hand, the 20:1 solution is used as a glue that is placed in the glass slides. For that, a spin-coater is used ("pdms50s" program as a standard in CEFT microfluidics laboratory) to guarantee a uniform spread of a thin layer of 20:1 solution in the glass slides. The most used program ("pdms50s") is composed by 3 steps: acceleration (from 0 rpm to 5000 rpm, in 10s), rotation (5000 rpm for 50s time) and Slowdown (from 5000 rpm to 0 rpm, in 10s). The molds filled with PDMS without bubbles and the glass slides with 20:1 solution are placed in the oven for 20 minutes at a temperature of 80º C for curing. After that period of time, the molds and the glass slides are removed from the oven and is necessary to cut out the microchannels from the mold, and the points where the fluids will enter are drilled. Using xurography molds, it is common that the removal of the channels makes damages to the mold, making them not reusable. Then,

the microchannels are bonded into the glass slide (the groove must be in the part that is connected with the glass slide). To finalize, the microchannels are placed in the oven for 12 to 24 hours.

3.3. Oxygen Plasma Treatment

Sometimes, due to the need of having hydrophilic channels or to connect PDMS to a glass slide, Oxygen plasma treatment can be used. At CEFT, this treatment has two different protocols available: PDMS-Glass and PDMS-PDMS. PDMS-glass treatment requires a previous cleaning that is performed with acetone in an ultrasonic cleaner. After that plasma asher is used. The glass slides and the PDMS are placed in the equipment and the power is set to 20W. After that, PUMP button is pressed and the plasma asher pressure decreases to 0.4 mBar. When that pressure is reached, the pressure is adjusted to the value pretended (1.2 mBar) and GENERATOR button is pressed to start the treatment. The treatment is applied for 30 seconds and, after that, GENERATOR and PUMP are turned-off, the ventilation knob is removed and VENTILATION is also turned-off. After removing PDMS and the glass slide, it is necessary to wait for at least 5 minutes to perform the bonding. PDMS-PDMS treatment is similar to the PDMS-Glass treatment presenting differences in the Power used (30W instead of the 20W), the need of a cleaning (for PDMS-PDMS, the procedure is not applied) and in the pressure used (0.4 mBar instead of the 1.2 mBar) and the period of time of the treatment (3 minutes instead of 30 seconds). Figure 25 presents the Plasma asher used for Oxygen plasma treatment.



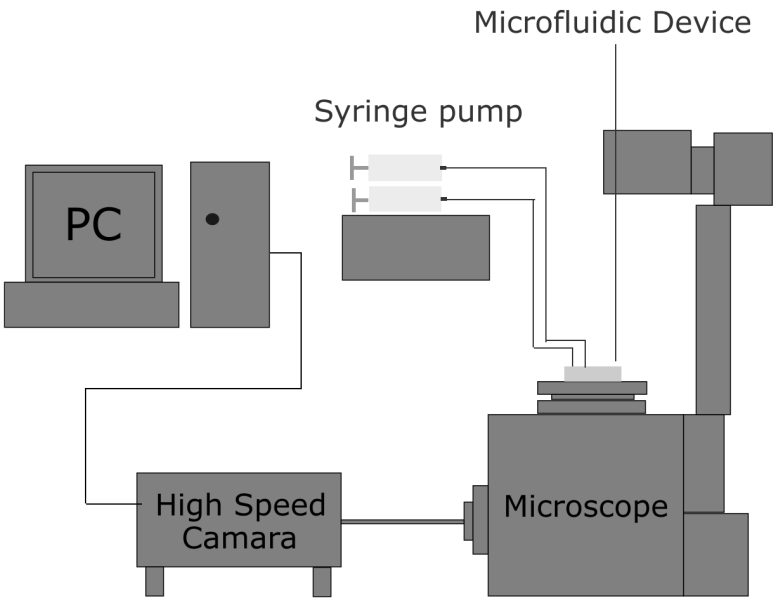
Figure 25: Plasma asher treatment example.

3.4. Particle and droplet characterization

As explored previously, rheological properties are critical to the effectiveness of the blood analogue fluid and the dimension of the particles that mimic RBCs is one of the most important characteristics. So, it is vital to control the characteristics of the particles, such as their dimension.

To characterise the particles that are formed through droplet microfluidics, the visualization of the droplet formations has to be performed. Figure 26 presents the experimental setup used.

A



B

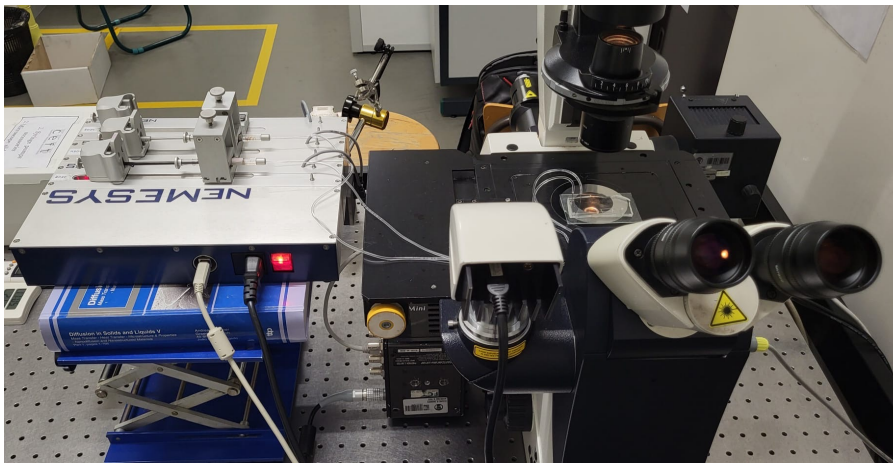


Figure 26: Experimental setup of visualization of the formation of droplets, using a microscope, a syringe pump and a High Speed Camera. A – Schematic version. B – Real experimental setup.

Considering the setup, syringes are placed in a syringe pump (neMESYS syringe pump) and are connected to the microchannel by polymeric tubes. The flow of the is controlled by a software called “neMESYS Userinterface” and a High Speed Camera is used to see (using the computer)

and to capture images from the droplet formation. Table 4 presents the calibration from the High Speed Camera.

Table 4: High Speed Camera calibration values.

Microscope objective	Pixels	Distance in micrometers (μm)
2.5×	1	4
5×	1	2
10×	1	1
20×	1	0.5
40×	1	0.25

The characterization of particles is related to properties from the particles, such as size, shape and microstructure [54]. The visualization of the particles is the first step to do this characterization. After the capture of the images, the analysis of the particles can be performed using images software's, such as, "Image J".

Images can be collected individually (frame by frame) or in video format. "Image J" is used to rebuild a video from a set of frames, using the following procedure: "File", "Import" and "Image Sequence" (in the last step, it is important to select the option "Use virtual stack", with the goal of avoiding problems with the storage of the video in the RAM memory of the computer). Figure 27 presents the Image import process in Image J software, used to make a virtual stack from individual frames.

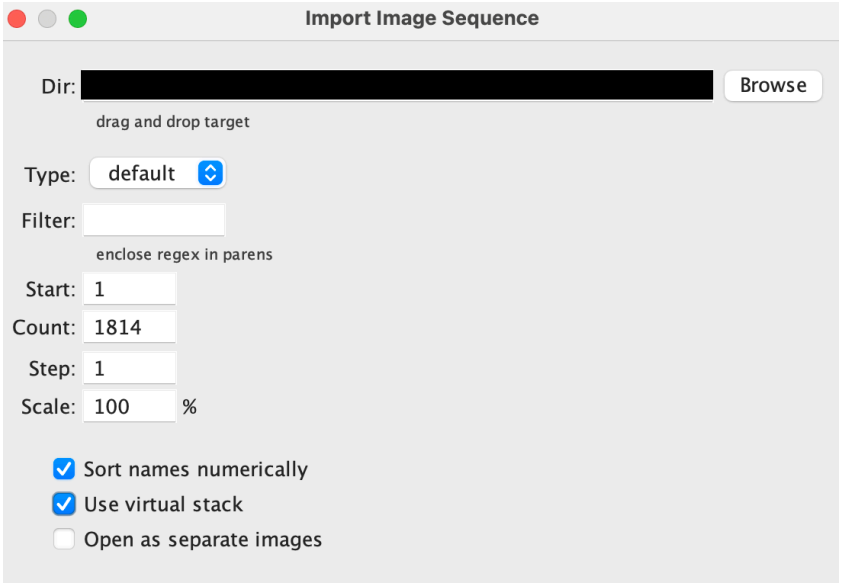


Figure 27: Image import process.

The values from Table 4 are used to the measuring of the length of the droplets, converting pixels in micrometers. To perform this measuring, the option "*Straight*" is selected. This

command is used to draw the line that measures the length of the droplet. After that, the command "Measure" is selected (Figure 28).

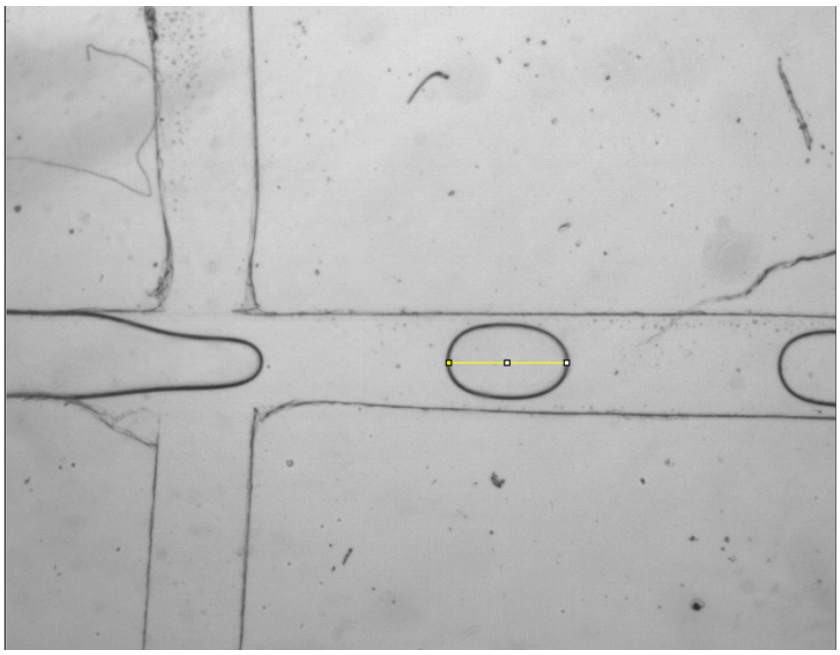


Figure 28: Example of the measuring procedure in Image J - 2.5x microscope objective.

The data collected in Image J is transferred to an Excel file, where the treatment was performed. The following equations correspond to the formulas that were used to calculate the speed of the droplet:

$$\Delta t = \frac{(Final\ frame\ number - Initial\ frame\ number)}{Frame\ rate} \tag{4}$$

$$v = \frac{Final\ position - Initial\ Position}{\Delta t} \tag{5}$$

3.5. Interfacial tension

Interfacial tension is a key concept in the study of the fluid's behavior, as will be shown in the following section. Interfacial tension is defined as the force that maintains the integrity of a fluid surface, enabling it to resist external forces [100]. In other words, it represents the work required to increase the surface area of a liquid by a unit amount (it can be measured following in mN/m, SI unit). Surface tension is a relevant property at microscale [52]. Considering this, surface tension is a property between the fluid and the gas phase and interfacial tension is characterized by the same phenomenon to other phases, by instance two fluids. Interfacial tension can be measured using a Force tensiometer. The equipment available used was a Force tensiometer Sigma 701 (Figure 29) and was used to measure several interfacial tensions.

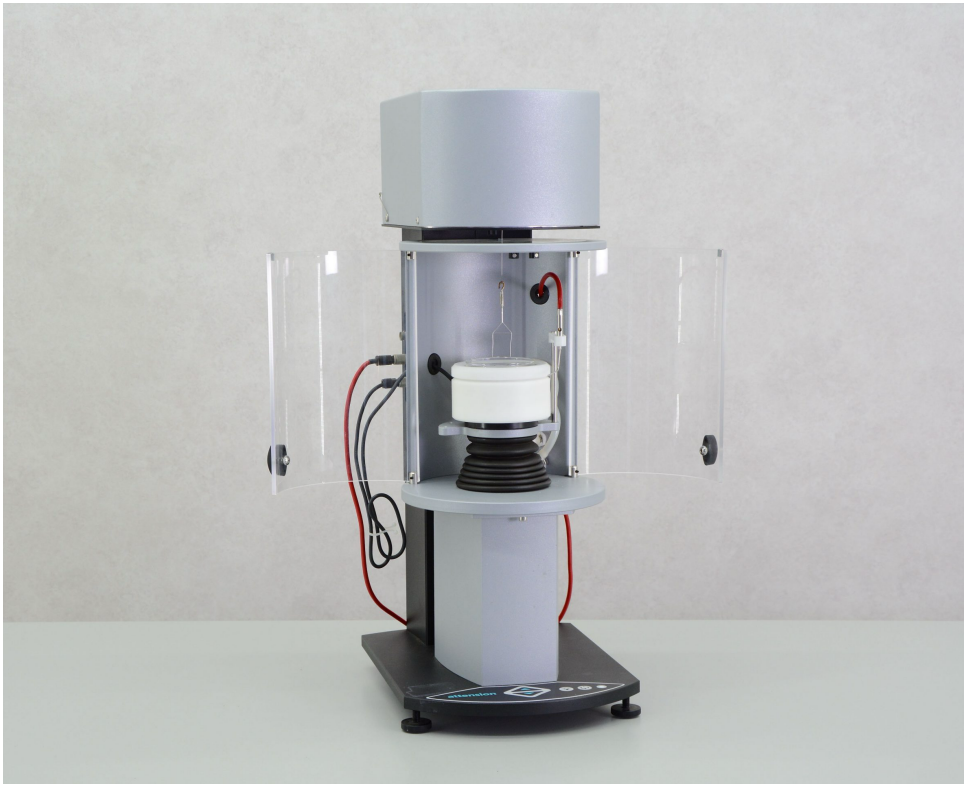


Figure 29: Force tensiometer Sigma 701.

In the force tensiometer was placed a glass recipient with the fluid(s) in study and the Platinium ring was placed in a level below the interface (2 fluids case) or above the interface (air-fluid case), depending on the fluids in study. Also, it was necessary to define important parameters, such as the light and the heavy phase of the measuring selecting the phases that were used. The ring moves into the interface and exert a force that changes the interface, measuring the interfacial tension through the changes in weight detected by the micro-balance from the equipment when the probe passes through the interface. The data from the tensiometer is obtained in the software OneAttension, that uses the values that are recorded to calculate the values of surface or interface tension. After executing the measurement, it is necessary to clean the Platinium ring, using a flame. A Bunsen burner was used. For the study of rheological properties, the values of interfacial tension of Oil-water and Oil-Glycerol (glycerol content of 40%, 50% and 60%) were measured. The Table 5 presents the values obtained in the measuring of interfacial tension.

Table 5: Interfacial tension values.

Fluids (Light phase-Heavy phase)	Interface tension (N.m^{-1})
Oil-water	0.05042
Oil-Glycerol (40%)	0.03250
Oil-Glycerol (50%)	0.03423
Oil-Glycerol (60%)	0.03595

3.6. Micro-Rheometer

To measure the viscosity of small samples, alternatives to rotational rheometer proposed were explored. Considering this, microfluidic devices were used to develop a micro-rheometer. To the development of the micro-rheometer, the following solutions were explored:

- Flow-focusing device.
- T-junction device.

3.6.1. Flow-focusing device

Flow-focusing microchannels were used for the development of a device capable of measuring the viscosity of a fluid. In this method, the Capillarity number (Ca) is an important concept. Ca can be calculated by:

$$Ca = \frac{v_{droplet} \times \mu}{\gamma} \tag{6}$$

μ – Viscosity
γ – Interfacial tension

The Ca parameter can be calculated using the speed of the droplet ($v_{droplet}$), that is obtained by the procedure previously explored, or the speed of the fluid (v_{fluid}). The speed fluid can be calculated by:

$$v_{fluid} = \frac{Q_c \times Q_d}{A} \tag{7}$$

Q_c – Continuous phase flow

Q_d – Dispersed phase flow

Considering the difference between the calculus of $v_{droplet}$ and v_{fluid} it was necessary to understand if the values were similar. If $v_{droplet}$ is divided by v_{fluid} and the value obtained is approximately 1, the values of speed are identical.

To use the device as a rheometer, it was necessary to test the Flow-focusing channels with fluids with a known viscosity to build up a graphic correlation that could be used to calculate the unknown viscosity of a fluid. To perform this procedure, oil (continuous phase) and water (dispersed phase) or a solution of water with glycerol (40%, 50% and 60%) were used. Glycerol properties are known (Table 6) and the increasing of the viscosity in the glycerol solution was implemented to having a solution with similar properties to the particulate fluids that were explored.

Table 6: Glycerol properties at 293K.

Glycerol content c (wt.%)	Density ρ_L (kg·m^{-3})	Viscosity μ_L (mPa·s)	Surface tension σ (mN·m^{-1})
40	1099.3	3.70	64.11
50	1124.7	5.66	64.02
60	1153.6	10.40	63.95
70	1181.1	21.80	63.52
80	1208.2	57.40	62.81

For peer review

The tests were performed choosing a certain flow rate of water or water + glycerol ($\mu L/min$) and generate droplets using different values of oil flow rate ($\mu L/min$). With the images captured, the length and the speed of the droplets were calculated. After calculating the parameters from the droplets formed with different flows (length and speed), a graphic with Ca in the x axis and L/W in the y axis. With Ca for a fluid that presents an unknown viscosity, it was expected that the viscosity value could be calculated. To demonstrate the use of the rheometer standard curve referred previously, particulate fluids were used as a fluid with unknown viscosity.

Particulate fluids were used as dispersed phase and oil as continuous phase, replicating the procedure described for the solution of glycerol. With the values of length of the droplets formed, width of the channel and speed of the droplets, Ca and L/W parameters can be calculated using different values of viscosity and superficial tension. It was expected that the graphics from the different fluids shown similar behaviors for the correct values of viscosity and superficial tension, allowing the use of T-junction microchannels as micro-rheometers. Also, micro-rheometer tests were applied to PFD particulate fluids developed, in particular the PFD (10%) fluid with Tween 80 (1%) and PVA (3%). Figure 30 presents the schematic from the micro-rheometer trials with flow-focusing microchannels.

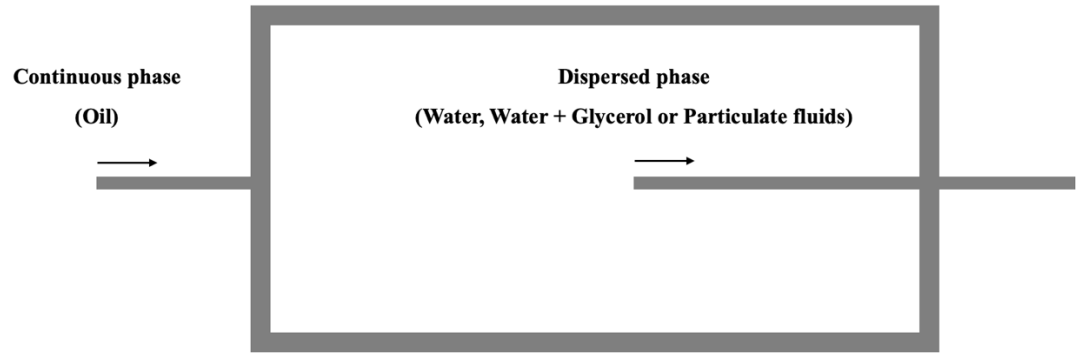


Figure 30: Schematic of the micro-rheometer trials - flow-focusing microchannels.

While at first, a standard curve based on the dependence of droplet length on the Capillary number was explored, an alternative approach was tested. In this approach, was based on the dependence of droplet length on the viscosity ratio between phases for fixed ratio between the flows of the continuous phase and of the dispersed phase (Q_c/Q_d). Considering this, different values of flow were used following the microfluidics method explored in this section, but with a certain value of ratio between the flows. The values of the ratios selected were 3 and 5 (Q_c is 3x and 5x higher than Q_d, respectively). The fluids used in calibration were also water and water + glycerol (40%, 50% and 60%).

In these approach, *L/W* parameter was used again (x axis) versus the ratio between the viscosity of the dispersed phase and the continuous phased (η_d/η_c) — y axis. After obtaining the standard curve, the procedure of testing particulate fluids was applied, with the parameter of η_d (viscosity of the particulate fluid) being estimated, according to the ratio of the flows and the behavior of the curve.

3.6.2. T-junction device

T-junction channels were also used to the study of a micro-rheometer solution. For this solution, the channels used presented a simpler design (Figure 23). For this method, to equal values of Flow ($Q_1 = Q_2$), was expected that the ratio of the thickness of the fluids in the channel (Figure 31) where equal to the ratio of viscosities. The behavior of the flow can be characterized by the viscosity of the fluids, because when the fluid presents a higher viscosity, the speed presented will be slower. Considering this, oil and a particulate fluid were used to perform the tests.

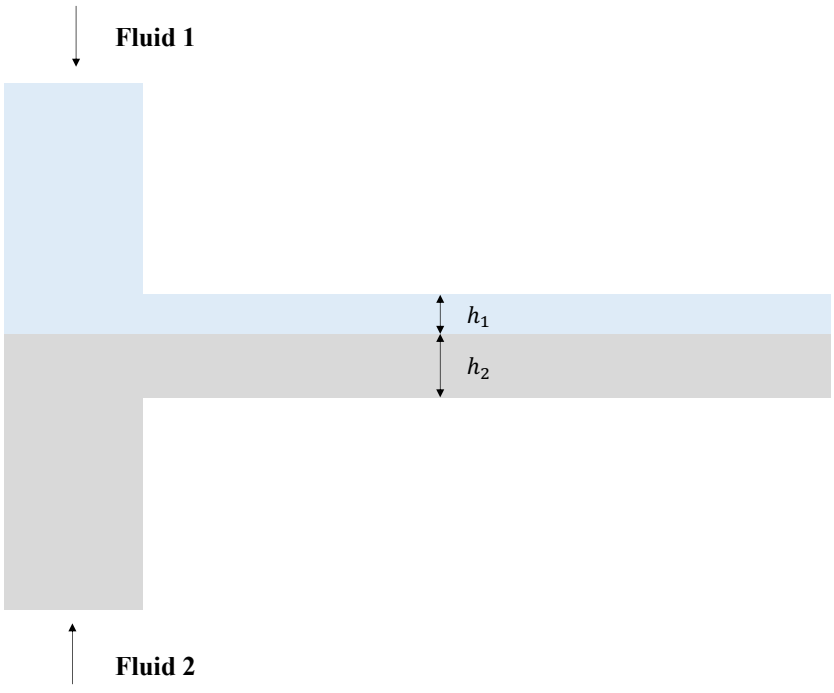


Figure 31: Schematic of the T-junction channel with 2 different flows (h as the thickness of the fluids).

3.7. Oxygen optical tests

3.7.1. Development of the oxygen sensor device setup

Oxygen optical tests were required to measure the oxygen concentration involved in the test with blood analogue fluid with PFC encapsulated particles. For this, it was necessary to incorporate an oxygen sensor. The solution implemented was the fluorescence detection and the Figure 32 presents the initial expected setup for oxygen sensor.

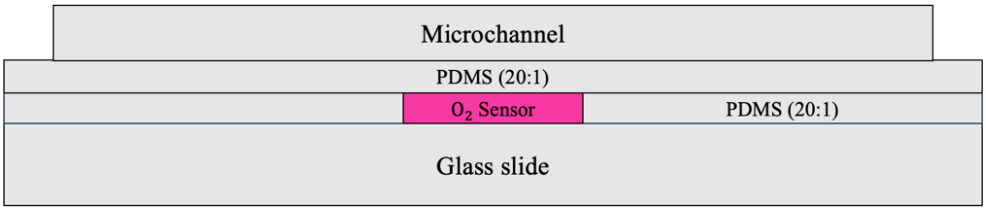


Figure 32: Schematic of the implementation of a fluorescence oxygen sensor.

To implement this solution, changes in the microfabrication procedure (section 3.2) were made, with changes in the program used in spin-coater and in the process of connecting the glass slide and the PDMS 5:1 structure. In fact, it was developed and tested an alternative program in the spin-coater to have a thicker layer of PDMS. This solution was required because the layer that is formed with the traditional program ("pdms50s") presents a thickness that is not enough to form the cavity and to place the solution with the oxygen sensor. The principal aspects of the development of this program (Figure 33) were to maintain the structure of "pdms50s", that is an optimized program. Considering this, the 3 steps of the program (acceleration, rotation and slowdown) and the times of execution were maintained. Spin rotation in the rotation step was reduced to 2000 rpm. To connect the PDMS to the glass slide, Oxygen plasma treatment (PDMS-glass) protocol was implemented, to prevent that oxygen sensor from suffering damages as a result of the long exposure to high temperatures (80 ºC for 12 to 24 hours). The first draft of the device was developed using a suspension of fluorescence particles, FluoSpheres® carboxylate-modified, 1.0 μm, nile red (535/575).

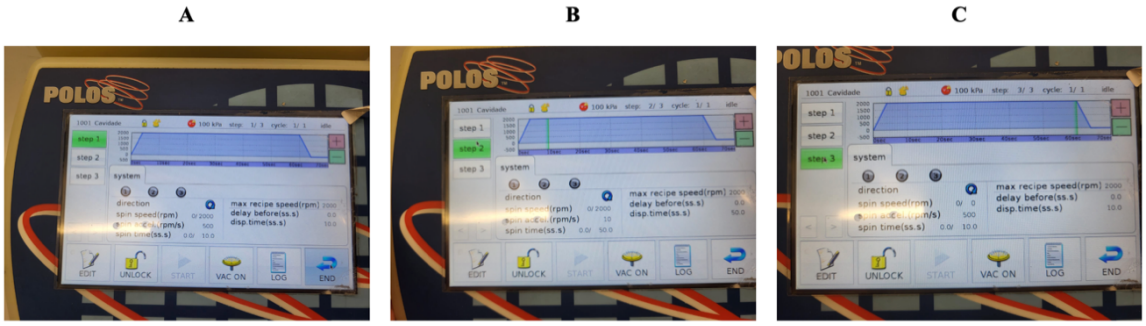


Figure 33: Spin-coater new program ("Cavidade" program). A – Step 1 (Acceleration); B – Step 2 (Rotation); C – Step 3 (Slowdown).

In the initial trials, the cavity was formed with the help of a circular adhesive paper, but the removal of the paper after the first curing process of 20 minutes was very difficult and the layer of PDMS was frequently damaged in the process. So, rectangular shaped pieces of paper were used instead (Figure 34) and the removal process is particularly easier, reducing the chances of damaging the PDMS layer.

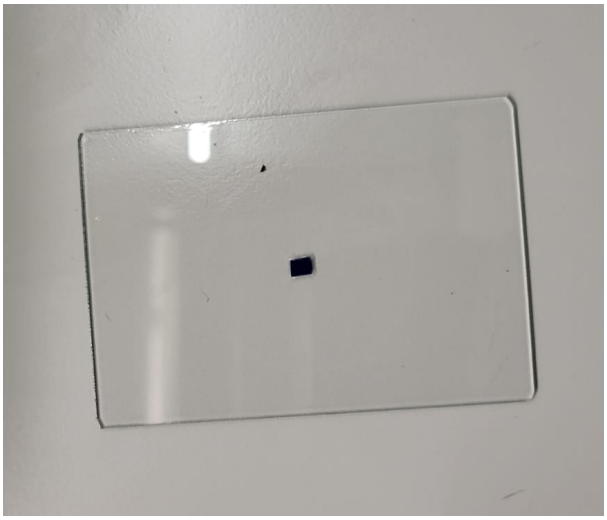


Figure 34: Glass slide with a rectangular piece of paper.

The implementation of the fluorescence substance (in initial trials, FluoSpheres® carboxylate-modified) must be carried out carefully to avoid the dispersion of the droplet (Figure 35). Considering this, it was necessary to let the fluorescence substance dry before the spreading of the second layer of PDMS 20:1. To avoid the dispersion of the fluorescence substance, it was necessary to dry the droplet, between the placement in the in first layer of PDMS 20:1 and the second one. A drying in the oven (80º C) for a 5-minute period of time was tested (Figure 36).

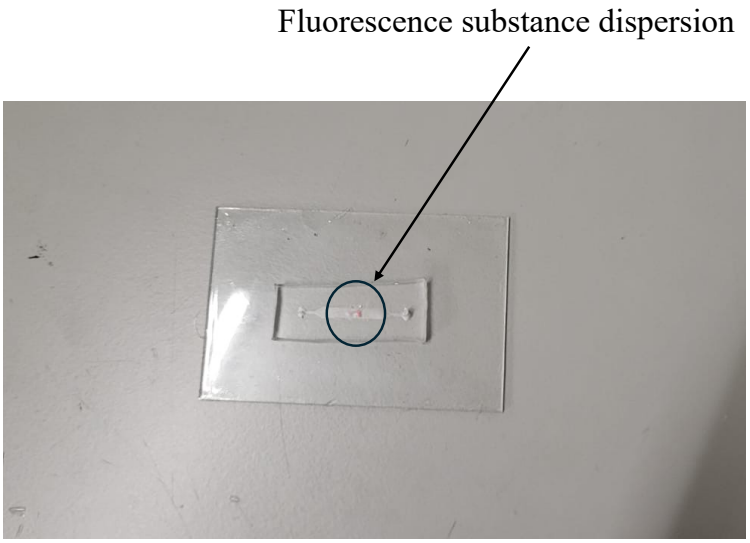


Figure 35: Implementation of the initial fluorescence substance without drying the substance.

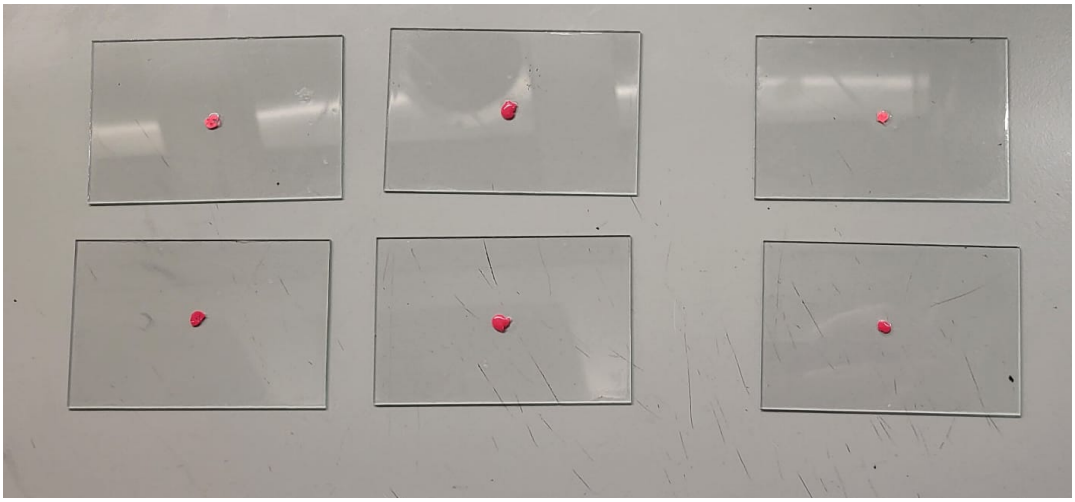


Figure 36: Glass slides after 5 minutes drying in the oven (80º C).

In Figure 37, it is possible to compare the differences between spreading the second layer of PDMS without drying the droplet of sensor (Figure 37 B) and the case where the droplet was dried in the oven for a 5-minute time (80º C temperature).

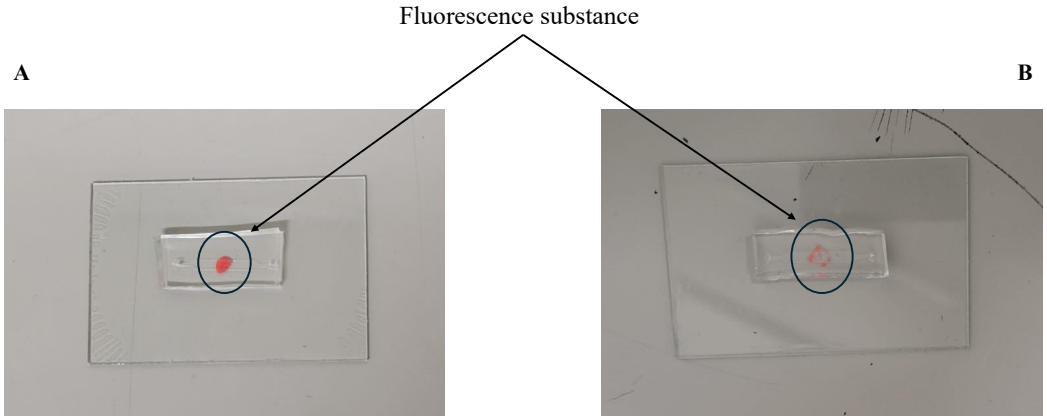


Figure 37: Fluorescence sensor implementing the drying procedure. A – Microchannel device with fluorescence droplet dried. B – Microchannel device where the dried conditions were not enough to ensure that the fluorescence substance maintains in the first layer of PDMS 20:1.

After testing the implementation, the fluorescence substance properties were tested using the microscope. Using the microscope, it was possible to visualize that FluoSpheres® carboxylate-modified, 1.0 μm, nile red (535/575) properties were not affected and the exposure to the light using a mercury filtering turned the fluorescence substance color to orange. The Plasma treatment was effective avoiding long exposure to high temperatures (80º C).

3.7.2. Oxygen sensor implementation

The encapsulation process was explored, but the low availably of PtOEP and difficulties associated to the process of encapsulations can cause challenges. Montagne, Komori [80] built

and tested an approach where the oxygen sensor is dissolved in toluene and in a polymeric material. In this approach, the sensor was implemented in the film and not in a space create between the films. However, encapsulation of the sensor was the selected approach. Preliminary trials were developed with rhodamine B ($C_{28}H_{31}CIN_2O_3$).

A solution of rhodamine B with toluene and PDMS (5:1) was prepared. After that, the procedure of encapsulation described in the microfabrication was applied, with the using of spin-coater and the program "Cavidade" (sector 3.7.1). Different methods were used to encapsulate PDMS embedded with rhodamine: glass slide without drying, glass slide with a drying for 5 minutes at 80º C and glass slide with the same temperature exposure for 10 minutes. Without drying, Rhodamine B was dispersed by the all surface of the second layer of PDMS.

After developing Rhodamine B encapsulated devices, PtOEP (1 mg) + toluene + PDMS (5:1) solution was prepared. In Montagne, Komori [80] trial, toluene was mixed successfully with PtOEP and the sensor was embedded in a PS (a polymer) film. So, PtOEP with toluene and polymer (PDMS) was previously tested and developed in the development of an oxygen sensor. PtOEP was mixed with toluene and that solution was mixed with PDMS 5:1. The procedure of encapsulation was applied to PtOEP using "Cavidade" program in spin coater. In certain situations, toluene can react with plastic, so the use of glass material is recommended. Also, the sensor devices were stored in conditions without light (were stored in a plastic box, covered by aluminum foil, to preserve the sensor functionality, avoiding PtOEP encapsulated droplet from suffering damages due to light continued exposure.

3.7.3. Oxygen sensor tests

Other important aspect to the measuring of the oxygen levels is the control of the expected percentage of oxygen in the blood analogue fluid. For this, a correct experimental setup is required. An effective setup is necessary to ensure that the oxygen detected by the fluorescence sensor is provided by the blood analogue fluid, in particular, by the encapsulated perfluorodecalin particles. So, to the development of the oxygen sensor, scavengers can be used also to approximate the values of oxygen from the ones observed in the biological environment and to test the functionality of the sensor, by creating a decrease of the oxygen levels and the variation of the fluoresce of the sensor. Sodium sulfite (Na_2SO_3) is used as a scavenger and presents the following chemical reaction [101]:

$$2Na_2SO_3 + O_2 \rightarrow 2Na_2SO_4 \quad (8)$$

Sodium sulfite is an oxygen scavenger that present several advantages, like being a low-cost product, produce a colorless product and it is a safe chemical [101]. Considering equation 8, for one mole of O_2, it is required 2 moles of Na_2SO_3 to consume the oxygen present in the system. So, it was calculated the quantities of Na_2SO_3 required to consume all the oxygen in the system in testing, and it was experimented in a preliminary version the addition of a large amount of Na_2SO_3 to water, to analyze if the behavior of the reaction. High levels of Na_2SO_3 were used to achieved conditions of 0% of oxygen in the trial space, but oxygen diffusion in the system and interaction of Na_2SO_3 with other chemicals, such as chlorine, can affect these trials.

To test the variation of fluorescence with the variation of the percentage of oxygen, a solution of water and Na_2SO_3 was placed over the oxygen sensor device. Assuming that Na_2SO_3 would consume all the oxygen in contact with the sensor, the experimental setup presented in Figure 38 was applied. In this test, the water solution presents an oxygen level of 0% and this situation will promote the diffusion of O_2 from the sensor to the water zone, where it is consumed by the Na_2SO_3. This setup promotes the decrease of the oxygen levels and the consequent changing of the color of the sensor (green light from the mercury light, obtained with Y3 filter, will be absorbed and the sensor will emit red light, in the absence of oxygen). The variation of fluorescence was recorded by Leica Camera from the microscope with the use of LAS software. A mercury light source and a Y3 filter were used and the test were executed in a dark room (lights off). The green that passes through the filter has a wavelength between around 520 nm and 565 nm. The green light excites the oxygen sensor, in the absence of O_2, and it emits and a red light with a wavelength between around 625 nm and 740 nm.

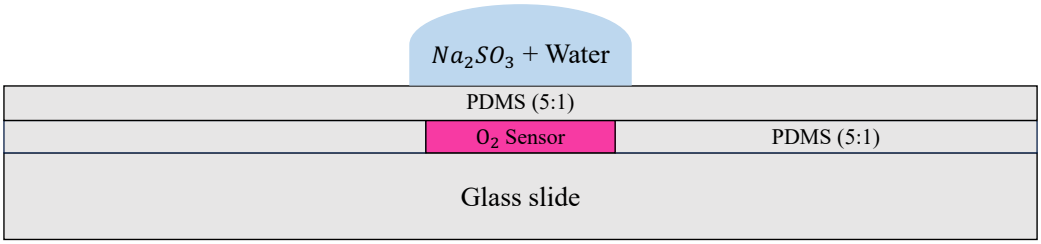


Figure 38: Oxygen sensor test experimental scheme.

After recording the images, the data was treated in Image J software. In first place, two different areas from the images were selected by using the commands "Analyze "-> "Tools" -> "ROI Manager" and creating a rectangular form that is saved by using the command "Add [t]". This procedure was implemented to guarantee that in the different frames, the same part of the image was analyzed. The areas selected are the following ones: an agglomerated formed in the sensor (Figure 39 A) and a normal zone (Figure 39 B).

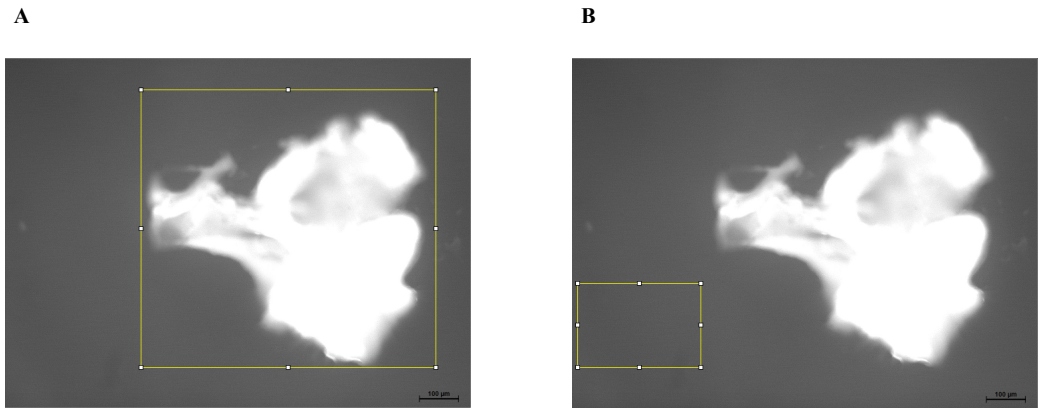


Figure 39: Selected areas of oxygen sensor to the measures or intensity of fluorescence (Image J). A – Agglomerate zone. B – Normal zone.

After selecting the target area in the different frames, “Measure” command was applied (“Set measurements was selected to define the correct parameters) with the objective of measuring the mean gray value, that represents the mean intensity value of the fluorescence in the black and white image that is recorded by Leica Camera.

3.8. Test with microorganisms

The tests with microorganisms were performed using *Saccharomyces cerevisiae*, known as baker’s yeast. This microorganism is probably one of the oldest domesticated organisms known and the first artificial cultivation goes back to 10,000 years [102, 103]. *Saccharomyces cerevisiae* is used in several applications in the food industry (fermentation), but can also be applied to other biologicals purposes.

The trial was performed using the oxygen sensor developed (sector 3.7) in similar conditions (dark room – lights off) and using the same experimental setup/equipment (Microscope with mercury light and Leica Camera). Mercury light source, Y3 filter, 20x objective and 20 intensity parameter were used. Also, Leica Camera parameters were the same in all the measurements (Exposure = 410.0 ms; Gain = 1.7 X and Gamma = 1.47). In the tests, a suspension of *Saccharomyces cerevisiae* was placed in the sensor device and after some time the fluorescence was recorded using Leica Camera. It was expected that *Saccharomyces cerevisiae* would be capable of consuming the oxygen and the system, making the sensor emitting red light. Also, in the same conditions, the sensor was tested with scavenger (Na_2SO_3), diluted scavenger (5:1 and 10:1), water and the PFD particulate fluid (Figure 22) with diluted scavenger (5:1). Figure 40 presents the experimental setup with the yeast suspension placed in the sensor.

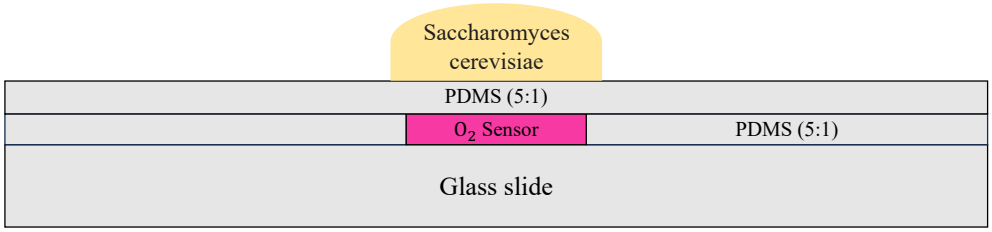


Figure 40: Microorganism test setup.

Chapter 4

Results and discussion

4.1. Microchannels production

Xurography was the most used technique to the production of molds to microfabrication (Figure 41), due to the advantages in the cost of production and in the time from design to fabrication. Flow-focusing design and T-junction were used, with the aim of developing micro-rheometers. Micro-Rheometer results will be presented in section 4.3. The microchannels (Figure 42) were produced by the soft lithography procedure in section 3.2.

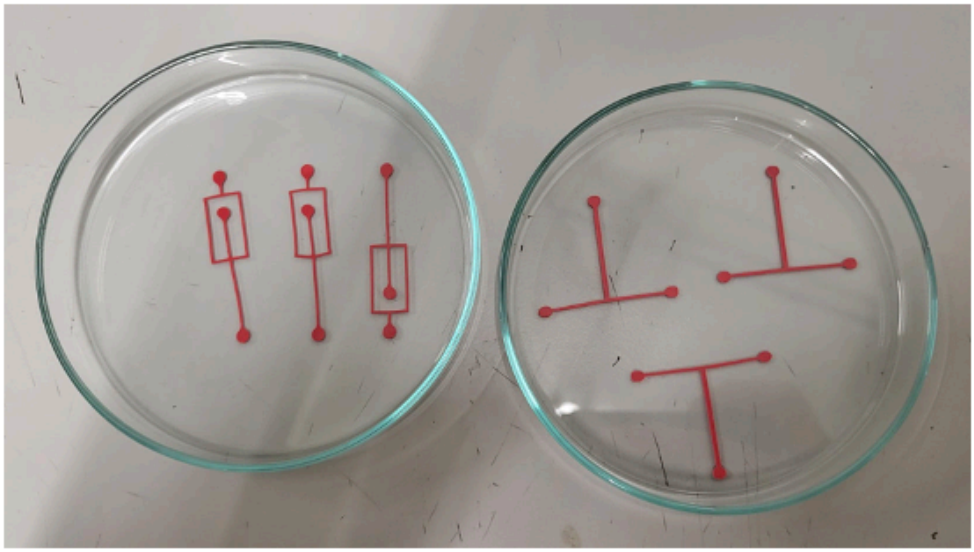


Figure 41: Microchannel molds (T-junction and Flow-focusing).



Figure 42: Example of microchannels procuded by soft litography (Flow-focusing design).

As explored in Chapter 3, the fabrication of the channels using of paper molds, produced by xurography method (section 3.2), is a procedure that depends more on manual work and skill than the ones that use SU-8 molds. Considering this, the production of some channels was affected. One of the major problems of microchannels is the presence of leaks, that makes them unusable. Also, the imperfections in the channels (Figure 43) can affect the production of the droplets, in particular, when the imperfection affect the interception zone or in the inicial zone after the interception, where droplets are forming and stabilizing.

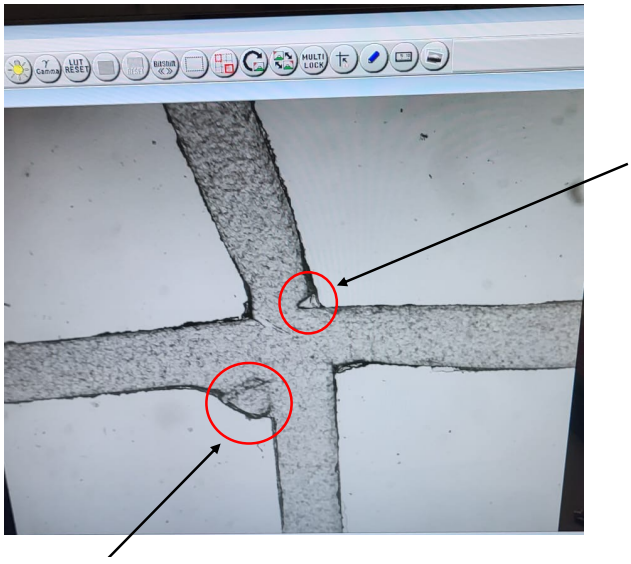


Figure 43: T-junction microchannel with imperfections.

4.2. Particulate fluids

A Blood analogue based on alginate microparticles [13] was provided by CEFT laboratory to the micro-rheometer trial. However, the study of the formation of the droplets, using oil, was difficulted by the properties of the fluid. In fact, the shear-thinning behavior of the fluid made that, at low flow rates, the viscosity of the fluid becomes extremely high. The shear-thinning behavior is expected from a particulate fluid with the main goal of mimicking blood, considering that blood presents that rheology due to the elevate presence of RBCs. Also, particles coalescence occurred, making the process more difficult. In fact, the formation of clusters causes the clog of the syringes and the tubes used in the connection to the microchannels. To overcome these, the fluid was diluted by 50%, but the difficulties were not totally solved. In fact, it was possible to perform the formation of droplets, but without the capacity of prevent the clogging of the equipment.

Other particulate fluids were prepared and were tested. The fluid production procedure was explored in section 3.1.1. The fluids images obtained using microscope and Leica Camera are presented in Figure 44. In the Figure 44 A shows PFD (10%) particulate fluid with Tween 80 (1%) and without PEG, Figure 44 B is for the same fluid with PEG (1%) and Figure 44 C is for PFD (10%) particulate fluid with Tween 80 (1%) and PVA (3%).

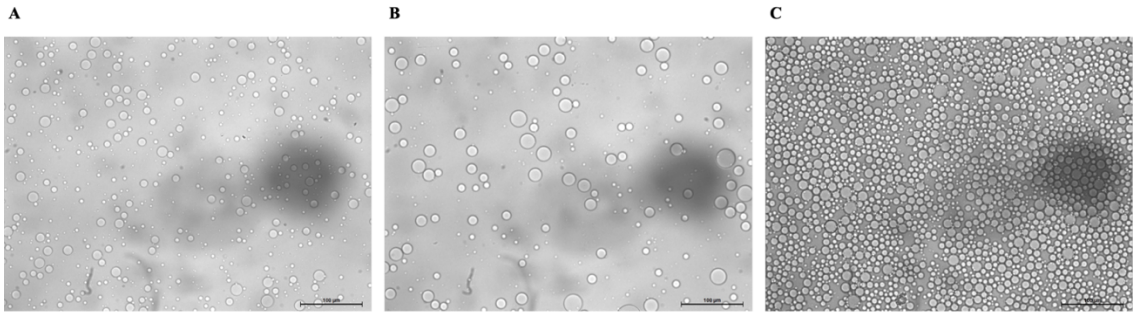


Figure 44: Particulate fluids images (20x objective). A – PFD (10%) particulate fluid without PEG; B – PFD (10%) particulate fluid with PEG (1%). C – PFD (10%) particulate fluid with PVA (3%). Scale bar: 100 μm.

One of the bigger challenges is the stability of the particles, that have the tendency to aggregate forming clusters of particles, like the situation explored previously in this section. Considering this, Tween 80 was used as a surfactant and a stabilizer was also used, in the cases of Figure 44 B and Figure 44 C (PEG and PVA respectively). It is possible to see that in Figure 44 A and Figure 44 B, the particles are not uniform and the dimensions are bigger than the expected maximum of 10 μm, considering that was used a filter of 10 μm and three passages were executed. This fact is even more relevant when the fluid without any stabilizer is compared to the one with addition of PEG, because it was expected that the formation of clusters was reduced in the fluid with PEG. However, particles present higher dimensions in the fluid with PEG when compared to the original fluid (without any stabilizer). This problem was solved with the use of PVA, another stabilizer, that was capable of reducing clustering phenomenon. In fact, the fluid

presented in Figure 44 C, shows particles with a size of 10 μm or lower and a more stable behavior.

4.3. Micro-Rheometers

Several trials were performed to test microchannels as micro-rheometers. In other words, Flow-focusing microchannels and T-junction microchannels were used with the objective of obtaining the viscosity of an unknown fluid, without the application of traditional methods, such as, the use of a rotational rheometer. This solution was developed with the aim of measuring the viscosity of small samples of fluids. To obtain a standard curve for the micro-rheometers, tests with water or water + glycerol and oil were performed, as presented in section 3.6.

4.3.1. Flow-focusing device

For the trials, Figure 26 setup was used (microscope, High Speed Camera and syringe pump). The first step to obtain the values is recording the images of the formation of the droplets using the High Speed Camera and treating them with the software Image J. In Image J, the width of the channel was measured, according to the example in Figure 45. The expected width of the Flow-focusing microchannels used was 600 μm and the expected height was 100 μm.

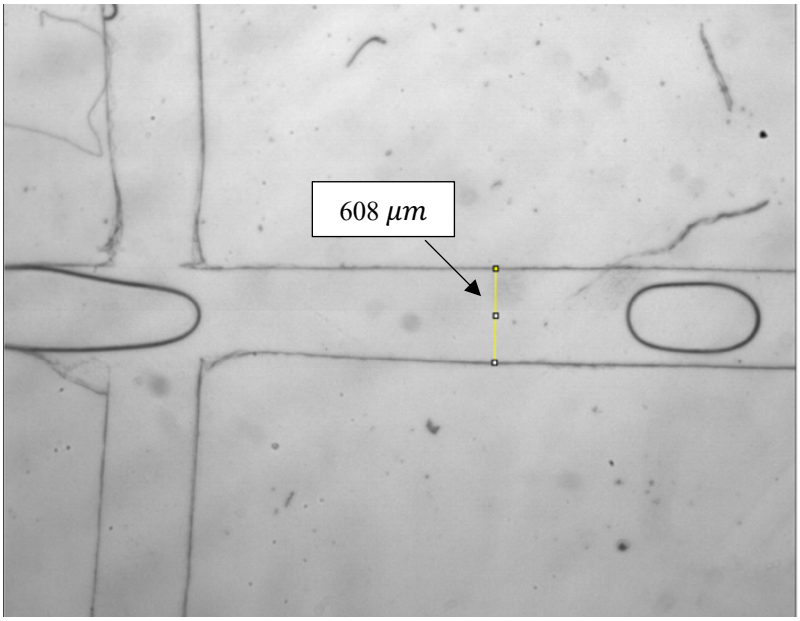


Figure 45: Example of the measuring of the width of the microchannel in Image J - 2.5x Microscope Objective.

To obtain the standard curve, several fluids were used as dispersed phase. Water and water + glycerol (40%, 50% and 60% of glycerol content) were used with fixed values of flow rate. Oil was used as continuous phase, with variable values of flow rate. The dispersed phase fluids were selected to have a standard curve that encompasses a wide range of viscosities. The graphic was

built following the process presented in section 3.6.1. Considering this, using the images recorded, droplets length and the width of the channel were measured. Also, were selected an initial frame and a final frame, where the *x* coordinate was measured (initial and final position). Speed of the droplet was calculated using position and frame parameters (equations 3 and 4). With speed of the droplet, Ca was calculated (equation 6). L/W was calculated dividing the length of the droplet by the width of the channel. Table 7 presents the fluids and the flow rates used in the trials and Figure 46 shows the variation of the length of the droplets, for fixed values of dispersed phase (water + glycerol 40% was selected in Figure 47). In the trials, to a certain value of Q_d, the values of Q_c (oil) was varied.

Table 7: Fixed values of dispersed phase flow used in the trials.

Dispersed phase	Q_d (µL /min)
Water	15
Water	20
Water	25
Water + Glycerol (40%)	10
Water + Glycerol (40%)	15
Water + Glycerol (40%)	20
Water + Glycerol (40%)	25
Water + Glycerol (50%)	2
Water + Glycerol (50%)	5
Water + Glycerol (60%)	5

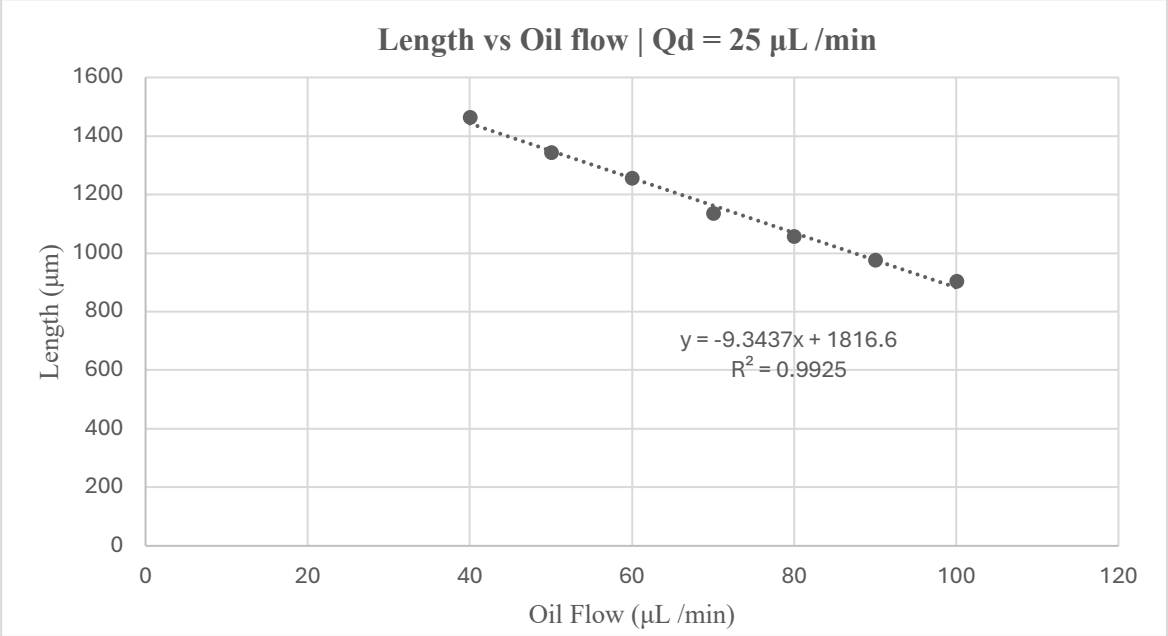


Figure 46: Length of the droplet's variation through the variation of oil flow to a flow of water (of 25 µL /min.

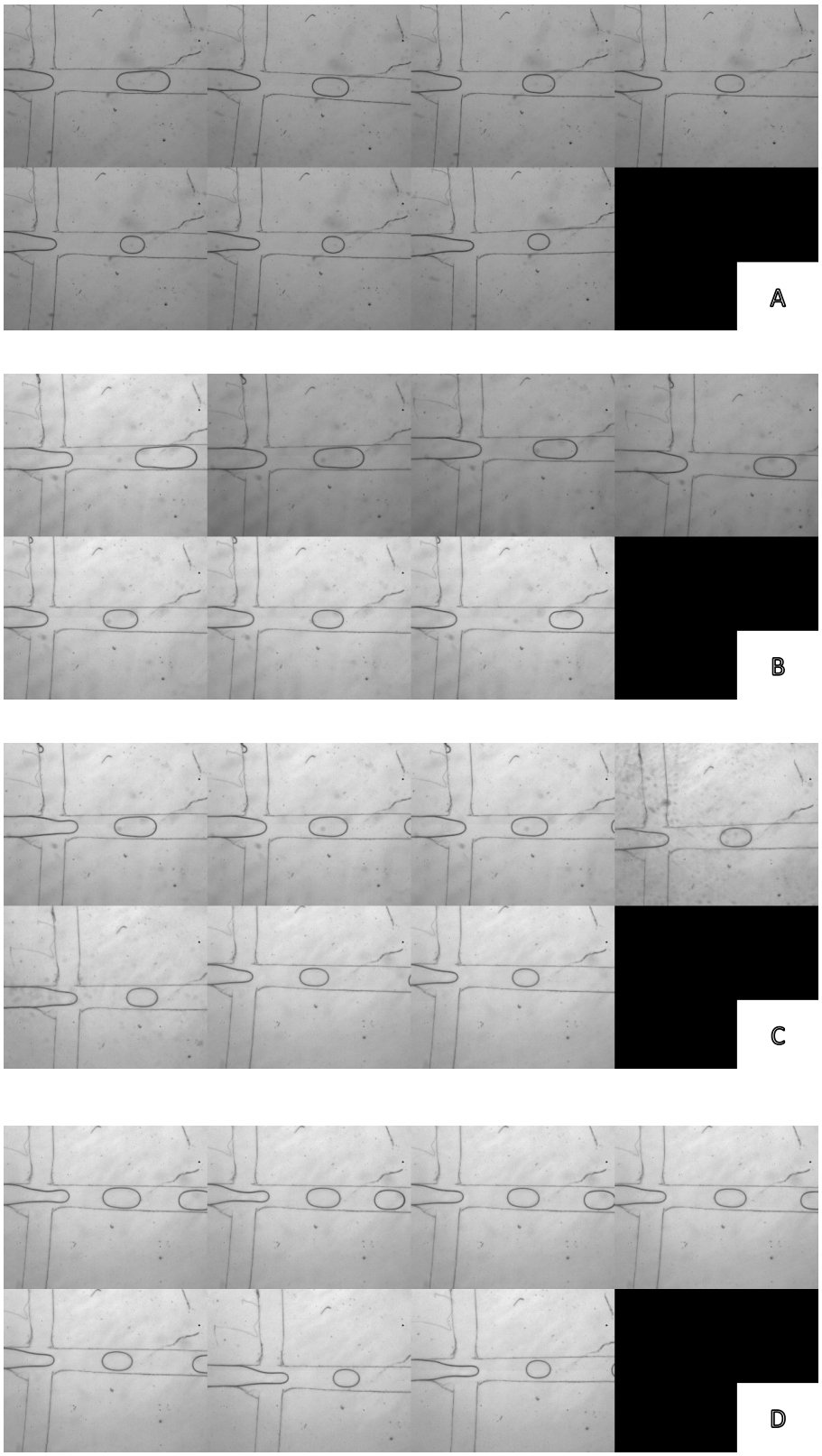


Figure 47: Droplet formation. A – Water + Glycerol (40%) flow: 10 µL/min; B – Water + Glycerol flow: 15 µL/min; C – Water + Glycerol flow: 20 µL/min; D – Water + Glycerol flow: 25 µL/min. Variable flow of oil (continuous phase) for a fixed value of dispersed phase. 2.5x microscope objective used.

Considering the values obtained, the decrease of the value droplet length when the oil flow increases was observed and follows a linear relation. After this, the speed of the droplet was calculated to obtain the necessary values to calculate Ca. As expected in a general way, the increase of the flow of the continuous phase (oil), causes an increase in the speed of the droplet, that was compared with the speed of the fluid (Figure 48).

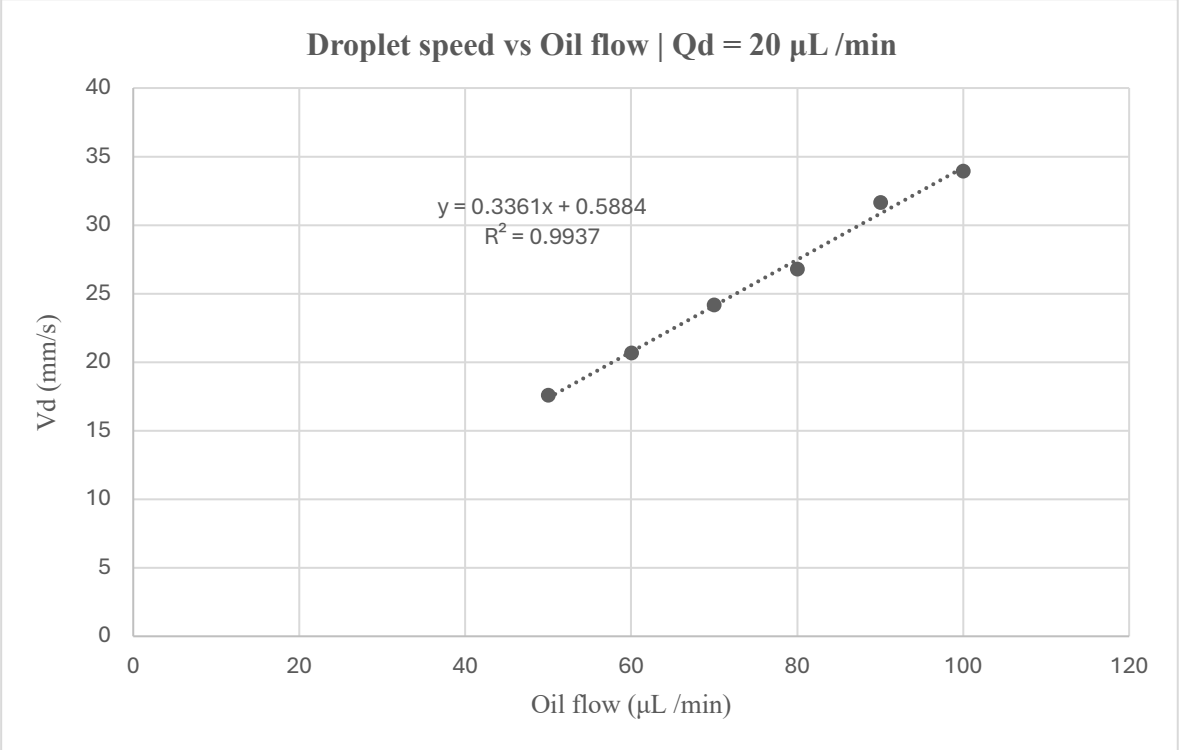


Figure 48: Speed of the droplet's variation through the variation of oil flow to a flow of water + glycerol (40%) of 20 µL /min.

To calculate Ca, interfacial tension between the dispersed phase of the droplet and the continuous one was necessary. Considering this, and the difference between the surface tension and the interfacial tension values (usually the tension between air and a fluid is higher than the same parameter between two fluids), the values of interfacial tension were measured in the Force tensiometer Sigma 701. The procedure of measurement used is described in section 3.5. With the values of interface tension (Table 5), Ca parameter to the different flows of continuous phase were calculated. Considering this, the graphic of the normalized length (*L/W*) in function of Ca was built (Figure 49). Water, water + glycerol (40%), water + glycerol (50%) and water + glycerol (60%) values where to finding a standard curve to estimate the value of viscosity to an unknown fluid.

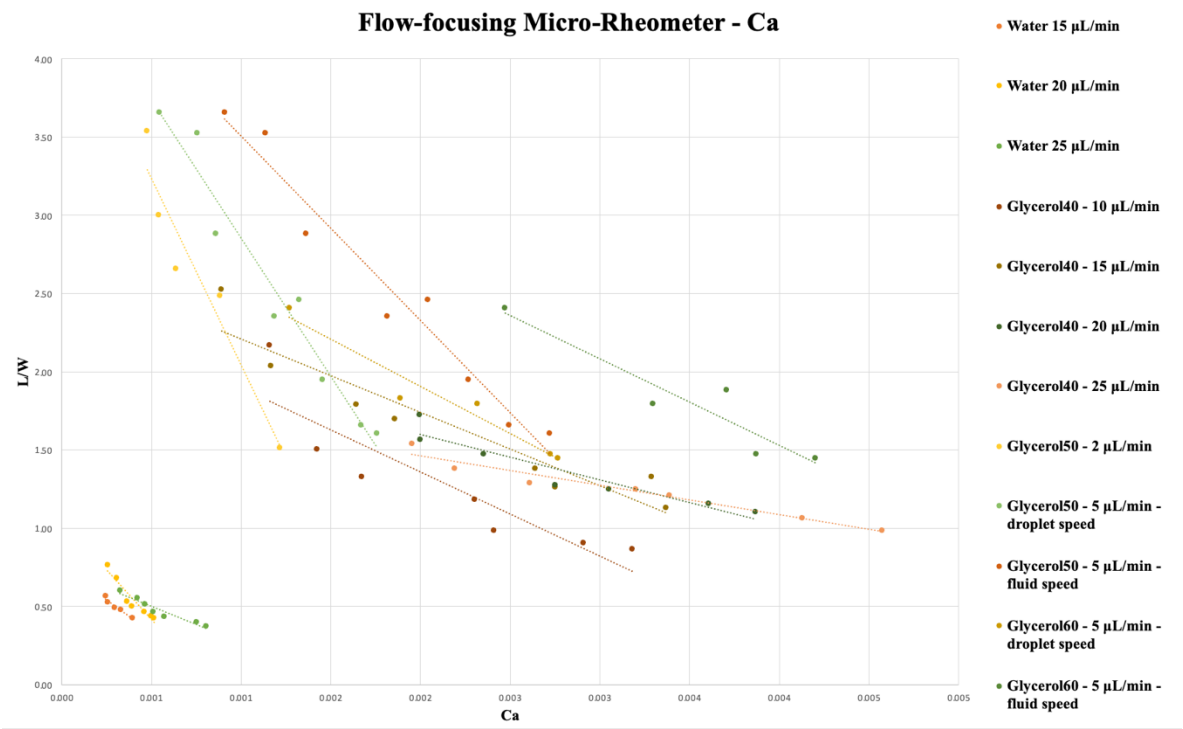


Figure 49: Ca x *L/W* graphic – Micro-rheometer.

As presented in Figure 49, it was not possible to obtain a unique standard curve for the values of water and water with the addition of glycerol. Considering this, the measurement of the viscosity by the calculation of Ca parameter cannot be applied. One factor that could explained the differences is the ratios between flows that were used, that were not the same to the different trials. Considering the results obtained, it is possible to conclude that viscosity doesn't depend exclusively on Ca, contrary to what was initially hypothesized. In fact, viscosity is affected by other parameters like the flow rate ratio and the ratio of the viscosities of the fluids.

Another approach was tested. In fact, ratios of flow (Q_c/Q_d) were selected, respectively 3 and 5, and droplet microfluidics technique was applied. For the ratios selected, different values of flow were used. Water and water + glycerol (40%, 50% and 60%) were used as dispersed phase and Oil was used as continuous phase. For the fluids of the dispersed phase, medium values of *L/W* were calculated and a curve for each ratio was built, using the values of *L/W* and the ratio of viscosities between dispersed phase and continuous phase (Q_d/Q_c). After that, blood analogue based on alginate microparticles [13] and PFD (10%) particulate fluid were assessed. In the case of these two fluids, the values of *L/W* were obtained as presented previously. Considering this, was estimated a value of viscosity to the fluids with unknown viscosity. The estimated values of viscosity were 0.008 Pa.s, 0.0026 Pa.s and 0.016 Pa.s, respectively for the PFD (10%) particulate fluid ratio 3, for the PFD (10%) particulate fluid ratio 5 and blood analogue based on alginate microparticles [13]. Figure 50 presents the graphic with the curves of ratio 3 and 5 and the particulate fluids values for the same ratios (ratio 3 and 5 for PFD particulate fluid and ratio 5 for the Blood analogue based on alginate microparticles [13]). Table 8 presents the results from the trials made with PFD particulate fluid.

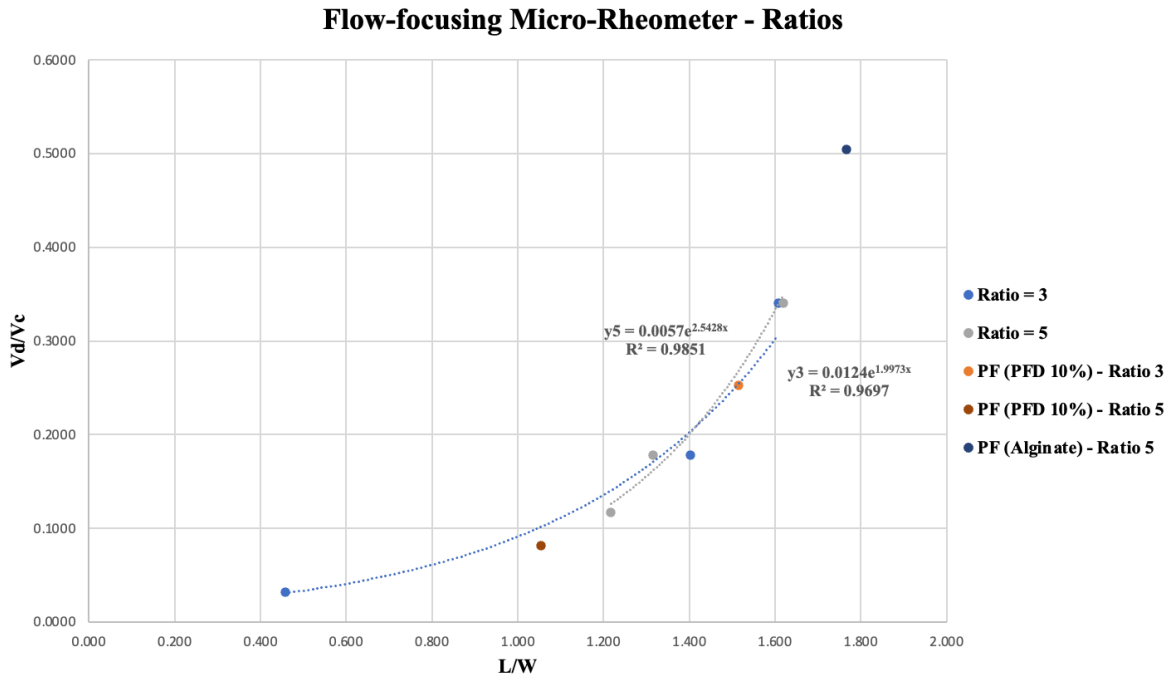


Figure 50: Ratio Micro-rheometer with the standard curves and estimations for alginate particulate fluid [13] and PFD (10%) particulate fluid. Ratio 3 standard curve is represented by blue dashed line and Ratio 5 standard curve is represented by gray dashed line.

Table 8: PFD (10%) particulate fluid results.

Q_{PF} (µL /min)	Q_{oIL} (µL /min)	Q_{Oil} /Q_{PF}	Length (µm)	Time gap (s)	Droplet speed (mm/s)	Fluid speed (mm/s)	L/W	η_{PF}/η_{Oil}
2	6	3	1120	0.23	2.46	2.22	1.867	1.107
3	9	3	1104	0.12	3.45	3.33	1.840	1.035
4	12	3	936	0.09	3.85	4.44	1.560	0.866
5	15	3	768	0.07	5.88	5.56	1.280	1.058
10	30	3	616	0.07	10.71	11.11	1.027	0.964
1	5	5	968	0.16	1.89	1.67	1.613	1.133
2	10	5	640	0.13	3.42	3.33	1.067	1.025
3	15	5	552	0.06	6.84	5.00	0.920	1.368
4	20	5	536	0.14	6.24	6.67	0.893	0.935

Analyzing the results obtained, it was possible to find a value of viscosity for the PFD (10%) particulate fluid in ratio 3 and ratio 5 (0.008 Pa.s and 0.0026 Pa.s, respectively). The value of viscosity for ratio 3 was directly obtained in the standard curve. For ratio 5, the value obtained was significantly lower due to the decrease of the *L/W* parameter. For ratio 5 of the PFD (10%) particulate fluid and for the particulate fluid based on alginate [13], the values were outside of the standard curve range. In these cases, it would be required to acquire more data, in particular from a solution of water + glycerol with a higher content of glycerol (80% for instance), that would be a solution with a higher viscosity than the ones used in the construction of the standard curve, and another with lower viscosity (water or water with the addition of glycerol at 20%). However, it

was possible to use the curves to extrapolate the values of viscosity for both fluids of ratio 5. Blood analogue based on alginate microparticles [13] presented a high value viscosity and the phenomenon of clustering was observed in the trials.

4.3.2. Preliminary results from T-junction device

The procedure of measurement and the experimental setup (Figure 26) are similar to the presented in section 4.3.1. Microscope, High Speed Camera and syringe pump were used to perform the trials and Image J was used to treat the data obtained. PFD (10%) particulate fluid and oil were used to test the micro-rheometer using T-junction microchannels (Figure 51). The results of the trials are presented in Table 9.

Table 9: T-junction micro-rheometer results with PFD (10%) particulate fluid and oil. Q_1/Q_2 = 1.

Q_{PF} (µL /min)	Q_{oil} (µL /min)	Particulate fluid thickness (µm)	Oil thickness (µm)	Total thickness (µm)	$\frac{h_{oil}}{h_{PF}}$
1	1	184.2	424.3	608.5	2.304
1	1	152.0	456.0	608	3.000
10	10	96.3	512.1	608.4	5.316
10	10	152.2	464.0	616.2	3.048
10	10	148.0	448.0	596.0	3.027

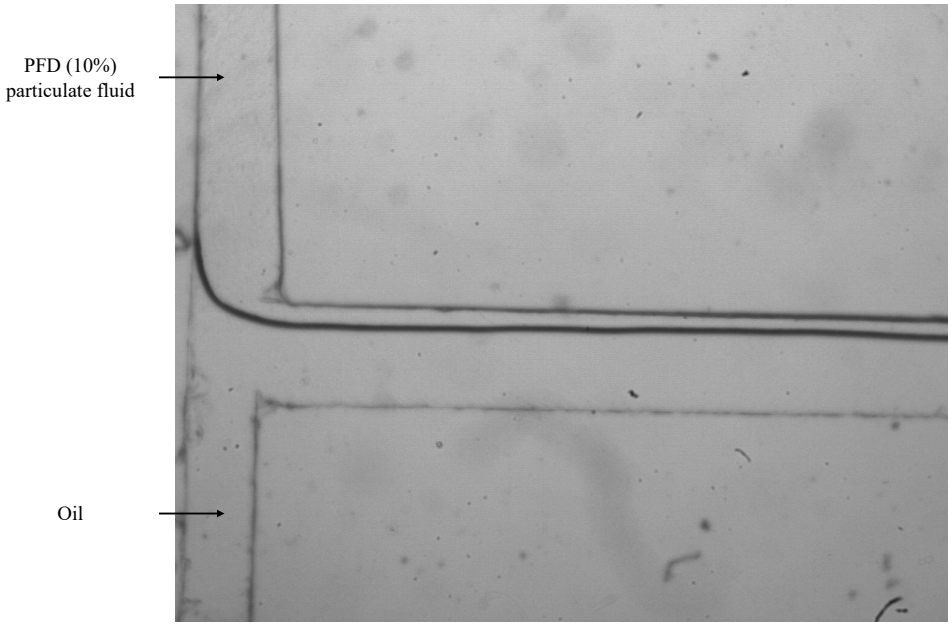


Figure 51: T-junction micro-rheometer trial example. $Q_{oil} = Q_{PF} = 10\ \mu L$/min.

Ratio of thickness are presented in table 7 and the average values were calculated. The medium values of ratio were calculated and are 2.652 and 3.797 for flows of 1 $\mu L/min$ and 10 $\mu L/min$ respectively. The global media for the values obtained in the trials were 3.339. The average value of total thickness is 607 µm, that is slightly the same from the measured value of

thickness of the channel (608 μm) and the value of expected thickness of the channel (600 μm). The average values from ratio are slightly different (2.652 and 3.797), but when individual values are compared, 3 of them, 2 from 10 $\mu L/min$ and 1 from 1 $\mu L/min$ present values of ratio around 3 (3.000, 3.048 and 3.027) and 2 of them (1 from each value of flow) are clearly different from these values (2.304 and 5.316). The values of viscosity were calculated considering that the ratio of viscosities is approximately equal to the ratio of thicknesses. Oil viscosity is 0.0317 Pa.s. Considering this, the viscosity of the particulate fluid is 0.012 Pa.s and 0.008 Pa.s for the flows of 1 $\mu L/min$ and 10 $\mu L/min$, respectively. These values can be used to make preliminary considerations to the relation from the ratio of thickness and the ratio of viscosities. However, the relation need to be verified experimentally.

4.4. Oxygen sensor

The oxygen sensor was developed using the procedure of encapsulation presented in section 3.7.2 and it was possible to achieve the goal of place a droplet of PtOEP + toluene + PDMS (5:1) in the cavity, with another PDMS (5:1) layer above. Figure 52 presents the sensor device that was obtained.



Figure 52: Oxygen sensor implementation - glass slide with PtOEP encapsulated.

The oxygen sensor was tested using a solution of water with an oxygen scavenger, Na_2SO_3 (Figure 38), to obtain a solution with a concentration of oxygen near zero. The variation of the fluorescence was recorded using LAS software, according to the method presented in section

3.7.3. Microscope, Leica black and white Camera, mercury lamp and Y3 filter were used (section 3.7.3). During the time, occurs the diffusion from the O_2 from the sensor to the water + Na_2SO_3 solution (O_2 levels close to 0% due to the saturation of scavenger). The oxygen are consumed by the Na_2SO_3 and the levels of oxygen decrease with the time. With the passage of the time and the increasing of the fluorescence, due to the consumption of O_2, the image goes from a black color to a white color. The time was registered during the trial. The variation of the color of the sensor is presented in Figure 53, where the initial images are the ones where oxygen was at high levels (approximately atmospherically level) and with time the images recorded became lighter, that corresponds to the decrease of oxygen level in the sensor util it is reaching a value close to 0%.

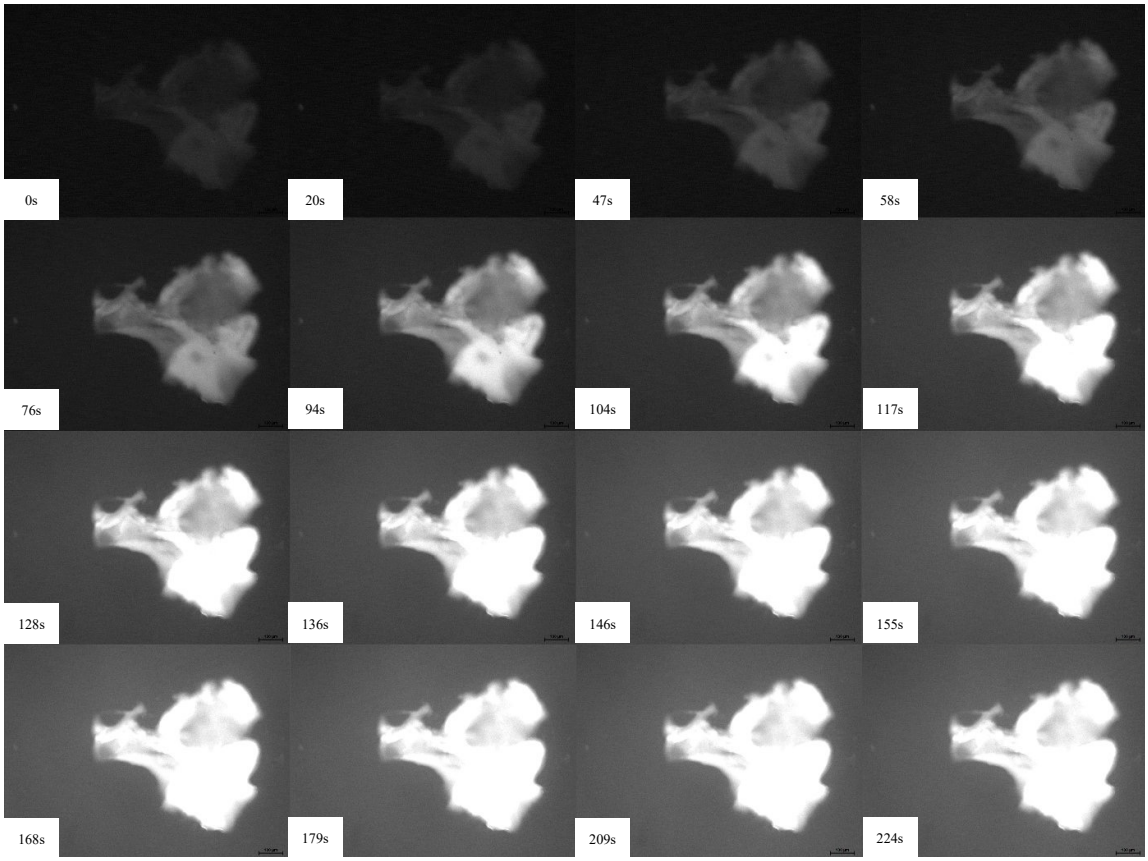


Figure 53: Images of the sensor fluorescence variation with the decrease of the oxygen level.

As presented, the fluorescence of the sensor increased with the time, that represents the decreasing of the level of O_2. One of the main threats to the process of encapsulation was the exposure of the sensor to high temperatures in microfabrication, but as presented, the properties of the sensor were not affected. Also, reflection of the light was not observed. The presence of two different zones allowed to observe the variation of fluorescence through two different perspectives. In fact, the agglomerate zone presents a higher variation of fluorescence and a higher capacity of fluorescence. The agglomerate is possibly a zone where the concentration of sensor is higher than the rest of the encapsulated PtOEP. Figure 54 presents the graphic variation of the mean gray value, that represents the mean value of fluorescence in the area selected in Image J, through time. Mean gray value is the measure of the average intensity of the pixels in a selected area of an image. This parameter corresponds to a gray scale, so the lower values correspond to a

black image and the higher ones to a white image. For an 8-bit image, the scale of mean gray value is between 0 and 255.

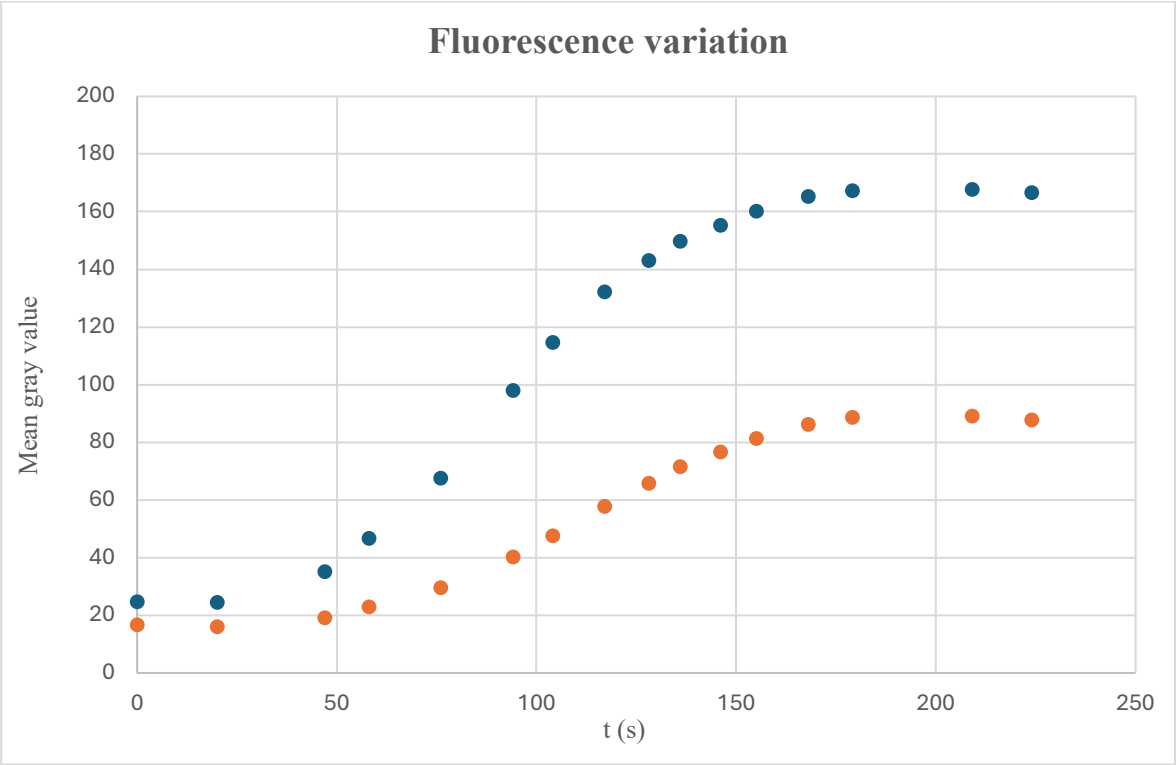


Figure 54: Fluorescence variation according to the time of the trial. Blue dots – Agglomerate zone (Figure 39 A); Orange dots – Normal zone (Figure 39 B).

Analysing the behavior of the curves, it is possible to confirm that the fluorescence increased with the time until reaching the maximum level, both to the case of the agglomerate structure (blue dots) and for the normal zone (orange dots). In the initial part of the measurements, the system presented high levels of O_2 (around the atmospheric level), because the reaction of consumption of the oxygen was at an initial stage. After 50s, the levels of oxygen started to decrease, according to the increase of the fluoresce values, until reaching the maximum limit of fluorescence (around 179s time). According to the setup of the experiment (high levels of Na_2SO_3), it is expected that the maximum level of the fluorescence represents a level of oxygen near 0%. It is possible to analyse also that the agglomerate zone presents a higher capacity to fluoresce when compared to the normal zone.

To quantify the levels of oxygen in the different stages, another method or a calibration of this method would be required. However, the assumptions of the levels of O_2 in the early stages (around 20,9% [23]) and at the end of the trial (approximately 0%) are probably correct. In fact, is possible to understand, considering the behavior of the graphic, that the levels of O_2 stabilized in the final part of the experiment, indicating that Na_2SO_3 consumed the maximum level of O_2 and that the reaction continues with the Na_2SO_3 that was not consumed and with the oxygen that enters in the system. In the early part, the assumption of the atmospheric level of oxygen in the

sensor zone is justified by the high O_2 permeability of PDMS and the exposure of the device to air.

As explored, the fluorescence of PtOEP was ultimately related to the levels of oxygen in the environment in study. Considering this, Figure 55 represents a limit situation where it is possible to see the behavior of the sensor with the presence of oxygen and in its absence. In Figure 55 B, it is possible to see the border between the zone with normal levels of O_2 and the zone with lower levels of O_2 (presence of $Na_2SO_3 + H_2O$). In Figure 55 A, it is possible to see the transition of color, from the zone with normal levels of oxygen and the zone with lower levels ($Na_2SO_3 + H_2O$).

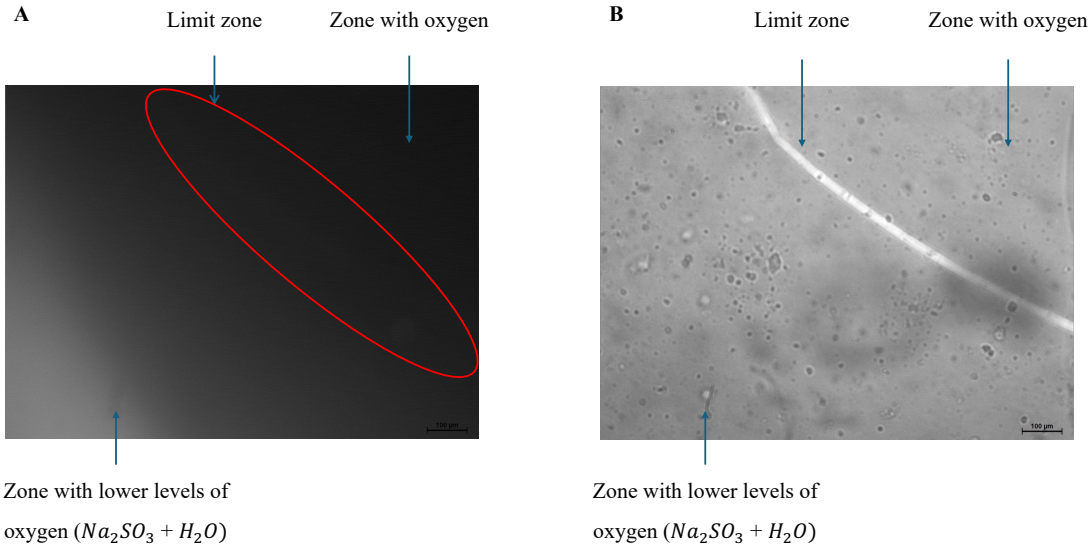


Figure 55: Oxygen sensor detection of fluorescence in a limit zone. A – Fluorescence light on; B – Image without fluorescence.

4.5. Test with microorganisms

Oxygen sensor was used to assess oxygen consumption of *Saccharomyces Cerevisiae* in suspension, as explored in section 3.8. Also, were executed tests with Na_2SO_3 solutions and with the particulate fluid developed in this work, to compare the values that were obtained. The images captured using Leica Camera are presented in Figure 56. Also, Table 10 presents the values of the Mean Gray Value obtained using Image J software.

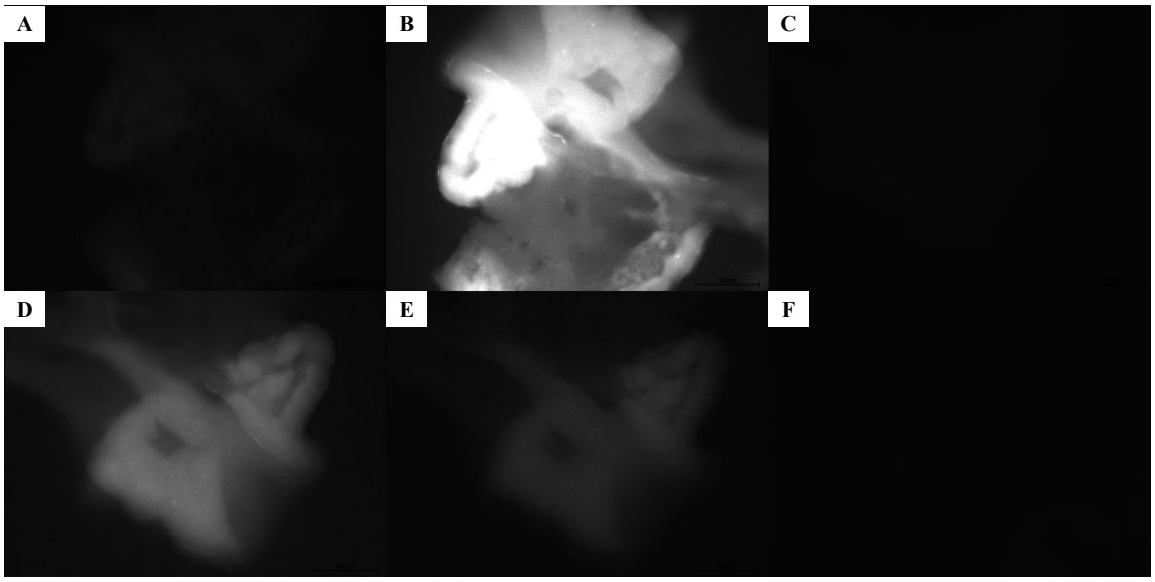


Figure 56: Recorded images from the microorganism's trials. A - *Saccharomyces cerevisiae* suspension; B – Scavenger (Na_2SO_3 + water); C – Water; D – Diluted scavenger (5:1); E – Diluted Scavenger (10:1); F – PFD particulate fluid + diluted scavenger (5:1).

Table 10: Mean Gray Value from Figure 57 images

Image	Mean gray value
A	9.42
B	124.55
C	5.68
D	44.77
E	18.00
F	5.02

The mean gray value from water (Figure 56 C) is 5.68 and is the reference in this trial to the atmospheric value of oxygen (around 20.9% [23]). Also, it is possible to evaluate the effects of the scavenger (Na_2SO_3) due to the use of three solutions, with different concentrations of Na_2SO_3. For a higher content of Na_2SO_3, the system present lower values of oxygen and the mean gray value is higher (more fluorescence).

Analyzing Figure 56 and the data from Table 10, it is possible to compare the suspension of *Saccharomyces cerevisiae* to the control (Water – Figure 56 C). In the trials, was possible to see a slight fluorescence in the *Saccharomyces cerevisiae* suspension that is represented by a mean gray value of 9.42. The fluorescence of the sensor in this situation is low, due to some factors. First of all, the microorganism could present low activity and it is expected that in this case the level of oxygen is around 20% of the saturation level. This value indicates that *Saccharomyces cerevisiae* had consumed oxygen. Also, this sensor presents a low definition, so, to observe clearly the differences between Figure 56 A and Figure 56 C, the difference of level of oxygen would

have to be higher or an amplification of the signal from the sensor would be required. For instance, with higher levels in the gain parameter, the differences between both images would be higher.

Other situation that could affect the results is the spatial resolution. In fact, due to the efforts to encapsulate the PtOEP solution, a PDMS layer was applied above the sensor. In this case, the PDMS is too thick. Considering the thickness between the sensor and the zone where the solution of *Saccharomyces cerevisiae* is placed and the permeability from the PDMS for oxygen, the oxygen enters laterally in the sensor and this affects the spatial resolution of the sensor. In this case, with a higher spatial resolution and an amplified signal, in Figure 56 A, it probably would be possible to see the zone with lower levels of oxygen (suspension of *Saccharomyces cerevisiae*) and the zone with more oxygen.

In Figure 56 F, it is presented a trial where PFD (10%) particulate fluid was used with diluted scavenger (5:1). The mean gray value obtained (5.02) is slightly lower than the one presented in the water measurement (Figure 56 C). In this trial, it was expected to have a scavenger solution that doesn't consume all the oxygen from the particulate fluid. In this case, the particulate fluid would be annulled partially and, with a higher spatial resolution, two zones would also be observed, one with higher levels of oxygen, due to the presence of PFD, (black image) and one with lower levels of oxygen (fluorescence).

Chapter 5

Conclusions

5.1. Conclusions

This work goal was to develop and characterize a blood analogue fluid with the capacity of transporting oxygen. To achieve that, an effective oxygen sensor and a micro-rheometer were required, respectively to measure the levels of oxygen for testing the RBCs substitutes (PFD encapsulated particles) and to measure the viscosity of a small sample. Also, the study of PFD particulate fluids was an important step to this work.

A PFD particulate fluid was developed with success using membrane emulsification approach (Figure 22). That fluid was used in tests of development of micro-rheometer and also in the final tests with the oxygen sensor.

To assess if the particulate fluid presents blood-like properties, some tools are needed. For measuring oxygen, PtOEP oxygen sensor was used to develop an oxygen sensor. The methodology of encapsulation of the PtOEP solution was implemented with success, in particular in the protection of the properties of fluorescence from the exposure to the curing process temperatures. Also, for a solution with water and Na_2So_3 (a scavenger), it was possible to detect the variation of oxygen through the time. The tests using microorganisms were inconclusive due to the low spatial resolution of the sensor that affects the measurements of fluorescence with *Saccharomyces cerevisiae*. So, tests with microorganisms need to be repeated as will be explored in future work.

In terms of mechanical behavior, the assessment of the viscosity of a particulate fluid using microfluidics techniques was explored, with Flow-focusing and T-junction microchannels. The trials with flow-focusing microchannels were conclusive in verifying that viscosity doesn't depend only on Ca. Ratio of viscosity as independent property was explored and some of the values of viscosity were measured to the viscosity of particulate fluids. Using flow-focusing

microchannels, it was possible to build two standard curves for ratio 3 and 5 of viscosities and to predict the value of viscosity for PFD (10%) particulate fluid (0.008 Pa.s for ratio 3 and 0.0026 Pa.s for ratio 5) and for alginate particulate fluid (0.016 Pa.s). For T-junction microchannels, preliminary values of viscosity were measured for PFD (10%) particulate fluid (0.008 Pa.s and 0.012 Pa.s).

5.2. Future works

This work was focused on microfluidics tools to the study blood analogue fluids, in particular in the development of the oxygen fluorescence sensor and in the development of a micro-rheometer. As explored, these two tools are very important in the development of a blood analogue fluid based in PFD, that present the capacity of transporting oxygen without losing the similarity in the mechanical properties. Also, a PFD particulate fluid was developed and tested using the membrane emulsification technique. Although, the work developed is not finished, so, future work steps could be explored.

The perfluorodecalin encapsulation is a major challenge to have a fluid that matches blood both in mechanical properties and in the capacity of transporting of oxygen. As explored in this work, it is possible to encapsulated PFD using double emulsion techniques in microfluidic devices. This would allow to overpass same issues in the production of particles by membrane emulsification, like the need to use large amount of product to obtain particles and the difficulties in the control of the size of the particles. Also, the particulate fluid developed in this work doesn't present encapsulated PFD and the encapsulation process is vital to PFD mimic RBCs. To perform encapsulation, it is vital to solve a problem explored in sector 2.3. In fact, the double emulsion of PFD in alginate and in oil would require respectively hydrophilic channel and a hydrophobic channel (Figure 15). Ideally, this double emulsion would be executed in a single channel (Figure 15 B) to avoid the coalescence of the droplets in the tubing,

Micro-rheometers were developed, using both flow-focusing and T-junction channels. Analyzing the results, it is not possible to use the Capillary Number as an independent variable to determine viscosity as viscosity depends on additional variables. The flow-focusing and the T-junction microchannels could probably be used as micro-rheometers using viscosity ratio as independent variable, but further trials and development of procedures. In future work, the test of more values for each method would be required. In the case of the flow-focusing microchannel trials, the standard curve as to extended to a zone of higher viscosity values, so droplet microfluidics technique should be used to collect values for a solution of water and glycerol, with a higher value of glycerol (80%) Also, more values should be obtained for particulate fluids. To T-junction microchannels, trials with water and oil could be performed to predict better the behavior of the micro-rheometer and the trials made should be repeated to have more values of thickness, to verify the conclusions obtained. After these procedures, the values of viscosity obtained from using micro-rheometer should be compared to the traditional methods of viscosity measuring. Also, it is necessary to verify, to other fluids, that the relation between ratio of thicknesses and ratio of viscosities is correct.

Oxygen sensor was developed with positive results, in particular the fluorescence of the sensor varies due to the variation of oxygen. Also, generally, the process of fabrication was designed and applicated with success. As future works, the calibration of the sensor is vital. Also, it is required to improve the spatial resolution and the testing of the new version of the sensor with microorganisms, such as bacterias. To solve the problem of spatial resolution, probably will be required to decrease the thickness of PDMS layers, by using a higher speed of rotation of the spin coater.

References

1. Timsit, J.-F., et al., *Expert consensus-based clinical practice guidelines management of intravascular catheters in the intensive care unit.* Annals of intensive care, 2020. **10**(1): p. 1-26.
2. Boulet, N., et al., *How to improve the efficiency and the safety of real-time ultrasound-guided central venous catheterization in 2023: a narrative review.* Annals of Intensive Care, 2023. **13**(1): p. 1-10.
3. Oliveira, T.G.P.d., et al., *Compliance with central venous catheter infection prevention practices after intervention with simulation.* Revista Brasileira de Enfermagem, 2023. **76**: p. e20220574.
4. van den Bosch, C., et al., *The efficacy of taurolidine containing lock solutions for the prevention of central-venous-catheter-related bloodstream infections: a systematic review and meta-analysis.* Journal of Hospital Infection, 2022. **123**: p. 143-155.
5. Murga, R., J. Miller, and R. Donlan, *Biofilm formation by gram-negative bacteria on central venous catheter connectors: effect of conditioning films in a laboratory model.* Journal of clinical microbiology, 2001. **39**(6): p. 2294-2297.
6. Wang, H., et al., *Effectiveness of antimicrobial-coated central venous catheters for preventing catheter-related blood-stream infections with the implementation of bundles: a systematic review and network meta-analysis.* Annals of intensive care, 2018. **8**(1): p. 1-12.
7. Lima, R., et al., *Fast, flexible and low-cost multiphase blood analogue for biomedical and energy applications.* Experiments in Fluids, 2020. **61**: p. 1-11.
8. de Pinho, D.M.D., *Blood rheology and red blood cell migration in microchannel flow*. 2018, Universidade do Porto (Portugal).
9. Jacob, M., D. Chappell, and B.F. Becker, *Regulation of blood flow and volume exchange across the microcirculation.* Critical Care, 2016. **20**(1).
10. Shah, S., et al., *The Heart: Anatomy, Physiology and Exercise Physiology*. Springer Berlin Heidelberg. p. 3-22.
11. Fred Shaffer PhD, B. and J.V. MAE, *Heart rate variability anatomy and physiology.* Biofeedback (Online), 2013. **41**(1): p. 13.

12. Shah, S., et al., *The heart: Anatomy, physiology and exercise physiology*, in *Integrating Cardiology for Nuclear Medicine Physicians: A Guide to Nuclear Medicine Physicians*. 2009, Springer. p. 3-22.

13. Moreira, A., et al., *Production and characterization of a blood analogue based on0020alginate microparticles.* Colloids and Surfaces A: Physicochemical and Engineering Aspects, 2024: p. 134022.

14. Carneiro, J., et al., *A microparticle blood analogue suspension matching blood rheology.* Soft Matter, 2021. **17**(14): p. 3963-3974.

15. Sadek, S.H., et al., *Blood particulate analogue fluids: A review.* Materials, 2021. **14**(9): p. 2451.

16. Rodrigues, R.O., et al., *In vitro blood flow and cell-free layer in hyperbolic microchannels: Visualizations and measurements.* BioChip Journal, 2016. **10**: p. 9-15.

17. Jansman, M.M. and L. Hosta-Rigau, *Recent and prominent examples of nano-and microarchitectures as hemoglobin-based oxygen carriers.* Advances in colloid and interface science, 2018. **260**: p. 65-84.

18. Baskurt, O.K. and H.J. Meiselman. *Blood rheology and hemodynamics*. in *Seminars in thrombosis and hemostasis*. 2003. Copyright© 2003 by Thieme Medical Publishers, Inc., 333 Seventh Avenue, New ….

19. Sousa, P.C., et al., *Extensional flow of blood analog solutions in microfluidic devices.* Biomicrofluidics, 2011. **5**(1): p. 014108.

20. Puig-de-Morales-Marinkovic, M., et al., *Viscoelasticity of the human red blood cell.* American Journal of Physiology-Cell Physiology, 2007. **293**(2): p. C597-C605.

21. Li, X., et al., *Probing red blood cell mechanics, rheology and dynamics with a two-component multi-scale model.* Philosophical Transactions of the Royal Society A: Mathematical, Physical and Engineering Sciences, 2014. **372**(2021): p. 20130389.

22. Sousa, P.C., et al., *Rheological behavior of human blood in uniaxial extensional flow.* Journal of Rheology, 2018. **62**(2): p. 447-456.

23. Palacio-Castañeda, V., et al., *Oxygen control: the often overlooked but essential piece to create better in vitro systems.* Lab on a Chip, 2022. **22**(6): p. 1068-1092.

24. Azimzadeh, M., et al., *Microfluidic-based oxygen (O2) sensors for on-chip monitoring of cell, tissue and organ metabolism.* Biosensors, 2021. **12**(1): p. 6.

25. Koens, R., et al., *Microfluidic platform for three-dimensional cell culture under spatiotemporal heterogeneity of oxygen tension.* APL Bioengineering, 2020. **4**(1): p. 016106.

26. Kodama, T., et al., *Volumetric and Angiogenic Evaluation of Antitumor Effects with Acoustic Liposome and High-Frequency Ultrasound.* Cancer Research, 2011. **71**(22): p. 6957-6964.

27. Michiels, C., *Physiological and Pathological Responses to Hypoxia.* The American Journal of Pathology, 2004. **164**(6): p. 1875-1882.

28. Organization, W.H., *Global status report on blood safety and availability 2021*. 2022: World Health Organization.

29. Jones, J.M., et al., *Slowing decline in blood collection and transfusion in the United States – 2017.* Transfusion, 2020. **60**(S2).

30. Custer, B., et al., *Addressing gaps in international blood availability and transfusion safety in low- and middle-income countries: a NHLBI workshop.* Transfusion, 2018. **58**(5): p. 1307-1317.

31. Kim, J.-H., E.-A. Jung, and J.-E. Kim, *Perfluorocarbon-based artificial oxygen carriers for red blood cell substitutes: considerations and direction of technology.* Journal of Pharmaceutical Investigation, 2024. **54**(3): p. 267-282.

32. Wisser, D., et al., *Blood Loss from Laboratory Tests.* Clinical Chemistry, 2003. **49**(10): p. 1651-1655.

33. Ahmed, H., E.A. Khan, and B.T. Stokke, *Microfluidic dual picoinjection based encapsulation of hemoglobin in alginate microcapsules reinforced by a poly (L-lysine)-g-poly (ethylene glycol).* Soft Matter, 2023. **19**(1): p. 69-79.

34. Gohel, M., et al., *How to approach major surgery where patients refuse blood transfusion (including Jehovah's Witnesses).* Annals of The Royal College of Surgeons of England, 2005. **87**(1): p. 3-14.

35. Hu, X., et al., *The Use of Microfluidics in Rheology.* Macromolecular Materials and Engineering, 2011. **296**(3-4): p. 308-320.

36. Barnes, H.A., J.F. Hutton, and K. Walters, *An introduction to rheology*. Vol. 3. 1989: Elsevier.

37. Baskurt, O.K., M.R. Hardeman, and M.W. Rampling, *Handbook of hemorheology and hemodynamics*. Vol. 69. 2007: IOS press.

38. Lee Waite, P. and J. Fine, *Applied biofluid mechanics*. 2007: The McGraw-Hill Medical Companies, Inc.

39. Sousa, P.C., et al., *Shear viscosity and nonlinear behavior of whole blood under large amplitude oscillatory shear.* Biorheology, 2013. **50**(5-6): p. 269-282.

40. Carneiro, J., et al., *Novel PDMS-based transparent suspensions suitable for fluid flow characterization by optical techniques.* Chemical Engineering Science, 2023. **280**: p. 119092.

41. Najjari, M.R., et al., *On the rheology of refractive-index-matched, non-Newtonian blood-analog fluids for PIV experiments.* Experiments in Fluids, 2016. **57**: p. 1-6.

42. Completo, C., V. Geraldes, and V. Semiao, *Rheological and dynamical characterization of blood analogue flows in a slit.* International Journal of Heat and Fluid Flow, 2014. **46**: p. 17-28.

43. Khan, F., K. Singh, and M.T. Friedman, *Artificial blood: the history and current perspectives of blood substitutes.* Discoveries, 2020. **8**(1).

44. Moradi, S., A. Jahanian-Najafabadi, and M.H. Roudkenar, *Artificial blood substitutes: first steps on the long route to clinical utility.* Clinical Medicine Insights: Blood Disorders, 2016. **9**: p. CMBD. S38461.

45. Jägers, J., A. Wrobeln, and K.B. Ferenz, *Perfluorocarbon-based oxygen carriers: from physics to physiology.* Pflügers Archiv-European Journal of Physiology, 2021. **473**: p. 139-150.

46. Clark Jr, L.C. and F. Gollan, *Survival of mammals breathing organic liquids equilibrated with oxygen at atmospheric pressure.* Science, 1966. **152**(3730): p. 1755-1756.

47. Schmieder, A.H., et al., *Recent advances in 19Fluorine magnetic resonance imaging with perfluorocarbon emulsions.* Engineering, 2015. **1**(4): p. 475-489.

48. Scott, M.G., et al., *Blood substitutes: evolution and future applications.* Clinical Chemistry, 1997. **43**(9): p. 1724-1731.

49. Novak, R., et al., *Robotic fluidic coupling and interrogation of multiple vascularized organ chips.* Nature biomedical engineering, 2020. **4**(4): p. 407-420.

50. Campo-Deaño, L., et al., *Viscoelasticity of blood and viscoelastic blood analogues for use in polydymethylsiloxane in vitro models of the circulatory system.* Biomicrofluidics, 2013. **7**(3): p. 034102.

51. Schöps, M., et al., *Ghost Cells for Mechanical Circulatory Support In Vitro Testing: A Novel Large Volume Production.* Biotechnology Journal, 2020. **15**(4): p. 1900239.

52. Beebe, D.J., G.A. Mensing, and G.M. Walker, *Physics and applications of microfluidics in biology.* Annual review of biomedical engineering, 2002. **4**(1): p. 261-286.

53. Wu, Q., et al., *Organ-on-a-chip: recent breakthroughs and future prospects.* BioMedical Engineering OnLine, 2020. **19**(1).

54. Moreira, A., et al., *Production of hydrogel microparticles in microfluidic devices: a review.* Microfluidics and Nanofluidics, 2021. **25**: p. 1-24.

55. Jalili-Firoozinezhad, S., C.C. Miranda, and J.M. Cabral, *Modeling the human body on microfluidic chips.* Trends in biotechnology, 2021. **39**(8): p. 838-852.

56. Kaminski, T.S., O. Scheler, and P. Garstecki, *Droplet microfluidics for microbiology: techniques, applications and challenges.* Lab on a Chip, 2016. **16**(12): p. 2168-2187.

57. Christopher, G.F. and S.L. Anna, *Microfluidic methods for generating continuous droplet streams.* Journal of Physics D: Applied Physics, 2007. **40**(19): p. R319.

58. Carneiro, J., J. Campos, and J. Miranda, *High viscosity polymeric fluid droplet formation in a flow focusing microfluidic device–Experimental and numerical study.* Chemical Engineering Science, 2019. **195**: p. 442-454.

59. Tumarkin, E. and E. Kumacheva, *Microfluidic generation of microgels from synthetic and natural polymers.* Chemical Society Reviews, 2009. **38**(8): p. 2161-2168.

60. Postek, W. and P. Garstecki, *Droplet microfluidics for high-throughput analysis of antibiotic susceptibility in bacterial cells and populations.* Accounts of Chemical Research, 2022. **55**(5): p. 605-615.

61. Liu, Y., et al., *A review on emulsification via microfluidic processes.* Frontiers of Chemical Science and Engineering, 2020. **14**: p. 350-364.

62. Tadros, T., et al., *Formation and stability of nano-emulsions.* Advances in colloid and interface science, 2004. **108**: p. 303-318.

63. Freire, M.G., et al., *Aging mechanisms of perfluorocarbon emulsions using image analysis.* Journal of colloid and interface science, 2005. **286**(1): p. 224-232.

64. Kamnerdsook, A., et al., *Formation of double emulsion micro-droplets in a microfluidic device using a partially hydrophilic–hydrophobic surface.* RSC advances, 2021. **11**(56): p. 35653-35662.

65. Wang, J., et al., *Formulation of water-in-oil-in-water (W/O/W) emulsions containing trans-resveratrol.* RSC advances, 2017. **7**(57): p. 35917-35927.

66. Leong, T.S., et al., *Preparation of water-in-oil-in-water emulsions by low frequency ultrasound using skim milk and sunflower oil.* Food Hydrocolloids, 2017. **63**: p. 685-695.

67. Guo, J., et al., *Encapsulation of β-carotene in calcium alginate hydrogels templated by oil-in-water-in-oil (O/W/O) double emulsions.* Colloids and Surfaces A: Physicochemical and Engineering Aspects, 2021. **608**: p. 125548.

68. Kim, H.S., C.-G. Lee, and E.Y. Lee, *Alginate lyase: Structure, property, and application.* Biotechnology and bioprocess engineering, 2011. **16**: p. 843-851.

69. Wong, T.Y., L.A. Preston, and N.L. Schiller, *Alginate lyase: review of major sources and enzyme characteristics, structure-function analysis, biological roles, and applications.* Annual Reviews in Microbiology, 2000. **54**(1): p. 289-340.

70. Duarte, A.R.C., et al., *Microfluidic production of perfluorocarbon-alginate core–shell microparticles for ultrasound therapeutic applications.* Langmuir, 2014. **30**(41): p. 12391-12399.

71. Bhattacharya, S., et al., *Studies on surface wettability of poly (dimethyl) siloxane (PDMS) and glass under oxygen-plasma treatment and correlation with bond strength.* Journal of microelectromechanical systems, 2005. **14**(3): p. 590-597.

72. Xiong, L., P. Chen, and Q. Zhou, *Adhesion promotion between PDMS and glass by oxygen plasma pre-treatment.* Journal of Adhesion Science and Technology, 2014. **28**(11): p. 1046-1054.

73. Jurado, E., et al., *Aerobic biodegradation of surfactants.* Biodegradation-life of science, 2013: p. 33-61.

74. Xu, Q., et al., *Soybean-based surfactants and their applications.* Soybean-applications and technology, 2011: p. 341-364.

75. Baret, J.-C., *Surfactants in droplet-based microfluidics.* Lab Chip, 2012. **12**(3): p. 422-433.

76. Khalfallah, A., *Structure and Applications of Surfactants*. 2024, IntechOpen.

77. Xu, J., et al., *The dynamic effects of surfactants on droplet formation in coaxial microfluidic devices.* Langmuir, 2012. **28**(25): p. 9250-9258.

78. Schroën, K., et al., *Linking findings in microfluidics to membrane emulsification process design: the importance of wettability and component interactions with interfaces.* Membranes, 2016. **6**(2): p. 26.

79. Bunge, F., et al. *µRespirometer to determine the oxygen consumption rate of mammalian cells in a microfluidic cell culture*. in *2017 IEEE 30th International Conference on Micro Electro Mechanical Systems (MEMS)*. 2017. IEEE.

80. Montagne, K., et al., *A micropatterned cell array with an integrated oxygen -sensitive fluorescent membrane.* Photochemical & Photobiological Sciences, 2009. **8**(11): p. 1529-1533.

81. Matsumoto, S., et al., *Investigation of the hepatic respiration and liver zonation on rat hepatocytes using an integrated oxygen biosensor in a microscale device.* Biotechnology Progress, 2019. **35**(5): p. e2854.

82. Charati, S. and S. Stern, *Diffusion of gases in silicone polymers: molecular dynamics simulations.* macromolecules, 1998. **31**(16): p. 5529-5535.

83. Palacio-Castañeda, V., et al., *Metabolic Switching of Tumor Cells under Hypoxic Conditions in a Tumor-on-a-chip Model.* Micromachines, 2020. **11**(4): p. 382.

84. Sleeboom, J.J.F., J.M.J.D. Toonder, and C.M. Sahlgren, *MDA-MB-231 Breast Cancer Cells and Their CSC Population Migrate Towards Low Oxygen in a Microfluidic Gradient Device.* International Journal of Molecular Sciences, 2018. **19**(10): p. 3047.

85. Funamoto, K., et al., *A novel microfluidic platform for high-resolution imaging of a three-dimensional cell culture under a controlled hypoxic environment.* Lab on a Chip, 2012. **12**(22): p. 4855-4863.

86. Harink, B., et al., *Microtiter plate-sized standalone chip holder for microenvironmental physiological control in gas-impermeable microfluidic devices.* Lab Chip, 2014. **14**(11): p. 1816-1820.

87. Virumbrales-Muñoz, M., et al., *Multiwell capillarity-based microfluidic device for the study of 3D tumour tissue-2D endothelium interactions and drug screening in co-culture models.* Scientific Reports, 2017. **7**(1).

88. Ayuso, J.M., et al., *Development and characterization of a microfluidic model of the tumour microenvironment.* Scientific reports, 2016. **6**(1): p. 36086.

89. Mehta, G., et al., *Hard top soft bottom microfluidic devices for cell culture and chemical analysis.* Analytical chemistry, 2009. **81**(10): p. 3714-3722.

90. Grist, S.M., et al., *Long-term monitoring in a microfluidic system to study tumour spheroid response to chronic and cycling hypoxia.* Scientific Reports, 2019. **9**(1).

91. Grist, S., et al., *Designing a Microfluidic Device with Integrated Ratiometric Oxygen Sensors for the Long-Term Control and Monitoring of Chronic and Cyclic Hypoxia.* Sensors, 2015. **15**(8): p. 20030-20052.

92. Lam, S.F., et al., *Microfluidic device to attain high spatial and temporal control of oxygen.* PLOS ONE, 2018. **13**(12): p. e0209574.

93. Ali, A., et al., *Microbial biofilms: applications, clinical consequences, and alternative therapies.* Microorganisms, 2023. **11**(8): p. 1934.

94. Yuan, L., et al., *Microfluidics for Biofilm Studies.* Annual Review of Analytical Chemistry, 2023. **16**(1): p. 139-159.

95. Gondil, V.S. and B. Subhadra, *Biofilms and their role on diseases.* BMC Microbiology, 2023. **23**(1).

96. Kilic, T. and E.B. Bali, *Biofilm control strategies in the light of biofilm-forming microorganisms.* World Journal of Microbiology and Biotechnology, 2023. **39**(5).

97. Lorenz, H., et al., *SU-8: a low-cost negative resist for MEMS.* Journal of Micromechanics and Microengineering, 1997. **7**(3): p. 121.

98. Bartholomeusz, D.A., R.W. Boutté, and J.D. Andrade, *Xurography: rapid prototyping of microstructures using a cutting plotter.* Journal of Microelectromechanical systems, 2005. **14**(6): p. 1364-1374.

99. Xia, Y. and G.M. Whitesides, *Soft lithography.* Annual review of materials science, 1998. **28**(1): p. 153-184.

100. Adamson, A.W. and A.P. Gast, *Physical chemistry of surfaces*. Vol. 150. 1967: Interscience publishers New York.

101. Harharah, H.N., S.A. Jafar, and L. IS. *Use of Sodium Sulfite as Oxygen Scavenger to Reduce the Corrosion Rate of Boiler Steel Pipes*. in *2nd International Chemical Engineering Conference*. 2010.

102. Que, Z., et al., *The powerful function of Saccharomyces cerevisiae in food science and other fields: A critical review.* Food Innovation and Advances, 2024. **3**(2): p. 167-180.

103. Winans, M.J., *Yeast hybrids in brewing.* Fermentation, 2022. **8**(2): p. 87.